NAVAL POSTGRADUATE SCHOOL
MONTEREY, CALIFORNIA

THESIS

A STUDY OF SOUTH ASIAN MONSOON CONVECTION AND TROPICAL UPPER EASTERLY JET DURING NORTHERN SUMMER 1991

by

Michael S. Nicklin

December, 1996

Thesis Advisor: Chih-Pei Chang
Co-Advisor: Peter S. Chu

Approved for public release; distribution is unlimited.

REPORT DOCUMENTATION PAGE

Form Approved OMB No. 0704-0188

1. AGENCY USE ONLY *(Leave blank)*	2. REPORT DATE December/1996	3. REPORT TYPE AND DATES COVERED Master's Thesis

4. TITLE AND SUBTITLE A STUDY OF SOUTH ASIAN MONSOON CONVECTION AND TROPICAL UPPER EASTERLY JET DURING NORTHERN SUMMER 1991

5. FUNDING NUMBERS

6. AUTHOR(S) Nicklin, Michael S.

7. PERFORMING ORGANIZATION NAME(S) AND ADDRESS(ES)
Naval Postgraduate School
Monterey CA 93943-5000

8. PERFORMING ORGANIZATION REPORT NUMBER

9. SPONSORING/MONITORING AGENCY NAME(S) AND ADDRESS(ES)

10. SPONSORING/MONITORING AGENCY REPORT NUMBER

11. SUPPLEMENTARY NOTES The views expressed in this thesis are those of the author and do not reflect the official policy or position of the Department of Defense or the U.S. Government.

12a. DISTRIBUTION/AVAILABILITY STATEMENT
Approved for public release; distribution is unlimited.

12b. DISTRIBUTION CODE

13. ABSTRACT *(maximum 200 words)*

This work studies the 1991 northern summer monsoon over India and surrounding areas using Japanese (GMS) and Indian (INSAT) geostationary satellite data, the ECMWF objective re-analysis, and the NMC sea surface temperature analysis. Monthly and weekly mean fields are first used to examine the development of the monsoon over the entire domain and to identify the timing of the onset over India. Latent heat fluxes are shown to be important in the monsoon development process. The relationship between the synoptic variations of a convective index derived from satellite data and the upper tropospheric easterly jet show two possible effects of cumulus convection on the easterly jet. The first is a forcing of the jet maximum near southern India when convection flares up to the north in the monsoon trough. This is believed to be the result of the Coriolis acceleration of the southward outflow of the local Hadley cell. The second is a damping of the upper jet by cumulus momentum transport that occurs at the same location as the jet maximum. This second effect is most clearly shown in regions of strong vertical shear.

14. SUBJECT TERMS
UPPER EASTERLY JET, CUMULUS TRANSFER OF MOMENTUM, ONSET OF NORTHERN SUMMER MONSOON OVER INDIA, MONSOON CONVECTION

15. NUMBER OF PAGES 140

16. PRICE CODE

17. SECURITY CLASSIFICATION OF REPORT	18. SECURITY CLASSIFICATION OF THIS PAGE	19. SECURITY CLASSIFICATION OF ABSTRACT	20. LIMITATION OF ABSTRACT
Unclassified	Unclassified	Unclassified	UL

NSN 7540-01-280-5500

Standard Form 298 (Rev. 2-89)
Prescribed by ANSI Std. 239-18 298-102

Approved for public release; distribution is unlimited.

A STUDY OF SOUTH ASIAN MONSOON CONVECTION AND TROPICAL UPPER EASTERLY JET DURING NORTHERN SUMMER 1991

Michael S. Nicklin
Lieutenant, United States Navy
B.S., University of Washington, 1990

Submitted in partial fulfillment
of the requirements for the degrees of

MASTER OF SCIENCE IN METEOROLOGY
MASTER OF SCIENCE IN PHYSICAL OCEANOGRAPHY

from the

NAVAL POSTGRADUATE SCHOOL
December 1996

Author: _____
Michael S. Nicklin

Approved by: _____
Chih-Pei Chang, Thesis Advisor

_____
Peter S. Chu, Co-Advisor

_____
Carlyle H. Wash, Chairman, Department of Meteorology

_____
Robert H. Bourke, Chairman, Department of Oceanography

ABSTRACT

This work studies the 1991 northern summer monsoon over India and surrounding areas using Japanese (GMS) and Indian (INSAT) geostationary satellite data, the ECMWF objective re-analysis, and the NMC sea surface temperature analysis. Monthly and weekly mean fields are first used to examine the development of the monsoon over the entire domain and to identify the timing of the onset over India. Latent heat fluxes are shown to be important in the monsoon development process. The relationship between the synoptic variations of a convective index derived from satellite data and the upper tropospheric easterly jet show two possible effects of cumulus convection on the easterly jet. The first is a forcing of the jet maximum near southern India when convection flares up to the north in the monsoon trough. This is believed to be the result of the Coriolis acceleration of the southward outflow of the local Hadley cell. The second is a damping of the upper jet by cumulus momentum transport that occurs at the same location as the jet maximum. This second effect is most clearly shown in regions of strong vertical shear.

TABLE OF CONTENTS

I. INTRODUCTION

Data sparse areas of the tropical oceanic regions, particularly the Indian Ocean and, to a lessor extent, the tropical Pacific, have historically challenged the research efforts of meteorologists and oceanographers. Recently, global numerical model analyses and satellite data assimilation techniques (Murakami, 1984) have contributed to the availability of better data sets for observational studies, but many significant questions still remain regarding the extent that the large-scale flow in these regions are adequately represented in these new data sets. The quality of these analyses is coupled to the quality of the observations used to initialize the models, and these same observations are the basis for validating model forecasts. Where these observations are lacking, high resolution (both in time and space) satellite infra-red (IR) data has been available for over two decades as an independent and proxy measure of tropical deep convective activity in the tropical eastern Pacific and western Atlantic by the U.S. Geostationary Operational Environmental Satellites (GOES). In the tropical western Pacific, similar data has been available from the Geostationary Meteorological Satellite (GMS) since 1979. However, data from the Indian Ocean Satellite (INSAT) system

has not been widely available for operational or research purposes outside of India, and this has hampered research efforts in the Indian Ocean.

In this study variations in large-scale convection over the Indian Ocean region during the northern summer monsoon season (May to August) of 1991 are examined using 3-hourly IR data from both the GMS and INSAT satellites. Specifically, the variability of tropical convective activity during this time frame is studied through a comparison between observed fluctuations in a satellite-derived convection index and analyses produced by a global numerical model assimilation system. The convective index is based on the equivalent black-body temperature data from the composite GMS-INSAT. The re-analyses produced by the European Center Medium Range Weather Forecast (ECMWF) is chosen for this comparison. In addition, possible air-sea interactions are further investigated utilizing the National Meteorological Center (NMC) satellite sea surface temperature (SST) fields, which are produced weekly on a one degree grid.

Even though the ECMWF re-analysis data are available at rather high temporal (4 times daily) and spatial (1.125°) resolutions that make it possible to match the data with the high resolution of the composite GMS-INSAT TBB (black body temperature) data, the observational radiosonde basis is very

sporadic over the region. The upper tropospheric analyses near 200 hPa are supplemented by the cloud top satellite winds and the abundant AIREP data from jumbo jets, whereas the lower levels do not have these supplemental data sources. The lower level cloud base wind vectors are often difficult to determine under deep convective regions. So in this study, the investigation of the possible relationships between the organized monsoon convection and the large scale circulations in the Indian monsoon region will be focused on general statistical relationships involving broad scale circulations, rather than specific cases. The dominant circulation feature in the upper troposphere during northern summer is the tropical upper level easterly jet with its maximum over southern India (Krishnamurti and Surgi, 1987). Two aspects concerning the possible relationships between deep cumulus convection and this upper easterly jet will be examined: 1) the possible forcing mechanism of the easterly jet by the subtropical monsoon convection poleward of the jet maximum, and 2) the effect of cumulus-scale vertical momentum transport on the easterly jet.

During the northern winter monsoon several studies (Chang and Lau, 1980; Lau, Chang, and Chan, 1983; Lau and Chang, 1987) showed that the synoptic time scale flare-up of deep convection over the Maritime Continent (the chain of island

nations between -10°S, 100°E and 10°N, 145°E) can remotely influence the East Asian upper tropospheric westerly jet streak in the mid-latitudes. This influence occurs following low-level northeasterly surges, which enhance the Maritime Continent convection and latent heat release, leading to a speeding-up of the local Hadley cell. The condensation heating occurs in the equatorial trough region with little planetary vorticity, but the relative vorticity is positive due to the presence of a low-level monsoon vortex over the Maritime Continent. The rising motion causes vortex stretching and hence acquisition of cyclonic vorticity. Thus, the air parcels tend to move poleward at upper levels in order to keep their relative vorticity small. The influence of the Coriolis torque causes these air parcels to move eastward, and the net effect is to accelerate the mid-latitude westerly jet downstream.

There have been some arguments that the enhancement of the mid-latitude westerly jet during cold surges may be itself a part of the increased baroclinicity associated with the surges, rather than a result of the increased tropical convection (which is also a result of the cold surge penetrating into the Maritime Continent region). But other situations of an enhancement of the northern winter mid-latitude jet in the upper troposphere by tropical

convection have also been observed. For example, Chang and Lum (1985) found a positive correlation at synoptic time scales between the tropical upper tropospheric poleward wind over the western North Pacific and the jet stream intensity over East Asia. They showed specific cases of tropical cyclones that produced the strong poleward divergent winds at the upper levels, and that these winds result in a westerly acceleration of the East Asian jet. Since the tropical cyclones originate in the tropics, there is little doubt that the sequence of events starts from the tropics, and that the mid-latitude jet acceleration is a result of the Coriolis torque of the northward outflow from the tropical cyclones.

In the present study, the INSAT-GMS data set will allow us to examine the effect of northern summer deep convection in the South Asian monsoon region. During this season, the local Hadley cell has its rising branch situated between 15°N-30°N in south and southeast Asia, and the sinking branch is situated in the Southern Hemisphere mid-latitudes. The tropical upper tropospheric easterly jet has its maximum located near southern India around 15°N. Thus, the jet maximum is on the equatorward-side of the maximum upper divergence in the region of the southward divergent flow. Based on the convection-jet stream interaction model of the northern winter monsoon (Chang and Lau, 1980), one may expect

that the easterly jet may be influenced by a weak Coriolis torque of the upper level equatorward flow of the monsoon-related Hadley cell. Thus, this will be one of the key questions that will be studied.

The mechanism of cumulus-scale transport and its effect in large scale motion systems is most well known in strong tropical cyclones. The intense eye-wall convection in typhoons and hurricanes transports low-level properties (including equivalent potential temperature, horizontal momentum and vorticity) upward at the cumulus time scale, resulting in the near moist-adiabatic, weak vertical wind shear and cyclonic outflow structure surrounding the eye of the typhoon (Gray, 1979). This structure is unique to typhoons and hurricanes and is responsible for the maintenance of the storms. During some northern summers, the upper tropospheric divergence and vorticity centers associated with the planetary scale Asian monsoon may become nearly in-phase (Krishnamurti, 1971). Holton and Colton (1972) argued that a strong viscous damping is required to balance the generation term in the vorticity equation, and cumulus scale transport of low-level vorticity upward may be the mechanism to fulfill this requirement. Chang (1977) also proposed a viscous damping model to explain the large-scale equatorial waves based on the cumulus momentum transports. On the other hand,

Sardeshmukh and Held (1984) proposed that the cumulus transport process in the tropical large scale motions is not important, as the required effect may be explained by the nonlinear processes that were neglected in the linear models.

The satellite IR data may be used reliably to represent the degree of convection only for the tropical band between 30°S-30°N (Murakami, 1984). A main upper tropospheric vorticity feature in the northern summer monsoon is the Tibetan anticyclone which is centered near 30°N, or the border region of this band. The suitability of using the satellite IR data to study the cumulus transport of vorticity around the Tibetan anticyclone is therefore questionable. On the other hand, the upper easterly jet maximum is near 15°N, and there are significant convection activities in southern India around this latitude that can be represented by the satellite IR data. In the lower troposphere, monsoonal southwesterly winds in this region prevail throughout the northern summer, and a strong vertical shear exists under the upper easterly jet maximum. Therefore, signals of the cumulus transport of momentum may be strong in this region and may show up in the present data. If this process is important, we may expect to see a negative correlation of the vertical shear and the degree of cumulus convection, as the upper and lower level winds will be mixed through the cumulus transport, thus

dampening the shear between the two levels. This will be another key question to be studied.

The dominating wind and convective regime typical of the northern summer monsoon does not exist continuously for the entire four month period from May through August. Rather, a transition occurs annually near the end of May that signals the beginning of the monsoon in the Indian Ocean. Characteristics of the transition include an increase in horizontal moisture and vertical latent heat fluxes (Pishnaroty, 1981); a movement of the monsoon trough (and associated convection) away from the equator to a position centered over the Tibetan Plateau (Cornejo-Garrido and Stone, 1977); a drop in average sea surface temperatures across the Indian Ocean (Pishnaroty, 1965); and a strengthening of the low level southwesterly winds and upper tropospheric easterly jet (Krishnamurti, 1971). A precise definition of the transition event, encompassing all significant meteorological and oceanographic phenomena, does not yet exist. Rather, most of the aforementioned research has centered on singular observations made using the sporadic data available at the time. Hence, it is important to clearly distinguish between the pre-monsoon and monsoon environments, and to isolate this transition or "onset" event.

Pisharoty (1965, 1981) studied the moisture and latent

heat fluxes in the northern Indian Ocean from May through September using ten years of data. He computed weekly mean water vapor and latent heat fluxes across the equator into the Arabian Sea, and across the Indian west coast from the Arabian Sea. He found that a large drop in areal averaged sea surface temperature occurred in conjunction with the onset of predominately southwesterly winds, and that a large, negative latent heat flux from these adjacent waters bore a strong positive correlation with the onset of strong convection over the Indian sub-continent. However, a lack of observational data and sporadic satellite coverage suggests that his conclusions may be somewhat speculative.

Additional studies (Cornejo-Garrido and Stone, 1977; Ramage and Hori, 1981; Rasmussen and Carpenter, 1982; Liebman and Hartmann, 1982) suggest that convective flare-ups in the tropics are closely associated with anomalies in sea surface temperature, which in turn govern the transfer of latent and sensible heat to and from the atmosphere. Before the transition, the highest average sea surface temperatures observed in the northern Indian Ocean ranged between 30.5 and 31.0° C. After the transition, the average sea surface temperatures were observed to range between 28.0 and 29.0 °C, demonstrating a drop of approximately 2.0 °C during the onset event.

Finally, studies by Krishnamurti (1971) and Murakami (1984 and 1987) describe the phenomenon known as the "onset vortex": a weak, low level cyclonic circulation that generally originates in the vicinity of the southern tip of India at the end of May. Formation of this vortex corresponds to substantial thermal low pressure development over the Indian sub-continent (due to latent heating), inducing positive vorticity and low level convergence. Warm, moist air from the Bay of Bengal and Arabian Sea flows into this cyclone, promoting strong convection and associated latent heat release. This sets up a positive feedback mechanism, whereby heating of the column lowers the surface pressure, which in turn induces low level convergence and continued development.

The vortex moves northward along the west coast of India, and winds south of the circulation align to the southwest. This signals the transition to the northern summer monsoon in the Indian Ocean, as these southwesterly winds strengthen and dominate the Arabian Sea, India, and the Bay of Bengal. Prior to this transition, the upper and lower level winds do not exhibit the strong vertical wind shear so prominently associated with the northern Indian summer monsoon.

Thus, an important consideration will be to discern if the three independent data sources used in this study are of sufficient quality that they can be used to identify the onset

of the monsoon regime. Specifically, isolating the transition is pertinent to the discussion of the local Hadley circulation and to the question of vertical momentum transfer, which are the central focal points of our study.

II. DATA AND METHODOLOGY

The initial data used in this study was the three-hourly infrared (IR) data of the GMS and INSAT satellites from May through August of 1991. This data was provided by Dr. Matsuto Murakami of the Meteorological Research Institute (MRI) in Tsukuba, Japan. The INSAT during 1991 was located above 82°E over the equator and its observation footprint covered the latitudinal range roughly from 40°E to 120°E. The GMS was located above 140°E over the equator and its observation footprint covered the longitudinal range roughly from 80°E to 160°W. The three-hourly, IR-equivalent black body temperature (TBB), averaged over the one degree latitude/longitude mesh, were taken from both satellites. The inter-calibration between GMS and INSAT was carried out by MRI utilizing the overlapping area from 110°E-115°E. The composition of these two geostationary satellites enabled full coverage of the entire Asian monsoon region (40°E-160°W, 50°N-50°S) with the finer spatial and temporal resolution than OLR (Out-going Longwave Radiation) data used in many previous studies.

A sub-section of the initial data coverage was chosen to concentrate on the Asia-Pacific-eastern Indian Ocean portion of the 1991 northern summer monsoon. The longitudinal range (63°E-153°E) and the latitudinal range (18°S-45°N) were chosen

to match boundary grid points of subsequent data sets used in these investigations. Quality control of each data point was necessary (particularly in the case of the INSAT data, which was less reliable than the GMS), and missing data points were arbitrarily set to -10°K. This cleaner version of the raw TBB data was then converted to high resolution MPEG-2 movie format (a compressed binary visualization scheme) to allow visual inspection of the data and to begin data analyses.

The European Center for Medium Range Weather Forecasting (ECMWF) Advanced Operational Data Set was also used in this study. Fields were un-initialized re-analyses of geopotential, temperature, vertical velocity, u- and v-components of horizontal wind, and relative humidity. These data were high resolution, upper air analyses of fourteen pressure levels in the troposphere (in a spherical harmonic representation). We converted the data from spherical harmonics to a gaussian grid, yielding a final horizontal resolution of 1.125°. Temporal resolution was four times daily at 0000Z, 0600Z, 1200Z, and 1800Z.

National Meteorological Center (NMC) optimum interpolation (OI) global sea surface temperature (SST) data was used, together with ECMWF gridded data, to study air-sea thermodynamic relationships. Produced weekly on a one-degree grid, these analyses use insitu and satellite SST. Satellite

data were adjusted for biases using the method of Reynolds (1988) and Reynolds and Marsico (1993). The bias correction does add a small amount of noise in time, which was eliminated using a 1/4-1/2-1/4 binomial filter. The weeks were defined to be centered on Wednesday at 0000Z, in agreement with the definition used for ocean modeling. Each data point was then linearly interpolated in time between weeks to match the temporal frequency of the ECMWF data (0000Z, 0600Z, 1200Z, and 1800Z daily). More exact interpolation schemes were not used because the SST variance is small.

Large scale synoptic convective activity was represented by converting raw TBB data to a convective index (CI), utilizing the following equation (Nitta, 1983):

$$CI = 255 - TBB \qquad (1)$$

Here, 255°K is the presumed black body temperature at the 400 hPa level. Values of CI that were less than zero represent little or no deep convection, and were thus set to zero.

The convective index was then plotted for each 3-hourly time increment from May through August 1991, and an MPEG-2 movie was generated. Additionally, the monthly mean average CI was compiled (Figures 1-4). After visual inspection of the individual frames of CI and the monthly mean values, it was determined that two particular areas exhibited frequent,

persistent, and active convection throughout the entire summer monsoon period. The first area chosen was near the southern tip of India and west of Sri Lanka (see Figure 5), hereafter referred to as area TI. The second area, (designated area NB in Figure 5), was selected in the northern Bay of Bengal, extending north and inland into the low lying coastal region.

The initial choice of TI and NB were further refined by calculating correlation coefficients of areal average CI for each area with the CI for all grid points in the entire domain (Figures 6 and 7). The periphery of the rectangular areas were adjusted to include isopleths of correlation coefficient greater than 0.7 (approximately). The final determined areal extent of area TI was forty eight square degrees (from 6°N-14°N and 74°E-80°E). For area NB, the areal extent was thirty five square degrees (from 20°N-25°N and 85°E-92°E).

ECMWF upper air wind data at 850 hPa and 200 hPa were used to compute the U (or zonal) component and V (or meridional) component of vertical wind shear for the entire domain using equations (2) and (3):

$$U_{vertical\ shear} = U_{200} - U_{850} \qquad (2)$$

$$V_{vertical\ shear} = V_{200} - V_{850} \qquad (3)$$

The vertical shear, particularly the zonal component in

equation (2), is used as a "monsoon index" to represent the intensity of the summer monsoon (Webster and Yang, 1992). A mean monthly average vertical wind shear was plotted using only $U_{\text{vertical shear}}$ because the meridional winds at 200 hPa are much weaker than the zonal winds (being dominated by the strong upper level tropical easterly jet known to persist throughout the northern summer monsoon). During May the average maximum vertical shear was situated over the northern Arabian Sea (near 25°N latitude), extending longitudinally from northern India to the Strait of Hormuz. Note that negative (positive) values of vertical wind shear correspond to an easterly (westerly) tilt of the vertical shear with height. The average maximum vertical wind shear during May averaged approximately -10 m/s, as illustrated in Figure 8.

By June, the average maximum wind shear (Figure 9) moved east and slightly south, covering the entire breadth of northern India. However, this average maximum wind shear had strengthened considerably over that for May, reaching values of approximately -32 m/s, indicative of the strong shear after the onset of the monsoon.

In July and August, strong vertical wind shear dominated the northern tropics (Figures 10 and 11), extending from the equator north to approximately 35°N. The average maximum vertical wind shear had migrated south, extending across

southern India along 13°N from the Arabian Sea well into the Bay of Bengal. Thus, a third area (designated SI in Figure 5) was chosen to study the relationship between strong active convection and the possible effect it has on vertical momentum transport.

The SST data noted previously were contoured at each 6-hourly time interval and a movie was generated in MPEG-2 format. By looping through the individual frames, a general assessment of sea surface temperature variation was made. As expected, little variation occurred on a daily basis. However, over the entire four month period, an average decrease of approximately 1.5 °C was noted, with the greatest decrease occurring in the first two weeks of June.

To study the exchange of heat across the air-sea boundary, and its possible effect on convective flare-ups (specifically in the areas TI and NB), the vertical latent and sensible heat fluxes were computed as detailed below. The long wave radiation (and, hence, the net heat flux) was not computed because no reasonable method of ascertaining cloud cover was available.

Three areas in the Arabian Sea and Bay of Bengal (Figure 12), designated SST1, SST2, and SST3, were chosen due to individual proximity to areas TI and NB, and because the horizontal wind patterns were predominately southwesterly

during most of the northern summer monsoon. Hence, these over-water areas can reasonably be expected to contribute to the horizontal heat and moisture flux by simple advection. Gridded data were converted from the standard one-degree by one-degree grid of the original NMC SST data set to the gaussian grid used by the ECMWF by using an optimum interpolation scheme and finite difference methods described by Schlatter (1975). The remainder of this chapter describes the method used to calculate the latent and sensible heat fluxes.

The magnitude of total velocity (W_{10}) at 10 meters was calculated from individual components of velocity as:

$$W_{10}=\sqrt{U_{10}^{2}+V_{10}^{2}} \qquad (4)$$

Surface latent heat flux was computed using the method of Buck (1981), beginning with the following equation for saturation vapor pressure (e_s):

$$e_s=6.1121\exp^{\frac{17.502T_{sfc\ air}}{240.97+T_{sfc\ air}}}(1.0007+3.46E\text{-}6\ P_{SFC}) \qquad (5)$$

$T_{sfc\ air}$ is air temperature in °C just above the ocean surface; and P_{SFC} is surface pressure in hPa. The saturation mixing ratio (w_s) was then defined as:

$$w_s = .62198 \frac{e_s}{p - e_s} \qquad (6)$$

Since the relative humidity (r) was also given from the ECMWF data, the mixing ratio (w) was approximated as:

$$w \approx r w_s \qquad (7)$$

The specific humidity of air at the surface of the water and the specific humidity in the air above the surface (q_s and q, equations (8) and (9), respectively) were then derived as:

$$q_s = \frac{w_s}{w_s + 1} \qquad (8)$$

$$q = \frac{w}{w + 1} \qquad (9)$$

The air density was calculated using the virtual temperature (T_v) and the ideal gas law:

$$T_v = T_{sfc\ air} \frac{(1 + 1.60779w)}{(1 + w)} \qquad (10)$$

The neutral value for the drag coefficient of momentum was taken from Garratt (1977):

$$\rho_{air}=3.4838 \times 10^{-4}\frac{P}{T_v} \qquad (11)$$

$$C_{DN}=7.5 \times 10^{-7}W_{10} \qquad (12)$$

The transfer coefficients for latent and sensible heat exchange were assumed to be constant ($C_{EN}=C_{SN}=.0014$) for our purposes. The variation of these transfer coefficients with wind speed is much smaller than that of the drag coefficient, and only at wind speeds exceeding 25 m/s will there be any significant source of error.

The stability correction to the neutral drag coefficients was taken from Kondo (1975), starting with a stability parameter (S) defined as:

$$S=S_o\frac{|S_o|}{|S_o|+0.01} \qquad (13)$$

where

$$S_o=\frac{T_{SST}-T_{SFC\ AIR}}{W_{10}^{\ 2}}\ (for\ z=10m) \qquad (14)$$

Applying the stability correction to the neutral transfer

coefficients yielded the transfer coefficients for diabatic conditions (SI units):

(a) *for stable condition* ($T_{SST}-T_{SFC\ AIR} < 0$):

$$C_{DN\ corrected}=C_{DN}[0.01+0.03S+0.9e^{4.8S}],\ (for\ -3.3<S<0) \quad (15)$$

$$C_{EN\ corrected}\approx C_{EN}[0.01+0.03S+0.9e^{4.8S}],\ (for\ -3.3<S<0) \quad (16)$$

$$C_{SN\ corrected}\approx C_{SN}[0.01+0.03S+0.9e^{4.8S}],\ (for\ -3.3<S<0) \quad (17)$$

$$C_{DN\ corrected}\approx C_{EN\ corrected}\approx C_{SN\ corrected}\approx 0,\ (for\ S \le -3.3) \quad (18)$$

(b) *for unstable condition* ($T_{SST}-T_{SFC\ AIR} > 0$):

$$C_{DN\ corrected}\approx C_{DN}[1.0+0.47S^{0.5}] \quad (19)$$

$$C_{EN\ corrected}\approx C_{EN}[1.0+0.63S^{0.5}] \quad (20)$$

$$C_{SN\ corrected}\approx C_{SN}[1.0+0.63S^{0.5}] \quad (21)$$

The magnitude of the surface wind stress (τ) was then computed using:

$$\tau=\rho_{air}C_{DN}W_{10}^{2} \quad (22)$$

The vertical latent heat flux (Q_E) and vertical sensible heat flux (Q_S), respectively, were then computed using standard

bulk formulae (after Wyrtki, 1965) as follows:

$$Q_E = -\rho_{air} C_{EN} L (q_s - q) W_{10} \qquad (23)$$

$$Q_S = -\rho_{air} C_{SE} C_P (T_{SST} - T_{SFC\ AIR}) W_{10} \qquad (24)$$

These formulae utilize the convention that negative (positive) values represent a heat transfer from (to) the ocean to (from) the atmosphere. Note that these values of latent and sensible heat flux are only good "over water", as are the values of moisture flux that follow.

Finally, the 850 hPa moisture flux (M) was computed using the specific humidity and 850 hPa combined winds:

$$\vec{M} = q\vec{V}_{850} \qquad (25)$$

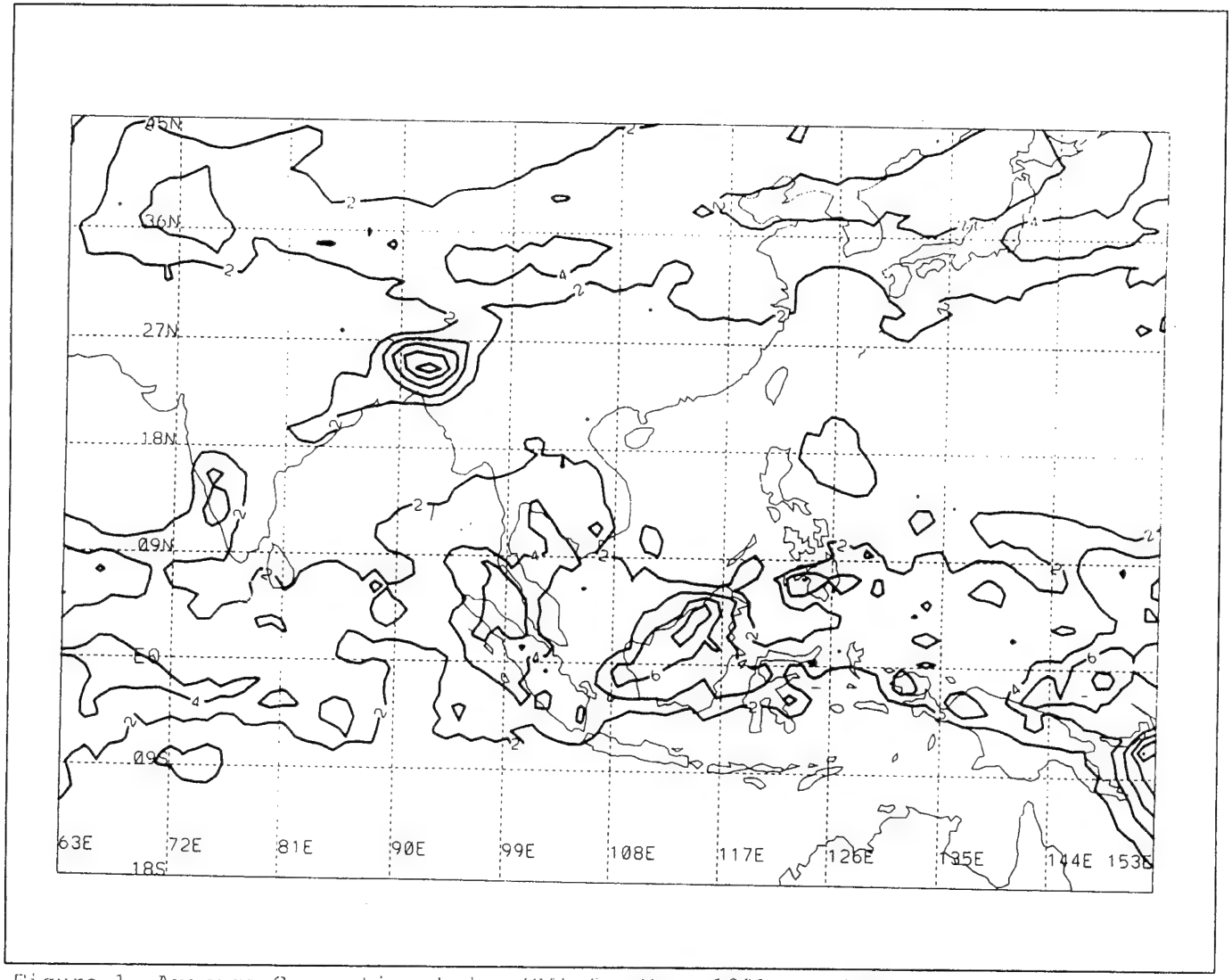

Figure 1. Average Convective Index (CI) for May, 1991. Values of CI are in °K.

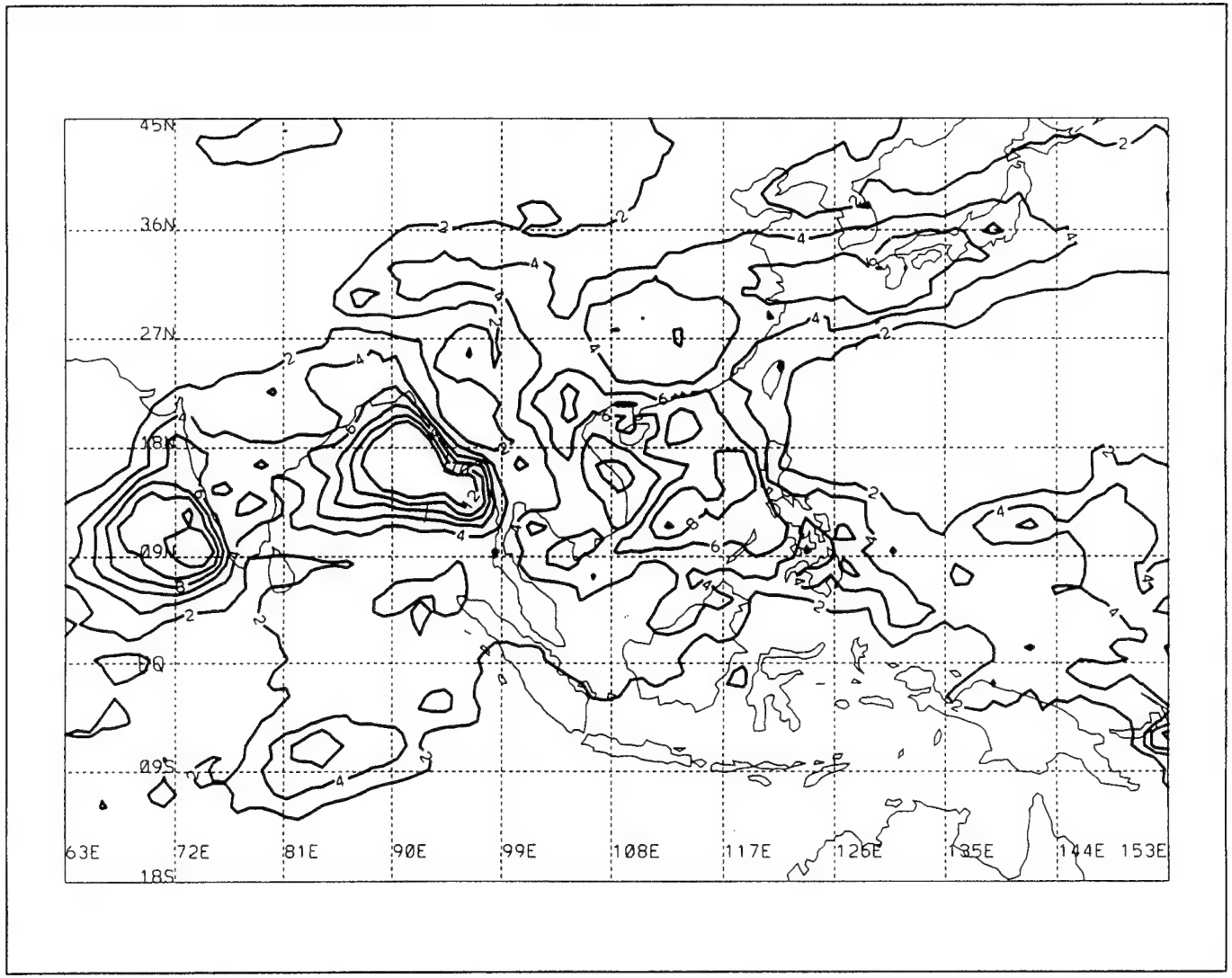

Figure 2. Average Convective Index (CI) for June, 1991. Values of CI are in °K.

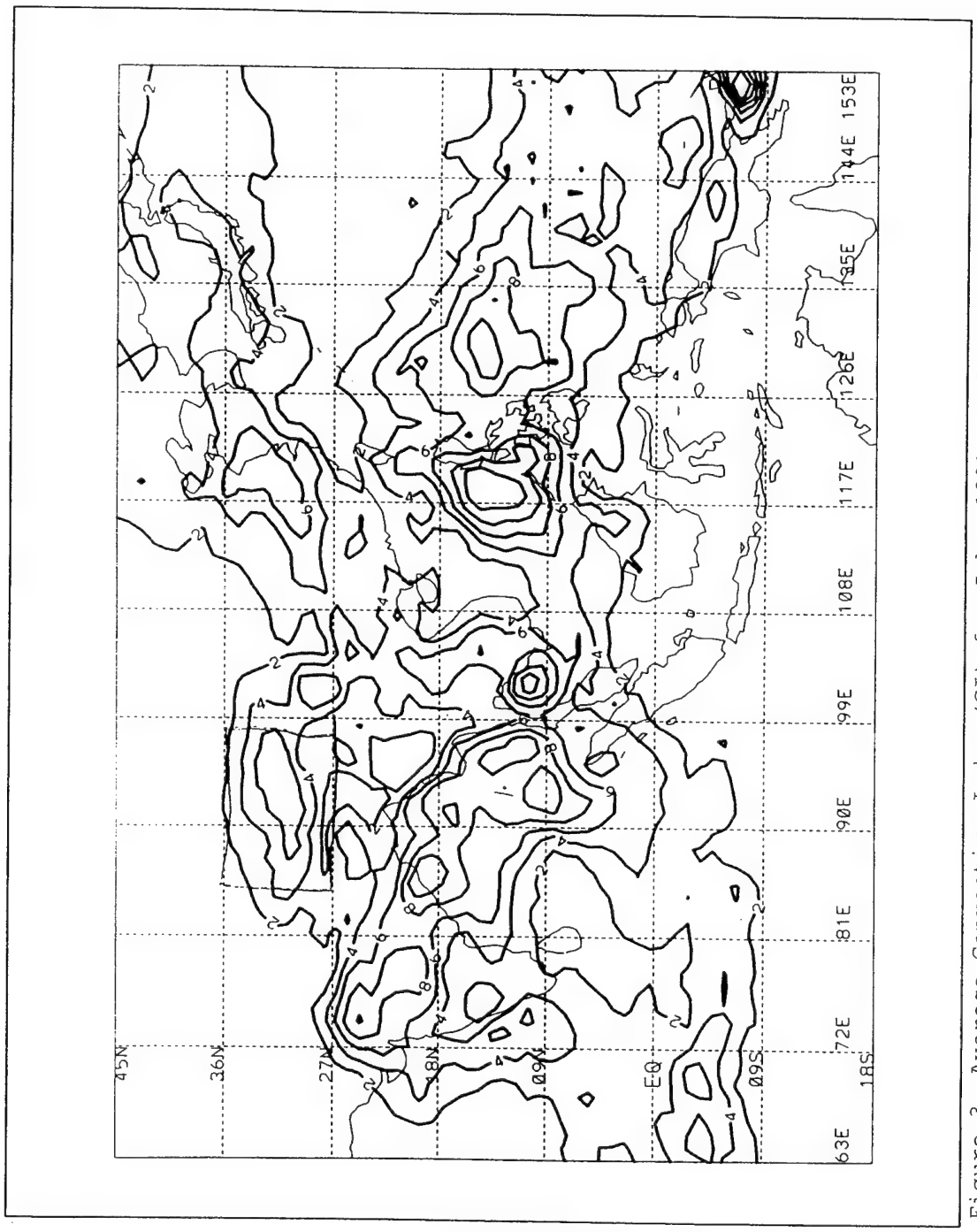

Figure 3. Average Convective Index (CI) for July, 1991. Values of CI are in °K.

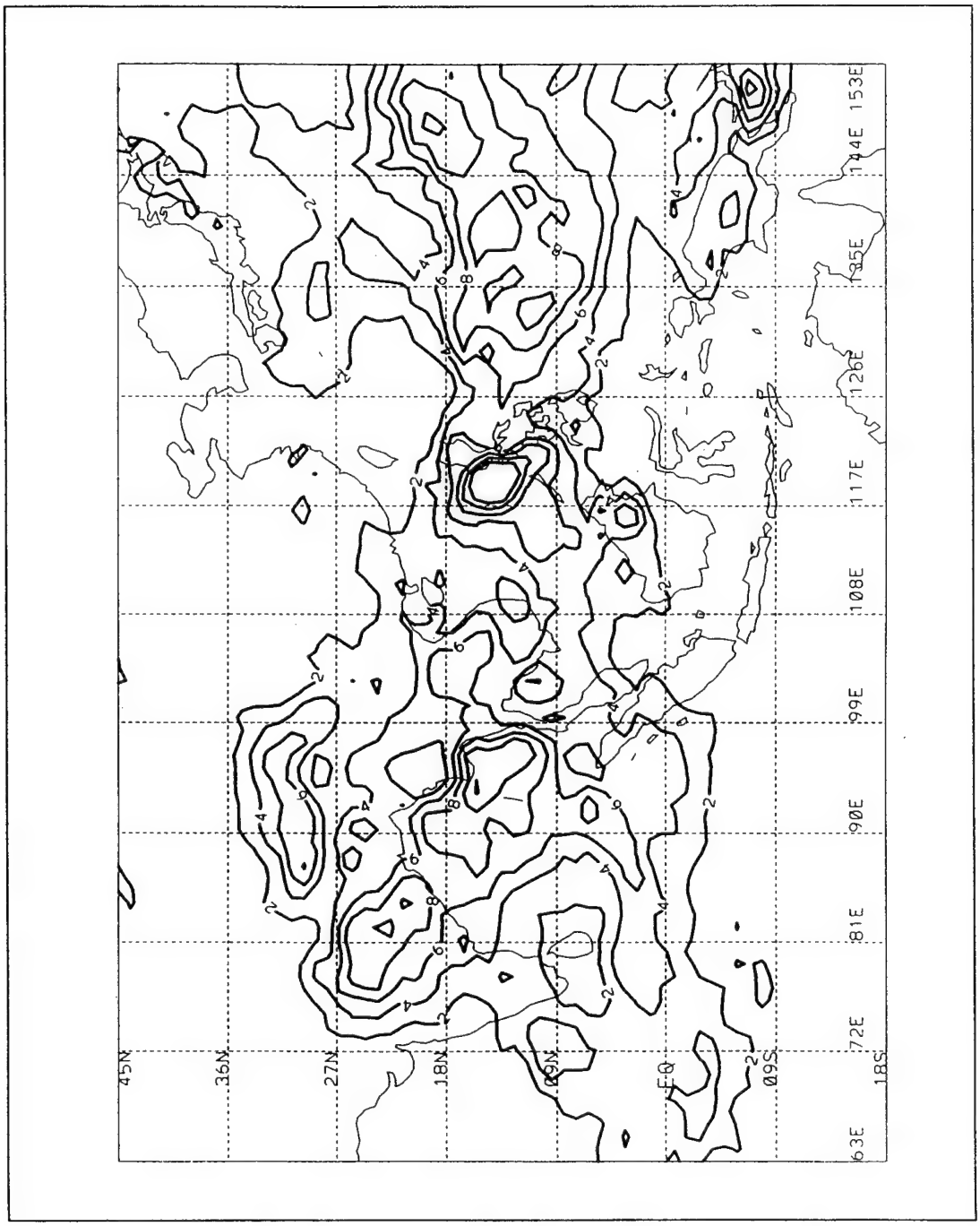

Figure 4. Average Convective Index (CI) for August, 1991. Values of CI are in °K.

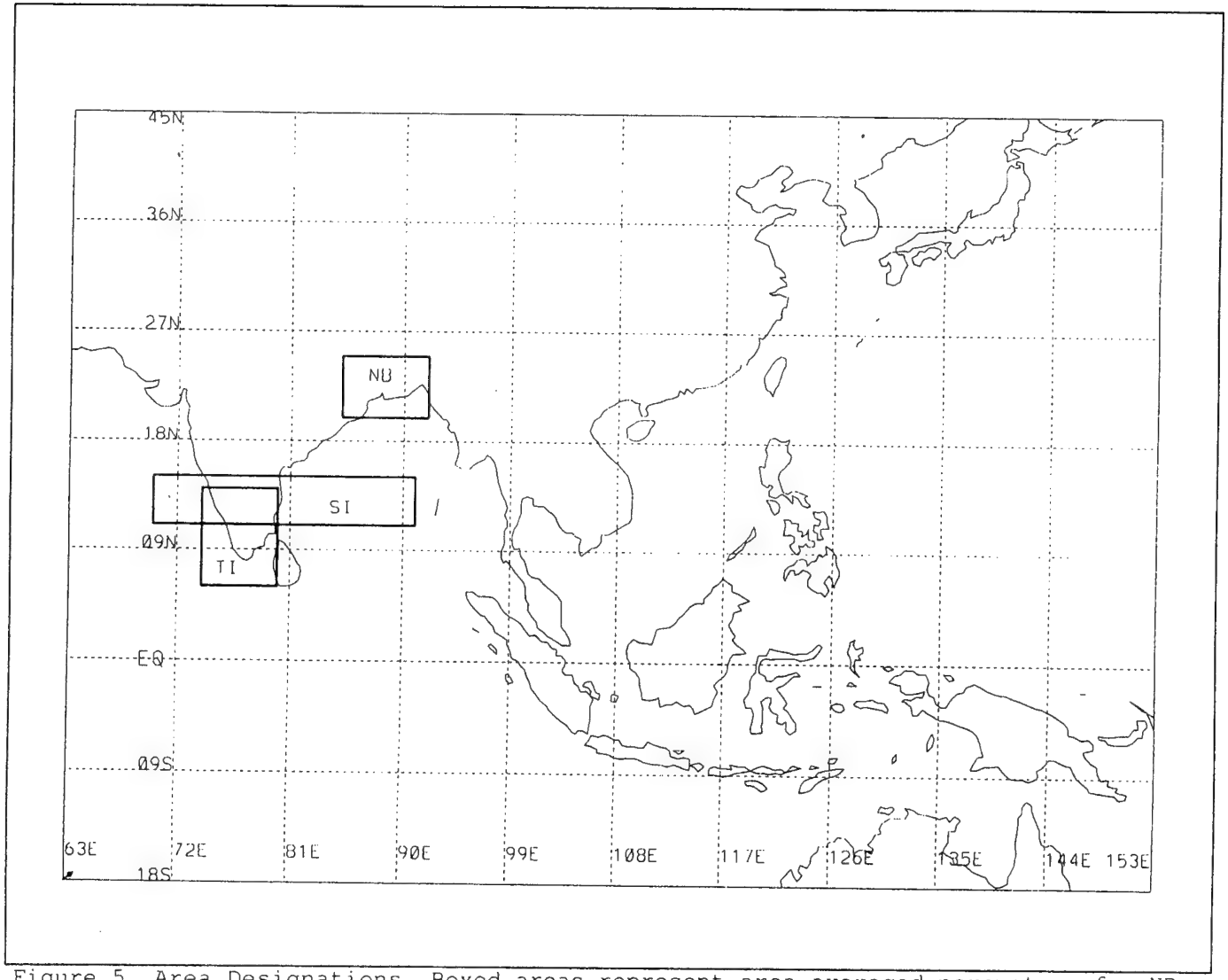

Figure 5. Area Designations. Boxed areas represent area-averaged parameters for NB (Northern Bay of Bengal), TI (Tip of India), and SI (Southern India).

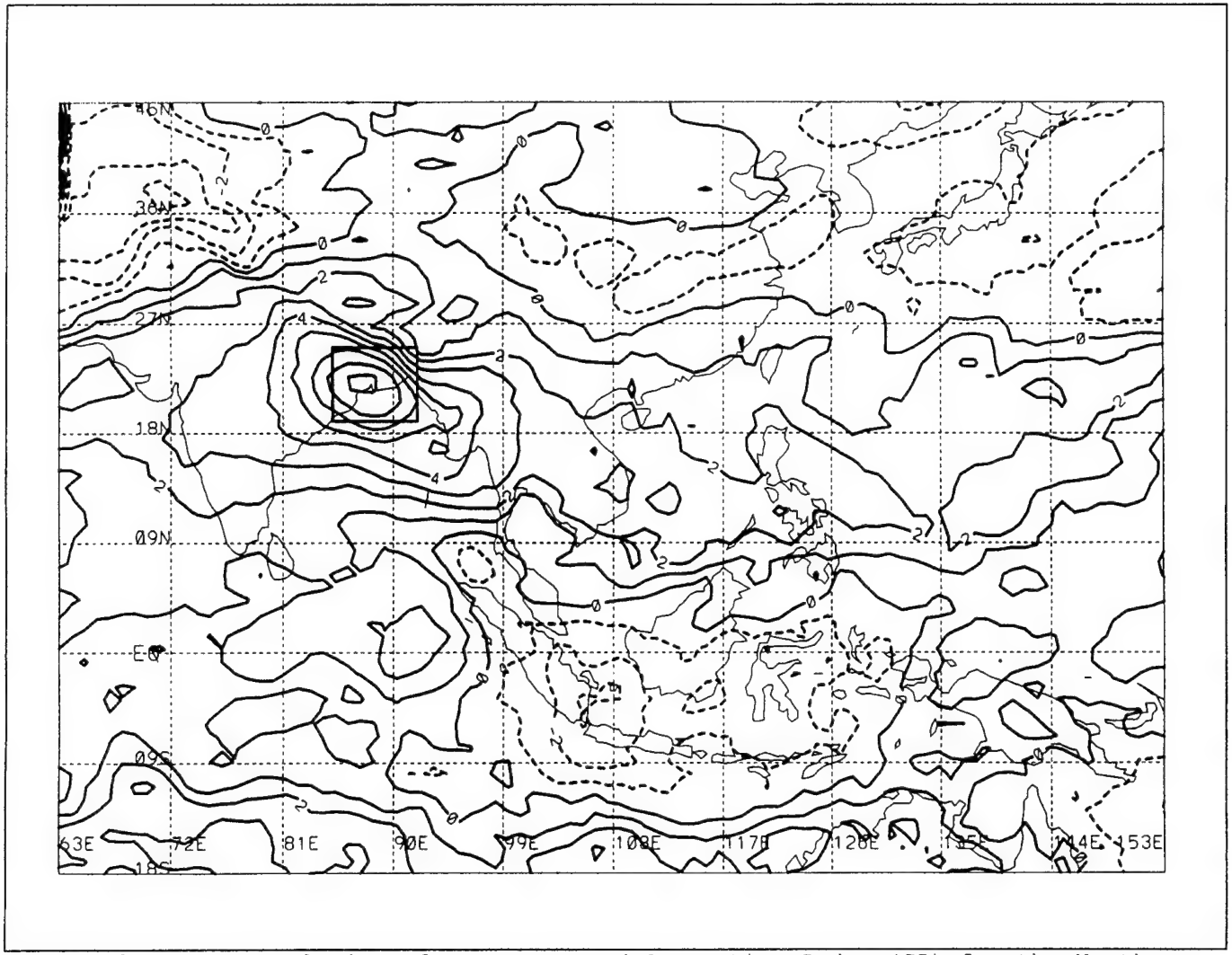

Figure 6. Auto-correlation of area-averaged Convective Index (CI) for the Northern Bay of Bengal (NB) with CI for the entire domain. Values greater than zero represent positive correlation, while values less than zero represent negative correlation.

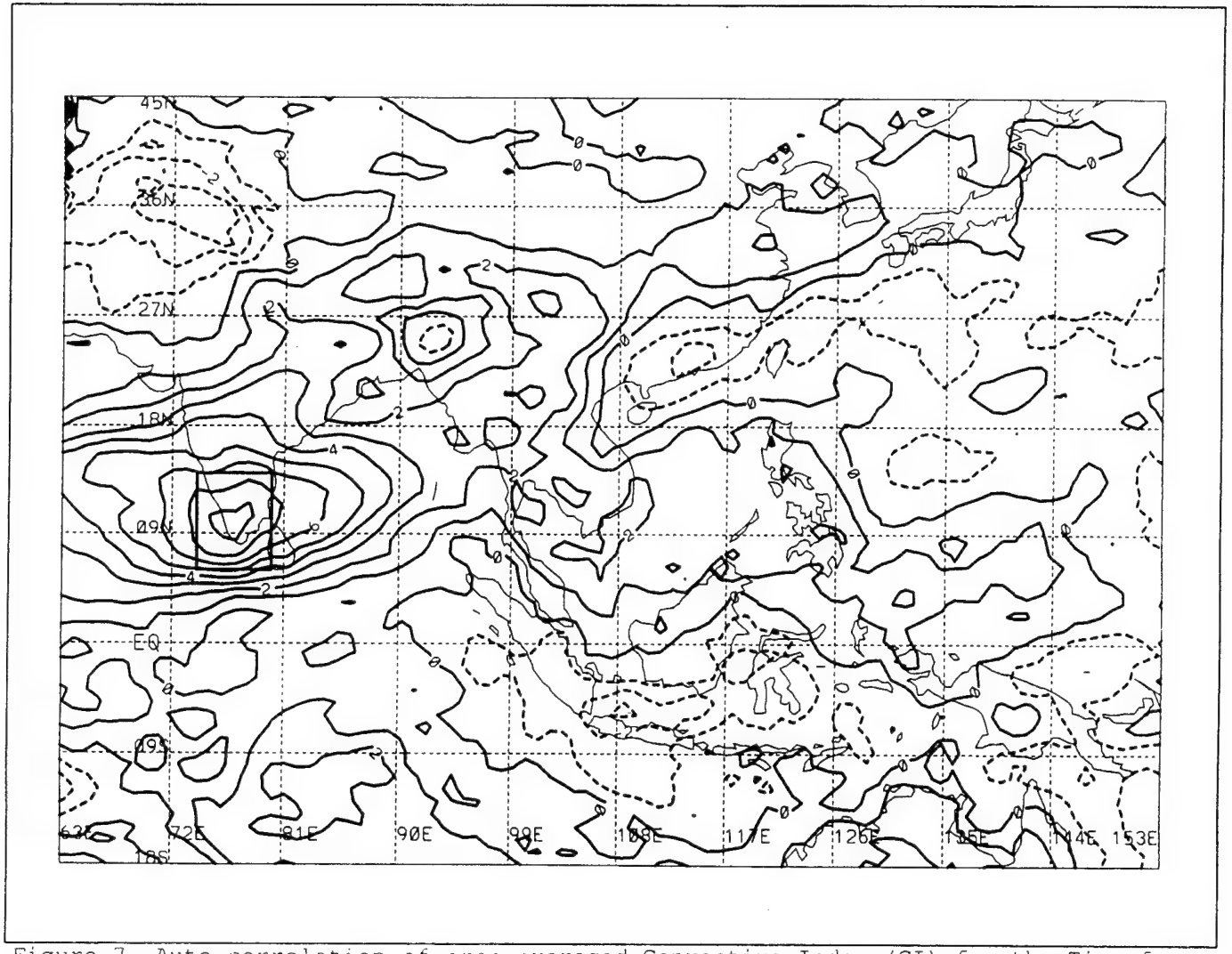

Figure 7. Auto-correlation of area-averaged Convective Index (CI) for the Tip of India (TI) with CI for the entire domain. Values greater than zero represent positive correlation, while values less than zero represent negative correlation.

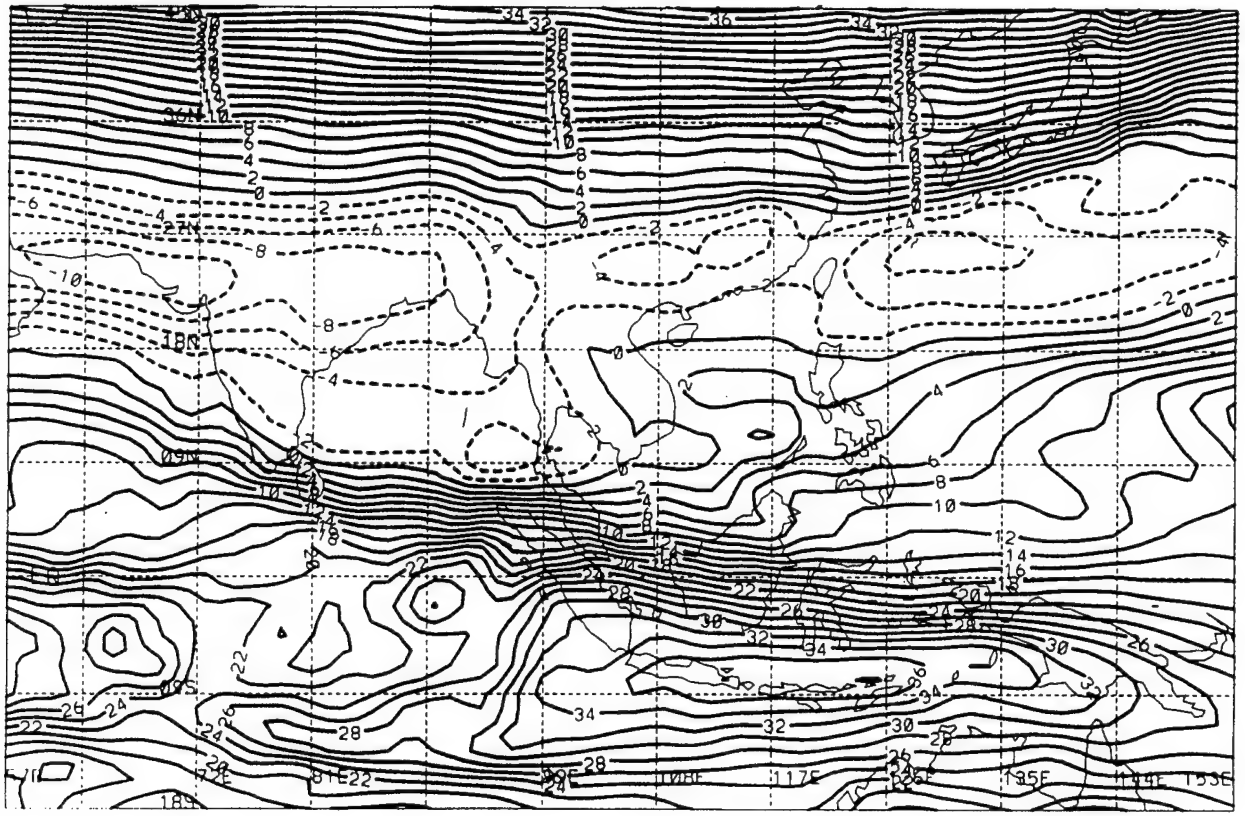

Figure 8. Average Vertical Wind Shear (U_{850} - U_{200}) for May, 1991 (m/s). Zonal component only.

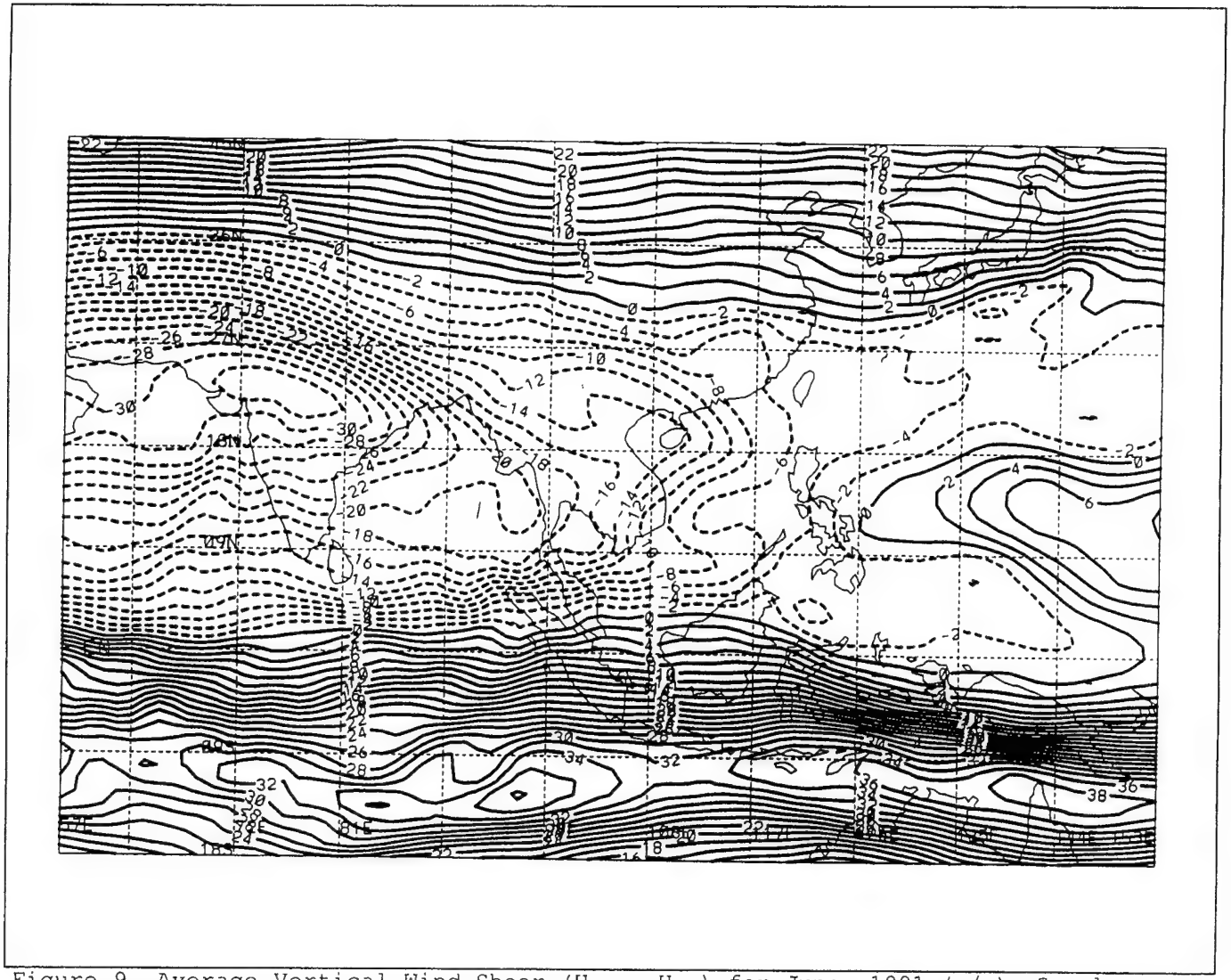

Figure 9. Average Vertical Wind Shear (U_{850} - U_{200}) for June, 1991 (m/s). Zonal component only.

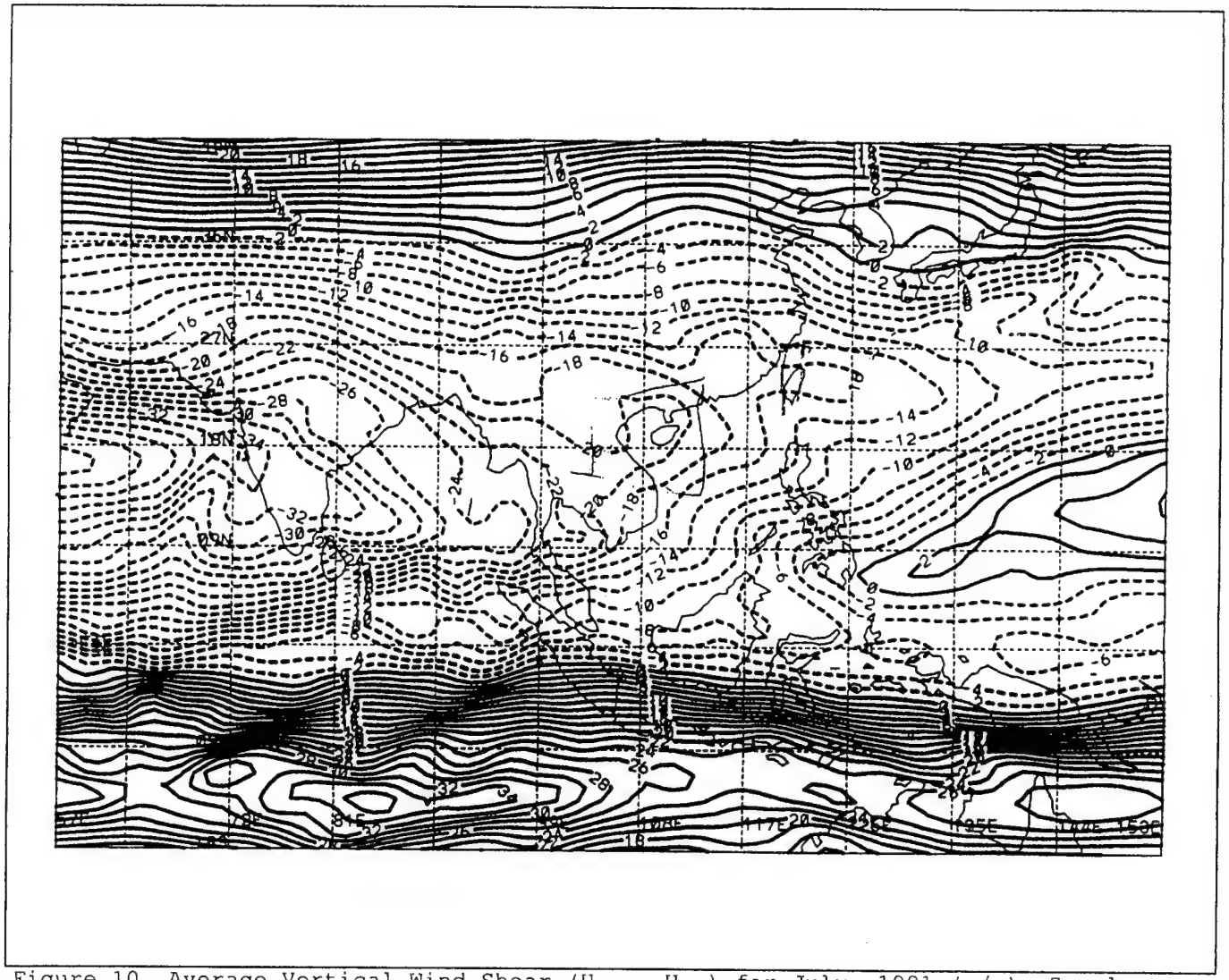

Figure 10. Average Vertical Wind Shear (U_{850} - U_{200}) for July, 1991 (m/s). Zonal component only.

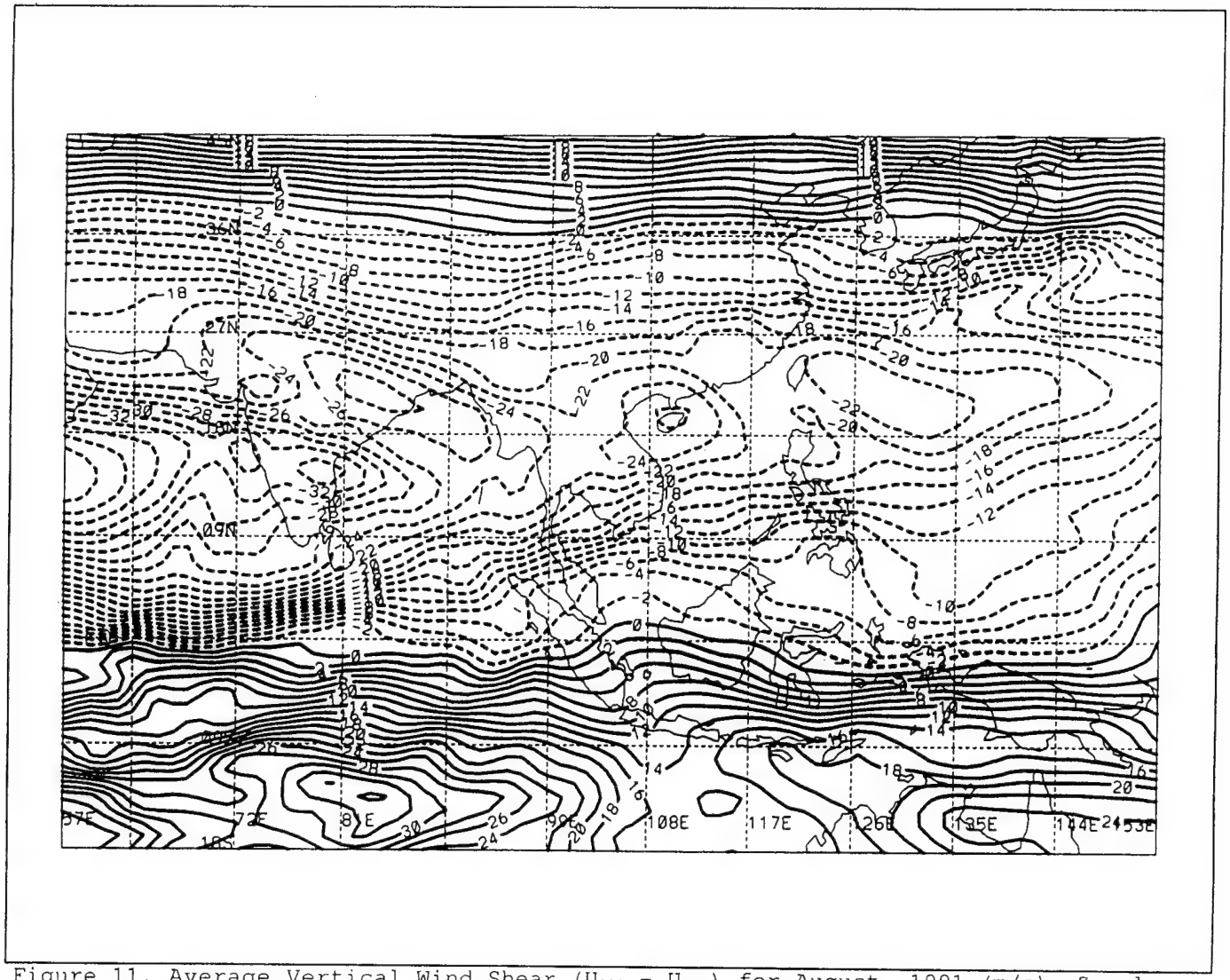

Figure 11. Average Vertical Wind Shear (U_{850} - U_{200}) for August, 1991 (m/s). Zonal component only.

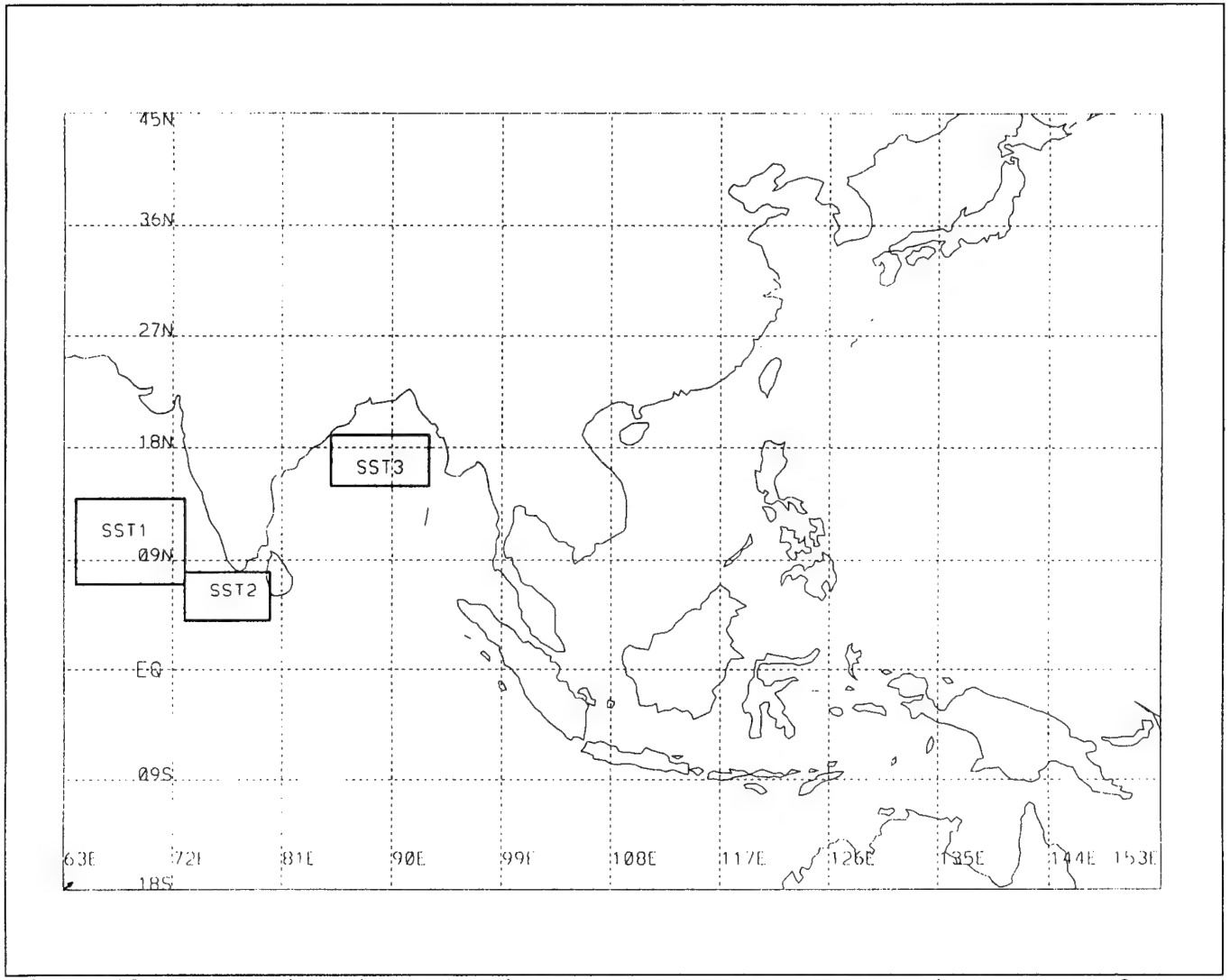

Figure 12. Area Designations. Boxed areas represent area-averaged parameters for over water areas SST1, SST2, and SST3.

III. RESULTS

A. OVERVIEW OF THE 1991 NORTHERN SUMMER MONSOON OVER INDIAN OCEAN REGION

1. Upper Level Winds (200 hPa)

During the northern winter, a pair of upper level, climatological anticyclones is located on the poleward sides of the low level, equatorial convergence zone (Krishnamurti and Surgi, 1987). This is the result of deep convection and latent heat release near the equator, where the Coriolis effect is near zero. During the northern spring, the maximum convection region extends to the Indochina Peninsula, with the resultant upper level anticyclone centered near the Malay Peninsula. In early May, the northern-most anticyclone migrates from Southeast Asia toward the Tibetan Plateau, becoming firmly established near 25°N by July. Analyses of the 200 hPa monthly mean wind fields during the northern summer monsoon of 1991 (Figures 13-16) indicates that this climatological pattern is represented well by the ECMWF wind data. In May, an upper level anticyclone is situated over Hainan, enhancing easterly flow throughout the southern South China Sea, across the Malay Peninsula, and into the southern Bay of Bengal. Associated ridging extends west-southwest from the center of the anticyclone, across the Bay of Bengal,

influencing flow as far west as the Arabian Sea. The flow over northern India and most of the Asian sub-continent is dominated by strong, nearly zonal westerly flow. Diffluent upper-level flow dominates the near-equatorial regions of the Indian Ocean, and this a characteristic feature above regions of monsoon rainfall.

By June, the anticyclone is situated just north of the Bay of Bengal, enhancing strong easterly flow throughout the Indian Ocean, extending east across the Malay Peninsula. An upper level easterly jet maximum forms across the southern tip of India, clearly situated over area SI in Figure 5.

In July and August, the anticyclone has strengthened significantly and migrated north to the Tibetan Plateau. A continuous subtropical ridge emanates zonally from this anticyclone outward along 30°N to the boundaries of our domain. By this time, the upper level easterly flow dominates the entire tropical region from 10°S northward to approximately 27°N. The aforementioned upper level easterly jet maximum has strengthened as well, and the jet axis has migrated zonally to include the Bay of Bengal, Malay Peninsula, and the South China Sea.

2. Low Level Winds (850 hPa)

The average 850 hPa winds for May (Figure 17) shows a weak low level trough extending south from the southern

foothills of the Tibetan Plateau to the southern tip of India. Here the 850 hPa wind represents the surface wind over the mountain plateau regions. During the summer monsoon months, the thermal equator and the Inter-tropical Convergence Zone (ITCZ) are displaced to about 27°N near northern India. The ECMWF data appear to indicate this manifestation in May, with two areas of convergent wind located at 26°N, 86°E and 28°N, 100°E, respectively. Thus, winds along the west coast of India are generally from the north-northwest, further enhanced by a weak anticyclone over the Arabian Sea. Winds on the east coast of India exhibit cyclonic turning in most areas, and are predominately south-southwest. An anticyclone, centered on the equator at 90°E, ridges west and enhances moderate cross equatorial south westerlies.

By June (Figure 18), the strong southwesterly flow clearly dominates the Bay of Bengal, extending south to the equator. The anticyclone noted previously at 90°E has expanded zonally and meridionally into a strong sub-equatorial ridge, extending eastward to Sumatra and southwest across the equator toward Madagascar. Similarly, the ITCZ south of the Tibetan Plateau has expanded toward the southeast across northern Thailand, enhancing southwesterly flow in the South China Sea. Flow across India has significantly strengthened, backing from west-northwest to west-southwest, exceeding 8 m/s

across the whole region from the Arabian Sea to southern Asia. The summer monsoon now completely dominates the northern hemisphere.

In July and August (Figures 19 and 20), the only discernable change in low level winds from June occurs near the equator, where the near-equatorial ridge is represented by the ECMWF data as a near continuous ridge line. We would expect the strongest anticyclonic flow to occur near Madagascar and the southern tip of Africa, as this has been observed climatologically in many studies (e.g., Krishnamurti, 1971; Ananthakrishnan, 1970; Findlater, 1969). It is not known whether the lack of low level observations may account for the near zonal easterly winds represented by the model south of the equator.

3. Tropical Cyclone Activity

Of the four tropical disturbances developing in the northern Indian Ocean in 1991 (Figure 21), only two (Figures 22 and 23) had any direct or indirect influence on the northern summer monsoon. Tropical Cyclone 02B (TC 02B) developed on April 22, 1991, near 10°N, 92°E, in the southern Bay of Bengal, reaching Typhoon strength by 0000Z on April 27. Following a north-northeasterly track through the central Bay of Bengal, TC 02B reached super typhoon strength (maximum sustained winds of 130 knots or greater) by 0600Z on April 29,

making landfall thirty nautical miles south of Chitagong approximately 2100Z that same day. Over the next twenty four hours, TC 02B weakened rapidly as it experienced significant shear passing across Indochina.

For the purposes of our study, TC 02B had only an indirect impact, as the residual storm remnants continued to influence convective activity and wind fields over Burma and Indochina well into the first week of May. TC 02B was also the deadliest and most destructive natural disaster of 1991, devastating the coastal city of Chittagong, with an estimated death toll of over 138,000 and damage at US$1.5 billion.

TC 03B began to develop on May 29,1991, at 13°N, 92°E. Although a poorly organized low-level circulation, over the next thirty hours it gradually intensified and tracked westward. A much smaller storm than TC 02B, it recurved to the north-northeast by 1200Z on May 31, and followed almost an identical track as 02B. TC 03B made landfall midway between Dacca and Chittagong on the coast of Bangladesh at 0400Z on June 2, with maximum sustained winds of 50 knots. It rapidly weakened over mountainous terrain inland and was completely dissipated by 1800Z on June 2, accompanied by torrential rains and extensive flooding.

TC 03B had a direct impact on the northern Bay of Bengal area (NB), as the storm actually passed through eastern edge

of the area, enhancing convection toward the end of May and beginning of June. Because of its relatively small size and intensity, however, the storm had little impact on the mean wind fields. Additionally, the time of occurrence of this storm was near the time of the transition or onset event, but there is no evidence suggesting that the storm itself played any role in the transition.

4. Convection and Thermodynamic Response

The average convective index for May (Figure 1) shows that the majority of significant convection is isolated along the equator, in the latitudinal band between 9°S and 9°N. Values of CI seldom exceed 2°K, except over the land-dominated regions of Indonesia, Borneo, and the Malay Peninsula, where average values were generally 4-6°K.

Over India, significant convective activity occurs only along the southwest tip (with values of CI ranging from 2-4°K), and this is predominately due to the normal thunderstorm activity that occurs during May in this region annually (Yasunari, 1979).

The impact of TC 02B and TC 03B can be clearly seen over Bangladesh, where average CI values ranged from 2°K to a maximum of 11°K. TC 02B was only present over land during May, hence the lower values of CI over the Bay of Bengal. Moreover, TC 03B was a weak, cyclonic circulation during most

of its track through the Bay of Bengal, only developing significant convection and tropical storm intensity just prior to landfall.

The monthly mean horizontal moisture flux at 850 hPa during the northern summer monsoon is represented in Figures 24-27. During May (Figure 24), mean horizontal moisture flux was nearly constant throughout the northern Indian Ocean, exhibiting moderate convergence near the southern tip of India. The largest values in the northern Indian Ocean occurred in the northern Bay of Bengal, which ranged from 60 to 80 g/kg m/s, and this is probably due to the tropical storm activity noted previously. Because the low level winds in May throughout the Indian Ocean are relatively weak, horizontal moisture flux can be expected to contribute only sporadically to significant convective events.

In June, we expect that the higher average values of CI (Figure 2) in the northern Bay of Bengal to have some, albeit small, contribution from the remnants of TC 03B. However, one key contributor of the convection is associated with the movement of the monsoon trough away from the equator. The highest average convective indices occur in the northern Bay of Bengal and southwest of India, often exceeding 12 °K for a considerable area.

This corresponds to an increase in mean horizontal

moisture flux from May to June, as indicated in Figure 25. Values of horizontal moisture flux in parts of the Bay of Bengal and the Arabian Sea nearly tripled, ranging from 150 to 205 g/kg m/s. The largest increase in horizontal moisture flux occurred in those areas where we experienced the largest increase in CI, namely the southwest tip of India and the northern Bay of Bengal. The directional component of the horizontal moisture flux suggests a direct link between the low level moisture flux and convection in these areas, and this will be explored in more detail later in this study.

During July, the average CI (Figure 3) has increased over northern India and the Tibetan Plateau, whereas values near the tip of India and the Bay of Bengal have actually decreased. This suggests a partial re-distribution of convection to the north, where the monsoon trough is now firmly established. The highest values of CI still exist in the Bay of Bengal (values exceeding 10°K persist throughout much of the northern and eastern portions), but a local maximum is now observed over northern India, as well.

The mean horizontal moisture flux for July (figure 26) reveals that surface moisture flux has again increased, following the strongest low level winds in the Arabian Sea and Bay of Bengal. The highest values (in excess of 240 g/kg m/s) are located off the northern west coast of India, pumping

moisture toward northern India. Similarly, the magnitude of horizontal moisture flux in the Bay of Bengal ranges from 210 to 230 g/kg m/s, converging near the central basin and western shores of the Malay Peninsula. Thus, higher values of low level moisture flux again appears to align with higher values of CI.

Finally, in August (Figure 4), average higher values of CI are concentrated in the eastern Bay of Bengal, extending northward to encompass the entire Tibetan Plateau. Little significant convection remains along the northern west coast of India, although the southern coastal region is still experiencing convective flare-ups. Even in the more convective regions, the values of CI have dropped, topping out at 10 °K in only a few areas.

The magnitude of mean horizontal moisture flux for August (Figure 27) has also decreased in all areas, particularly over the Arabian Sea, where values have dropped to below 160 g/kg m/s in all coastal regions. The Bay of Bengal also experienced a decrease, with values ranging from 170-200 g/kg m/s over much of the central and eastern bay of Bengal. The directional component of horizontal moisture flux has remained nearly the same as July, remaining west-southwesterly in the Arabian Sea, and predominately southwesterly in the Bay of Bengal.

5. Summary

a. *May*

As the land begins to heat up over India and the Tibetan Plateau in May, strong thermal low pressure begins to dominate the region, favoring low level convergence and upward vertical motion. We have observed a pattern in the mean 850 hPa wind (Figure 17) suggesting the formation of two low level cyclonic systems over the Tibetan Plateau which would seem to substantiate this. Associated troughing from the western-most cyclone dips south across India, inciting cyclonic turning of the wind pattern, particularly near the southern tip of India and Sri Lanka. In turn, this region exhibits the most significant convection north of the equator (the convection over Burma and Bangladesh notwithstanding, as the remnants of tropical cyclone activity is thought to be the main influence of higher CI in this area during May).

Mean 200 hPa upper level winds (Figure 13) over the Tibetan Plateau are westerly and nearly zonal, exhibiting little diffluence. These strong upper level winds appear to inhibit significant convection over this region. An upper level anticyclone appears to be firmly established over Hainan and Thailand, ridging west across the Bay of Bengal to the southern tip of India, providing some upper level venting for the low level convergence (hence favoring the thunderstorm

activity noted previously).

The mean vertical wind shear (Figure 8) during May is relatively weak, as the low level winds do not exhibit the strong southwesterly flow and the upper level easterly jet is not yet fully established. The maximum easterly shear over the northern Arabian Sea (-10 m/s) is not a reflection of opposing low level and upper level winds, as is the case during the post-onset period (in early June). Rather, this vertical wind shear maximum is a manifestation of stronger westerly winds at 200 hPa than at 850 hPa, as the tropical upper tropospheric easterly jet has not yet developed.

b. June

The upper level 200 hPa anticyclone (Figure 14) now appears to be vertically aligned with the low level 850 hPa thermal trough (Figure 18) over the Tibetan Plateau, providing the difluence aloft necessary to sustain significant convective activity. The upper tropospheric easterly jet is also well established across the Indian sub-continent, as are the strong low level south westerlies (Figure 18).

The upper and lower wind patterns represented by the ECMWF data suggest conditions are favorable for a Hadley-type circulation, where the meridional winds at low levels (enhanced by thermal low pressure over the Indian sub-continent) set up a synoptic scale sea breeze across India and

southern Asia. These strong southwesterly winds gather latent heat and moisture over water (as evidenced by high values of mean 850 hPa horizontal moisture flux (Figure 25)). The warm, moist air arriving over land converges and is driven upward, creating an atmosphere favorable for sustained convective activity over the whole region. The role of latent heat release from the ocean to the atmosphere is thought to be an important contributor to convective flare-ups in June, but the temperature contrast between land and sea is the main driving force of the circulation.

Upper level divergence, provided by the anticyclone aloft, is a means of venting the convective columns and returning the flow southward, as represented by the southerly meridional mean wind component observed at 200 hPa. This return flow converges and sinks south of the equator, thus completing the loop of a northern summer local Hadley circulation.

The mean vertical wind shear in June (Figure 9) reflects the onset of the northern summer monsoon, with a maximum easterly shear located over northern India of -35 m/s. Unlike May, the upper level wind at 200 hPa is easterly (strengthened by the migrating anticyclone to the north) and dominates the low level southwesterlies. As a result, the mean vertical wind shear has tripled in magnitude across India

and south Asia, and the dominating influence of the tropical upper tropospheric jet is noted as far east as the western Pacific.

c. July

The 200 hPa anticyclone (Figure 15) situated over the Tibetan Plateau has moved a couple of degrees further north from its mean June position and strengthened considerably. This feature now dominates all of Asia, extending as far east as the East China Sea. The strongest low level winds during the northern summer monsoon are represented in the mean 850 hPa wind field (Figure 19) over the Bay of Bengal and the Arabian Sea, where mean values of greater than 12 m/s dominate most of pattern.

Significant convection (Figure 3) accompany the movement of the ITCZ north, with the greatest convection located over northern India, the Tibetan Plateau, and the Bay of Bengal.

The average vertical wind shear for July (Figure 10) shows that a local easterly maximum of -33 m/s has moved south from its June position, and the absolute easterly maximum is located over the western Arabian Sea (not shown). Thus, the southern tip of India is now directly underneath the tropical upper tropospheric easterly jet.

d. August

The average 200 hPa and 850 hPa winds (Figures 16 and 20, respectively) show little change in pattern from those in July. The upper level easterlies over northern India and the northern Bay of Bengal (near area NB) have strengthened somewhat, while the low level south westerlies have increased an average 4 m/s. A consequence of these enhanced winds is the formation of a second local maximum in the average vertical wind shear pattern for August (Figure 11). As a result, both the southern tip of India (area TI) and the northern Bay of Bengal (area NB) experience local easterly maximum vertical wind shear simultaneously. We will revisit this phenomenon later in this study.

B. ONSET OF THE 1991 NORTHERN SUMMER MONSOON

The mean monthly 200 hPa and 850 hPa wind fields for May (Figures 13 and 17) and June (Figures 14 and 18) have been shown to exhibit remarkably different characteristics. The well defined upper tropospheric easterly jet present in June is nonexistent in May. Further, the weak and somewhat variable low level winds of May have been replaced by organized and significantly stronger west-southwesterly winds that dominate the entire northern Indian Ocean in June. The contemplation of the possible effects of the local Hadley circulation and possible vertical momentum transfer due to

convection (the key foci of this study) requires that the transition or onset of the northern summer monsoon be identified. We may expect different results during the pre-onset and post-onset periods; and it is the post-onset period (namely, the months of June, July, and August) during which many of the meteorological and oceanographic parameters exhibit those attributes conducive to further analyses. Specifically, the strong vertical shear and the upper tropospheric easterly jet (present in these latter months) are the phenomena in which we are interested.

From the studies conducted by Krishnamurti (1971) and Murakami (1984), we would expect to see a weak low level cyclone or "onset vortex" form near the southern tip of India that acts as a catalyst to initiate the monsoonal wind pattern over the Indian Ocean region. The land-sea temperature contrast would than act to sustain the synoptic scale sea breeze that is the northern summer monsoon. As the low level winds increase and converge toward the thermal low pressure of the land masses, the oceanic response would be a lowering of the sea surface temperature and an increase in vertical latent heat flux from the ocean to the atmosphere (Pishnaroty, 1965 and 1981) as discussed previously. Increased low level winds and latent heat transfer would increase the horizontal moisture flux which, in turn, would be favorable to convective

activity.

The two main objectives of this portion of our study are 1) to see if the three independent data sets used are of sufficient quality to observe the transition event; and if so, 2) to identify the transition event temporally to distinguish the pre-onset and post-onset regimes, which are deemed pertinent to the subsequent study of the local Hadley circulation and vertical momentum transfer due to convection.

1. Low Level Moisture Flux

The mean weekly 850 hPa horizontal moisture flux for the week May 15-22, 1991, is shown in Figure 28. Two low level anticyclones dominate the Bay of Bengal and the Arabian Sea. Over Sri Lanka and the southern tip of India, an area of convergent moisture flux and cyclonic turning are induced between the anticyclones, drawing moisture northward from the equatorial region. Maximum values of horizontal moisture flux are 60-70 g/kg m/s over these northern waters, while values along the northern equatorial region are 20-40 g/kg m/s. From our previous discussion, this clearly represents a pre-onset stage, as the low level moisture flux is comparatively weak (to those observed in June) and do not exhibit the traditional west-southwesterly alignment associated with the northern summer monsoon.

By the following week (May 23-29, 1991; Figure 29), the

anticyclone over the Arabian Sea has moved approximately 300 nautical miles to the west. The anticyclone over the Bay of Bengal has subsequently weakened to become a narrow ridge line. Consequently, the low level cyclone over southern India and Sri Lanka has expanded, as the anticyclone and ridge move apart. South of the cyclone, the horizontal moisture flux has dramatically increased in the near-equatorial zone (from the equator to 9°N), with values now ranging between 120-160 g/kg m/s. The alignment of the vectors in this region are now west-southwesterly, suggestive of the beginning of the onset mechanism detailed by Krishnamurti (1971).

During the week of May 30-June 5, 1991, the ridge line previously over the Bay of Bengal has receded toward the east (Figure 30), merging with the subtropical ridge extending across the Indochina Peninsula. The cyclone over southern India now influences flow across the central basin of both the Bay of Bengal and the Arabian sea, while extending north across central India. As the cyclone begins to move north, the horizontal moisture flux to the south and southeast experiences a surge of cross equatorial flow, with values now ranging between 160-220 g/kg m/s. A noticeable southwesterly alignment of the wind extends north to the central Bay of Bengal, becoming due southerly in the northern portion.

By the second week of June (June 6-12, 1991), the low

level cyclone has moved over the central portion of northern India (Figure 31), and the horizontal moisture flux at 850 hPa veers from northwesterly in the north Arabian Sea to westerly across southern India. The pattern shifts to southwesterly across the entire Bay of Bengal, which also exhibits the highest flux magnitude (210-240 g/kg m/s). The transition is nearly complete.

Finally, during the following week (June 13-18, 1991) the mean horizontal moisture flux (Figure 32) exhibits the same relative pattern we observe in the monthly mean moisture flux profiles of June, July, and August (Figures 25, 26, and 27, respectively). The low level anticyclone has been absorbed by the monsoon trough situated over the Tibetan Plateau, signaling an end to the onset event.

Thus, it appears that the ECMWF data (specifically, the temperature, relative humidity, and wind profiles represented in the calculated horizontal moisture flux at 850 hPa) supports the findings of Krishnamurti (1971) and Murakami (1984) mentioned previously. In 1991, the monsoon development process represented in the ECMWF data takes about four weeks (from May 22 to June 18) to effect the complete transition to the northern summer monsoon over the entire northern Indian Ocean and south Asian regions. Over India and the Bay of Bengal, the onset itself occurred during the week of May 30-

June 5.

2. Convection

Previous studies by Pishnaroty (1965 and 1981) indicated that a positive correlation between convergent low level moisture flux and significant convective activity exists during the northern summer monsoon over the Indian Ocean. A natural extension of his analytical techniques would be to compare convective activity and low level moisture flux during the transition event, as the dynamic and thermodynamic processes are quite similar. In this section, we compare the mean weekly convective index (CI) during the five week period from May 15 to June 18, 1991, to the mean weekly horizontal moisture flux at 850 hPa discussed in the previous section, to see if the two independent data sources corroborate one another.

The mean convective index for the week of May 15-22, 1991, is shown in Figure 33. The induced low level circulation over Sri Lanka and southern India (Figure 28) appears to be located in the area of significant convection across southwest India, extending south and east, to include the equator. The monsoon trough is located in this equatorial region, extending east and west to the periphery of our domain. It is also worth noting that the two anticyclones over the Arabian Sea and Bay of Bengal are areas where there

is little significant convection. The higher convective indices landward of the northern Bay of Bengal is thought to be residual tropical storm activity, and not specifically related to the processes responsible for convection in other areas.

By the following week (May 22-29, 1991), the average convective index has increased considerably (Figure 34) along the equatorial region, extending north into southwest and central India. As the anticyclone over the Arabian Sea (Figure 29) recedes towards the west, moisture flux values to the north increase, feeding into the cyclone over southern India. The noticeable surge in moisture flux north of the equator to approximately 9°N corresponds to the increased convective indices in the same area (where values have increased, on the average, by 2-4 °K over the previous week). An area of convergent moisture flux over the Malay Peninsula exhibits elevated average convective indices over the previous week, while the northern Bay of Bengal (still under the influence of a weakened ridge) shows little significant convection.

Average values of CI during the third week (May 29-June 5, 1991) exhibit the most prolific increase noted throughout the four month period of our study (Figure 35). Average convective indices in excess of 10 °K extend from the southern

Arabian Sea, across southern India, and into the northern Bay of Bengal. This corresponds well with the moisture flux increase (Figure 30) over the entire region, as the cyclone over southern India begins to dominate. We observe the highest values of CI in those areas of convergent average moisture flux, namely the equatorial region southwest of India (where values of CI reach a maximum 27 °K) and the southern Bay of Bengal.

By the week of June 6-12, 1991, a compelling change again occurs from the previous week: the significant convection (values of CI greater than zero) near the equator has all but disappeared (Figure 36). The average moisture flux pattern (Figure 31) has significantly changed also, as the cyclone previously over southern India has moved 15° north. Thus, a surge of convergent moisture flux is observed near the central west coast of India, as well as the entire Bay of Bengal. We observe maximum convective indices of 24-26 °K concentrated in those areas of strongest average moisture flux and demonstrated convergent conditions. The overall pattern of convective activity has shifted away from the equator, suggestive of the movement of the ITCZ away from the equator to a position further north (as described by Murakami, 1984).

During the final week of the transition event (June 13-18, 1991), the low level cyclone is absorbed into the flow

pattern over the Tibetan Plateau (Figure 32), and a weakening of the average moisture flux over the central and north Arabian Sea is observed. The flow pattern is much less convergent in this region. The average convective index appears to reflect this change (Figure 37), as significant convection near the central and northern west coast of India has disappeared. Convergent average moisture flux now exists over southern India, extending northwesterly into and across the Bay of Bengal. Once again, we observe the most significant convection in the areas of strongest and most convergent low level moisture flux.

3. Oceanic Response

From the studies by Cornejo-Garrido and Stone (1977), and by Pishnaroty (1981), the sea surface temperature and vertical latent heat flux should respond to the onset of the northern summer monsoon. Increased low level winds (such as those observed previously during and after the transition) and northward movement of significant convective activity (as observed in the preceding section) can reasonably be expected to lower the sea surface temperature and increase the latent heat transfer from the ocean to the atmosphere.

The area-averaged sea surface temperature from May 15 to June 18, 1991, for areas SST1, SST2, and SST3 are plotted in Figure 38. The observed sea surface temperatures for SST1 and

SST2 (located west and south of the southern tip of India; Figure 12) indicate that a local maximum sea surface temperature occurs on May 22nd, just prior to the surge of near-equatorial low level moisture flux that occurs during the week of May 22-29, 1991, in Figure 29. The maximum sea surface temperature west of the southern tip of India is 31.0 °C (SST1), while the maximum to the south (SST2) is 30.2 °C. For the area over the northern Bay of Bengal (SST3), the maximum sea surface temperature does not occur until May 28th, reaching a value of 30.4 °C.

Once the moisture flux (and associated low level winds) begin to increase during the week of May 22-29, we observe a marked decrease in sea surface temperature in both SST1 and SST2, which continues until the transition is complete. The northern Bay of Bengal (SST3) begins to decrease on approximately June 4, also continuing until the end of the transition. SST1 registers a drop of 2.1 °C during the transition. SST2 decreases 1.9 °C, while SST3 decreases only 1.3 °C.

These findings support the study conducted by Pishnaroty (1981), where he observed an average decrease of 1.5-2.0 °C throughout the northern Indian Ocean during the transition event. He attributed this decrease in sea surface temperature to increased surface cooling and latent heat release in

response to increased low level winds associated with the onset of the northern summer monsoon. The time lag between decreasing temperatures near the southern tip of India (SST1 and SST2) and those of the northern Bay of Bengal (SST3) are presumably due to the lag in the transition event reaching these northern waters. If this is true, we would expect to see a similar response in the vertical latent heat flux in these same areas.

Figure 39 represents the average vertical latent heat flux for areas SST1, SST2, and SST3 during the same five week period beginning on May 15. Negative values of latent heat flux represent a transfer of latent heat from the ocean to the atmosphere. The vertical latent heat flux for SST1 ranges between -10 and -40 W/m^2 until May 30th, when a sharp increase begins to occur. From May 30th to June 9th, the increase in vertical latent heat flux for SST1 is approximately -7 W/m^2/day, going from -25 W/m^2 at the beginning of the period to -95 W/m^2 near the end. For SST2, average vertical latent heat flux experiences a similar increase, going from -37 W/m^2 on May 27th to -93 W/m^2 on June 3rd (which again corresponds to an increase of -7 W/m^2/day). For SST3, the increase does not begin until June 2nd, starting at -20 W/m^2. By June 9th, the average vertical latent heat flux is -70 W/m^2, increasing approximately -6 W/m^2/day.

The time period of largest increase in average vertical latent heat flux corresponds roughly to the largest decrease in sea surface temperature noted in Figure 38. Additionally, a time lag between an increase the areas near the southern tip of India (SST1 and SST2) and the area near the northern Bay of Bengal is noted, again similar to the time lag observed in the sea surface temperature decrease. There is considerably more variability in the average vertical latent heat flux than there is in the sea surface temperature, as the former is a calculated quantity dependent upon sea surface temperature, air temperature, wind speed, stability, vapor pressure, and relative humidity (Equation 23). However, even given its noisy nature, the average vertical latent heat flux appears to substantiate the findings of Pishnaroty (1981), namely that the vertical latent heat flux increased measurably from the pre-onset stage to the post-onset stage.

4. Timing of the Onset

Based on our findings from the previous three sections, the development of the 1991 northern summer monsoon over the entire Indian Ocean region occurred over a four week period, beginning approximately May 22nd and ending approximately June 18th. Three data sets (INSAT-GMS high resolution satellite IR, ECMWF upper air re-analyses, and NMC sea surface temperature analyses) independently reflect changing

parameters that tend to substantiate the aforementioned previous studies in this area.

However, the time and duration of the transition event is not the same for the equatorial region and the northern Bay of Bengal. The transition begins near the equator, with increasing low level moisture flux, higher than average sea surface temperatures, lower than average vertical latent heat flux, and strong convection (compared to the northern latitude land masses).

As the land over India and south Asia heats up, inducing thermal low pressure and low level convergence, a cyclone forms near the southern tip of India. Low level moisture flux and convergent low level winds into the cyclone create an area favorable for convective activity, and this is reflected in increasing average convective indices moving slowly northward away from the equator. As the winds at the surface increase, the average vertical latent heat flux increases south of the cyclone and sea surface temperatures drop.

As the cyclone moves northward toward the Tibetan Plateau, low level winds align to the southwest and strengthen, carrying even more moisture flux away from the equatorial regions to the Indian sub-continent and the Bay of Bengal. As a consequence, convective indices continue to rise in these areas and decrease near the equator. The sea surface

temperatures near southern India continue to drop and average vertical latent heat flux continues to increase.

Approximately three weeks into the transition, the low level cyclone has reached northern India, and the associated strong southwesterly winds and low level moisture flux are observed near the northern Bay of Bengal on June 4-6 (thus accounting for the time lag in higher latent heat flux increase and sea surface temperature decrease noted in this area). Convective activity has followed this cyclone north, and little convection remains near the equator.

By the fourth (and last) week of the transition, the low level cyclone has been absorbed by the re-located monsoon trough over the Tibetan Plateau, signaling the end of the transition for the entire domain. The low level winds are now west-southwesterly over the entire Indian Ocean, the upper tropospheric jet is well established over southern India, sea surface temperatures stabilize (do not continue to decrease), and vertical latent heat flux (presumably) follows variations in wind and convection (and additional processes not the subject of these investigations).

For the purposes of our study, we are interested in the onset event as it pertains to India and the Bay of Bengal. Both the low level wind, moisture flux, and convection indices over this area indicate that the onset occurred during the

week of May 30-June 5. As will be shown in Section C, the CI time series for the northern Bay of Bengal indicates the onset occurred June 4-6.

C. EFFECTS OF MONSOON CONVECTION ON THE TROPICAL UPPER TROPOSPHERIC EASTERLY JET

1. Introduction

The large scale monsoon circulation during the northern summer derives its main energy from the vigorous cumulus convection in South Asia. One of the most energetic motion components of this circulation is the tropical upper tropospheric easterly jet. The jet normally occupies the northern equatorial region and encompasses nearly two thirds of the longitudinal extent of the tropics (Krishnamurti and Surgi, 1987). The jet axis is centered between 10°N-15°N with the maximum speed zone occurring near southern India. The 1991 jet maximum is close to this normal location, as shown in Figures 14-16.

The jet maximum is situated to the south of the monsoon trough/ITCZ over the northern India - Bay of Bengal region where the center of cumulus convection is located. It is well recognized that the strength of the upper easterly jet depends on the strength of this monsoon convection (Krishnamurti, 1971). In fact, this relationship was the basis of Webster and Yanng's (1992) design of a monsoon index that is given by

the vertical shear between 200 hPa and 850 hPa. Their use of this convective index showed that this vertical shear is a good representation of the strength of the monsoon in the monthly, seasonal, and inter-annual time scales. As described in the introduction, we are interested in whether the synoptic time scale fluctuations of the northern summer monsoon convection center exert influences in the strength of the upper level easterly jet. Two possible effects of the synoptic time scale fluctuations are considered in this study. The first is the forcing of the easterly jet through the upper branch southward outflow of the local Hadley cell. The second is the cumulus transport of momentum from the low-level southwesterlies to the upper troposphere where the jet may be damped.

2. Forcing of the Upper Tropospheric Easterly Jet by Synoptic Time Scale Fluctuations of Monsoon Convection

During the northern winter monsoon the upper branch of the local Hadley cell causes an acceleration of the subtropical westerly jet on the synoptic time scale. The local Hadley cell fluctuations are directly related to the fluctuations in the tropical convection with the rising branch of the former caused by the latter. As a result, the strength of the subtropical westerly jet increases when the tropical convection increases. If a similar process is working during

the northern summer, then it may be expected that the strength of the tropical upper easterly jet may increase with enhanced convection midway through the summer monsoon. This is because the enhanced convection would give rise to enhanced upward branch of the summer local Hadley cell over South Asia. The upper branch of the cell will accelerate southward and cross the equator into the Southern Hemisphere. Since the strengthening of the southward divergent flow occurs in the region of the easterly jet maximum, the strengthening may cause a Coriolis torque to accelerate the jet.

To study this possibility, we will compare the time variations of the monsoon convection in the NB region and those of the upper level easterly jet strength. Figure 40 compares the time series of the u component at 200 hPa (U_{200}) that is area-averaged in the jet maximum region over southern India (SI) and that of the convective index over northern Bay of Bengal (NB) during May 1991. In general, there is no clear phase relationship between the two time series in this month when the monsoon has not started. Figure 41 compares the SI U_{200} time series and the NB convective index during June 1991. As discussed previously, the first increase of NB convection at the beginning of June is due partially to tropical cyclone 03B, but is mainly due the onset of the summer monsoon which occurs approximately June 4-5. Figure 41 shows that after

this onset the two time series began to show an out of phase tendency for most of the month. The only noted exception is near the end of the month after 24 June.

An out of phase relationship between U_{200} and CI indicates that the easterly jet strengthens when the convection index increases. The first flare up of convection occurred from June 4 to June 6 when the CI went from 0°K to a rather high peak value of 28°K. A strengthening of the easterly jet by a factor of almost three, from -4 to -11 m/s, was observed during this period. It is important to keep in mind that these are area-average indexes so that such changes are not negligible. After the monsoon onset in early June the CI also showed a clearly discernible diurnal cycle. Strong diurnal cycles in the convection index in the vicinity of the Tibetan Plateau has been reported previously by Murakami (1984), Nitta (1983), and others. After this first event, the CI had its largest increase for the entire summer 1991. It reached a peak value of 40°K in late June 9 and maintained high values for more than a week, with the exception of a temporary dip on June 12. In the meantime, the U_{200} series showed a sustained acceleration trend from -4 m/s on June 7 to -23 m/s on June 14. The area-average easterly wind speed exceeded -15 m/s most of the time during June 12-16. After June 16 the easterly speed relaxed back to less than -9 m/s on June 18.

This corresponds to a rapid decrease of CI from 11°K on June 17 to near 0°K on June 18.

Between June 18 and June 23 the easterly wind speed accelerated again, from -10 m/s to -24 m/s. The CI was 0°K during this period, hence the acceleration cannot be attributed to the NB convection, although between June 21-23 the CI showed a clear increase from 0°K to 20°K. This is followed by a rapid decrease of the easterly wind speed from June 23 to June 24 and a slowing down of the deceleration between June 24-26. A corresponding rapid decrease of the NB convective index also occurred from June 23 to June 24. As noted above, the last week of June is the exception where there was actually an in-phase relationship between the NB convective index and the SI U_{200}.

Overall, the June 1991 data in Figure 41 shows that the 200 hPa easterly jet speed contains a synoptic time scale fluctuation that is mostly in phase with the convective index over NB. This is consistent with the hypothesis that the upper easterly jet may be accelerated by enhanced monsoon convection to the north of the jet.

Figure 42 compares the time series of U_{200} area-averaged velocity over SI with that of the convective index over NB during July 1991. Here the general out of phase relationship between the two time series can again be observed for most of

the month. The only exception with an in-phase relationship also occurred near the end of the month centered around July 27. During July 1991 the CI over NB had two significant synoptic time scale flare-ups, each lasting a week or more. The first event covered the first seven or eight days of July, with the CI rising from near 0°K on July 1 to 20°K at 0600Z July 3, then falling to near 0°K again between July 8-9. This change in CI corresponded to a strengthening of the easterly wind speed from -11 m/s at 0000Z July 1 to -28 m/s at 1800Z July 3, and a deceleration in two stages from July 3 to July 9. The second general period of flare up of CI occurred between July 16 and July 22. This corresponded to a general high speed period of the easterly winds starting from July 16 and ending around July 23. In addition, there is also some suggestion of a correspondence between the two indexes between July 13-15, when a wind speed spike seemed to correspond to a small increase of CI over this period. This aspect cannot be ascertained due to the missing INSAT TBB data between June 15-16.

Figure 43 compares the time series of U_{200} area-averaged velocity over SI and that of the convective index over NB during August 1991. This diagram showed the best correspondence of the two time series in their out of phase relationship. This is also the month when the northern summer

monsoon was at its fullest and the upper tropospheric easterly jet was well established over south Asia. Five synoptic events of convective flare-up occurred with the peak CI value reaching above 15°K. They are: August 1-5, 9-12, 12-18, 20-21 and 24-28. With the exception of August 20-21, the other four events all corresponded to increased easterly wind speed events. However, the exact phase difference between the peaks in the two series cannot be consistently determined. This is probably because of the uncertainty involved in choosing the designated areas for area-averaging and the nature of the area averaging, as well as the fact that variations in the convective index and the easterly jet are complex and involve many factors.

In summary, the above results show that after the onset of the summer monsoon, the fluctuations of the easterly jet on the synoptic time scale are mostly in phase with those of the intensity of cumulus convection in the monsoon trough region. Thus, it appears that in both northern winter and northern summer monsoon regimes, the monsoon convection exerts an influence in the upper tropospheric jet that is downstream from the meridional outflow of the local Hadley cell through the Coriolis torque of the outflow. This influence results in an acceleration of the jet when the convection flares up.

3. Effects of Cumulus Momentum Transport on the Upper Tropospheric Easterly Jet

For a warm-core motion system the upper and lower level winds normally oppose each other and, in such a case, the vertical transport of momentum by cumulus convection is always a damping mechanism to the large scale circulation. The most well known example of this process occurs in tropical cyclones, where the transport by eyewall clouds is the main cause of the reduction of the vertical shear at the radius of maximum wind (Gray, 1979). The possibility of this mechanism operating in the northern summer monsoon was first raised by Holton and Colton (1972), who thought that the cumulus vertical transport mechanism was important in damping the generation of large-scale vorticity by divergence (which is itself a result of strong cumulus convection). This damping mechanism appears to be required to balance the 200 hPa vorticity budget of the summer monsoon analyzed by Krishnamurti (1971).

To examine the possibility of cumulus momentum transport as a damping mechanism, we will compare the time series of vertical zonal wind shear and the convective index at the southern tip of India (TI) area. This is not the center of the monsoon convection but it is near the region of the maximum velocity of the upper easterly jet and therefore

maximum vertical shear. It is also one of the most active convection areas, thereby affording the best opportunity of detecting the possible cumulus momentum damping. In Figures 44-47, the time series of the vertical shear of the zonal wind are compared with those of the convective index at TI. If cumulus damping is important, we expect to see strong convection associated with weak vertical shear and vice-versa. After the onset of the northern summer monsoon, the zonal wind is easterly at 200 hPa and westerly at 850 hPa. If we choose the normal vertical shear index (Webster and Yang, 1992) of $U_{200}-U_{850}$, the values will normally be negative. Plotting such values in units of m/s together with the positive values of CI will require a large range of the vertical coordinate. We therefore decide to plot the vertical shear defined by $U_{850}-U_{200}$, since these are normally positive values. In Figures 44-47, if the two time series appear out of phase it means that smaller values vertical shear correspond to higher values of CI, thereby supporting the theory that cumulus transports momentum to damp the large scale shear.

It may be argued that sometimes the deep cumulus convection itself may be affected by strong vertical shear, in that the vertical shear may "ventilate" the released latent heat causing the large-scale motion system supported by the cumulus heating to be less organized. This typically occurs

in tropical cyclones where the presence of strong vertical shear is unfavorable for tropical cyclone development. Therefore the cause-effect relationship between convection and vertical shear (when the two are out of phase) may not be easily deduced. However, in tropical cyclones this effect is present only in the center within the radius of the maximum wind, which is typically less than 100 km. In the present study the CI and the vertical shear are both averaged over a much larger area. Furthermore, this area (TI) still represents only a small fraction of the planetary scale monsoon circulation system, unlike the tropical cyclone example in which the eyewall convection and the maximum winds represent the major portion of the energy interactions for the entire system.

Figure 44 is the comparison for May 1991, before the monsoon onset. The fluctuations of both CI and vertical shear are small and no clear relationship is discernable. Figure 45 shows the comparison for June. Here a general out of phase relationship is seen, dominated by the events in the first 11 days of the month. The CI was at relative high values of above 10°K between June 2-4 (peak value of 30°K on July 3) when the vertical shear was relatively small (less than 20 m/s). As the CI declined from June 4 to June 11, the vertical shear showed a general increasing trend, reaching its maximum

of 42 m/s at 0000Z June 12. Additional patterns of weakened vertical shear associated with peak CI may be seen on June 14, 18, and 24-26; these patterns are less clearly defined and somewhat ambiguous (particularly for the last event). This is the first month after the monsoon onset and the vertical shear over TI averaged around 25 m/s.

Figure 46 shows the comparison for July, when the monsoon is more fully established and the vertical shear averages around 35 m/s. Here the out of phase relationship can be better seen throughout the entire month. The relationship becomes somewhat less clear in August (Figure 47). The convection over TI was active only during the first half of August, and the phase between CI and the vertical shear is more likely one quarter cycle out of phase than totally out of phase.

Another way to examine the possible cumulus damping mechanism on the upper easterly jet is a direct comparison of CI and the co-located zonal wind. The comparison for area TI for the four summer months are shown in Figures 48-51. Here a damping of U_{200} by cumulus convection will show up in the figures as an in-phase relationship (higher CI value, which is always positive, and lower negative U_{200} value). The May, 1991 results (Figure 48) again show no discernable pattern, as the monsoon has not started. The U_{200} was weak and variable

throughout the month. After mid-June (Figure 49) when the upper easterly jet developed an average speed exceeding -10 m/s, the in-phase relationship between U_{200} and CI began to emerge. The relationship was not clear during the first half of July (Figure 50), but was quite clear during the latter part of July and in the first half of August (Figure 51) when significant CI fluctuations occurred.

To summarize the comparisons shown in Figures 43-51 that cover the southern tip of India, there is some evidence of a reduced vertical shear or reduced U_{200} at the location of the jet maximum (area SI) when the convective index increases. This relationship was seen over 70% of the time after the monsoon onset, when convection was active over TI. The vertical zonal wind shear shown in Figure 11 shows the development of a second local jet maximum in northeast India and the northern Bay of Bengal in August 1991 that is not present during the preceding months. This second maximum in August provides another area to examine the possible damping mechanism due to cumulus momentum transport. In Figures 52-55 the time series of CI and vertical shear (U_{850}-U_{200}) are compared for all four months. Again, an out of phase relationship in these diagrams would indicate that weak shear is associated with strong convection and vice-versa. The May (Figure 52) and June (Figure 53) results do not show any clear

phase relationship. This was also true for most of July (Figure 54). However, for the last ten days of July a weak indication of an out of phase relationship is detected. This is close to the time of development of the secondary jet maximum developed over the northern Bay of Bengal. In August (Figure 55) the relationship becomes rather clear, with a strong indication of an out of phase relationship between the two time series. Thus, the evidence over the northern Bay of Bengal again supports the existence of a damping mechanism due to the transport of momentum by cumulus convection.

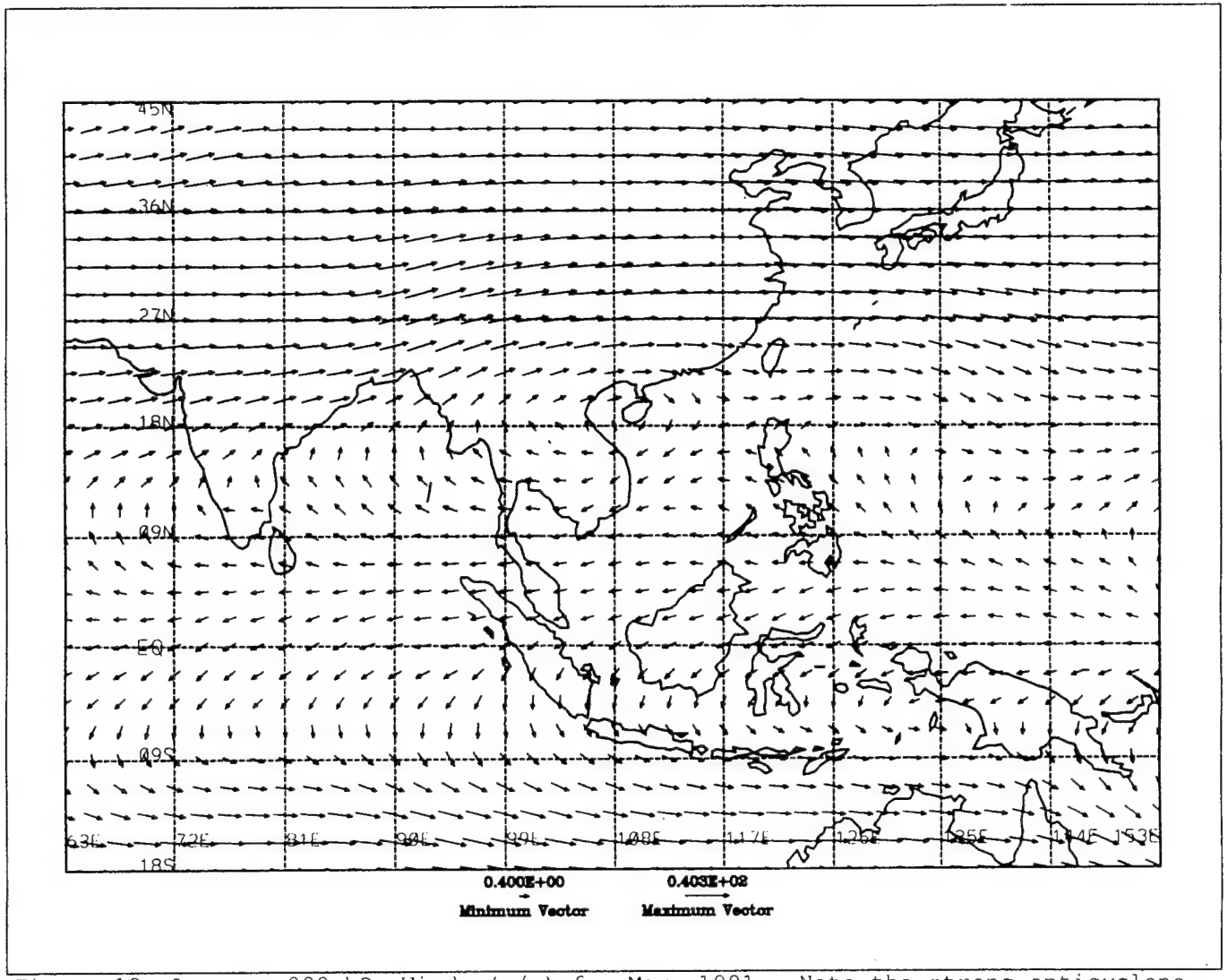

Figure 13. Average 200 hPa Winds (m/s) for May, 1991. Note the strong anticyclone over the Malay Peninsula.

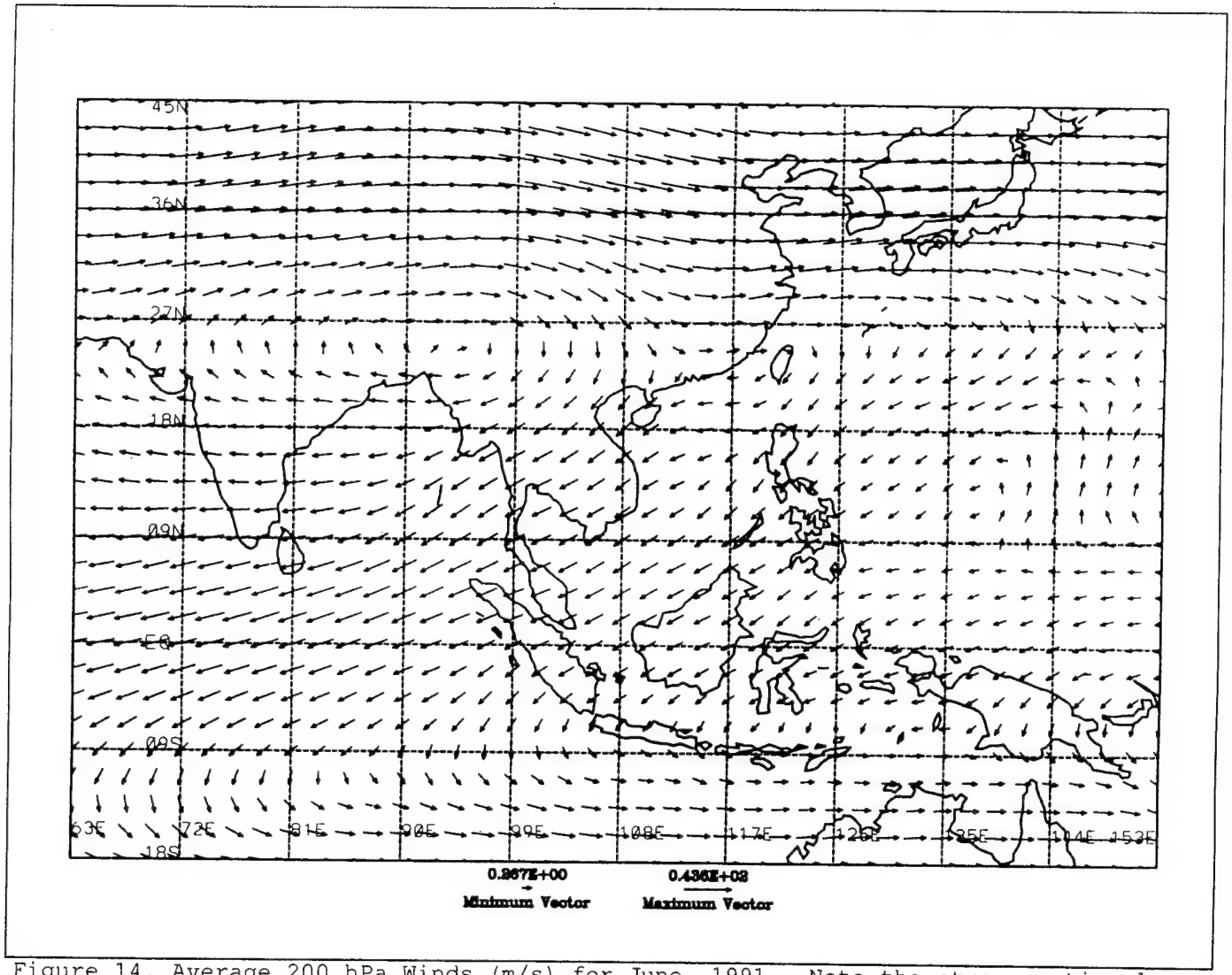

Figure 14. Average 200 hPa Winds (m/s) for June, 1991. Note the strong anticyclone and easterly winds over the northern Bay of Bengal.

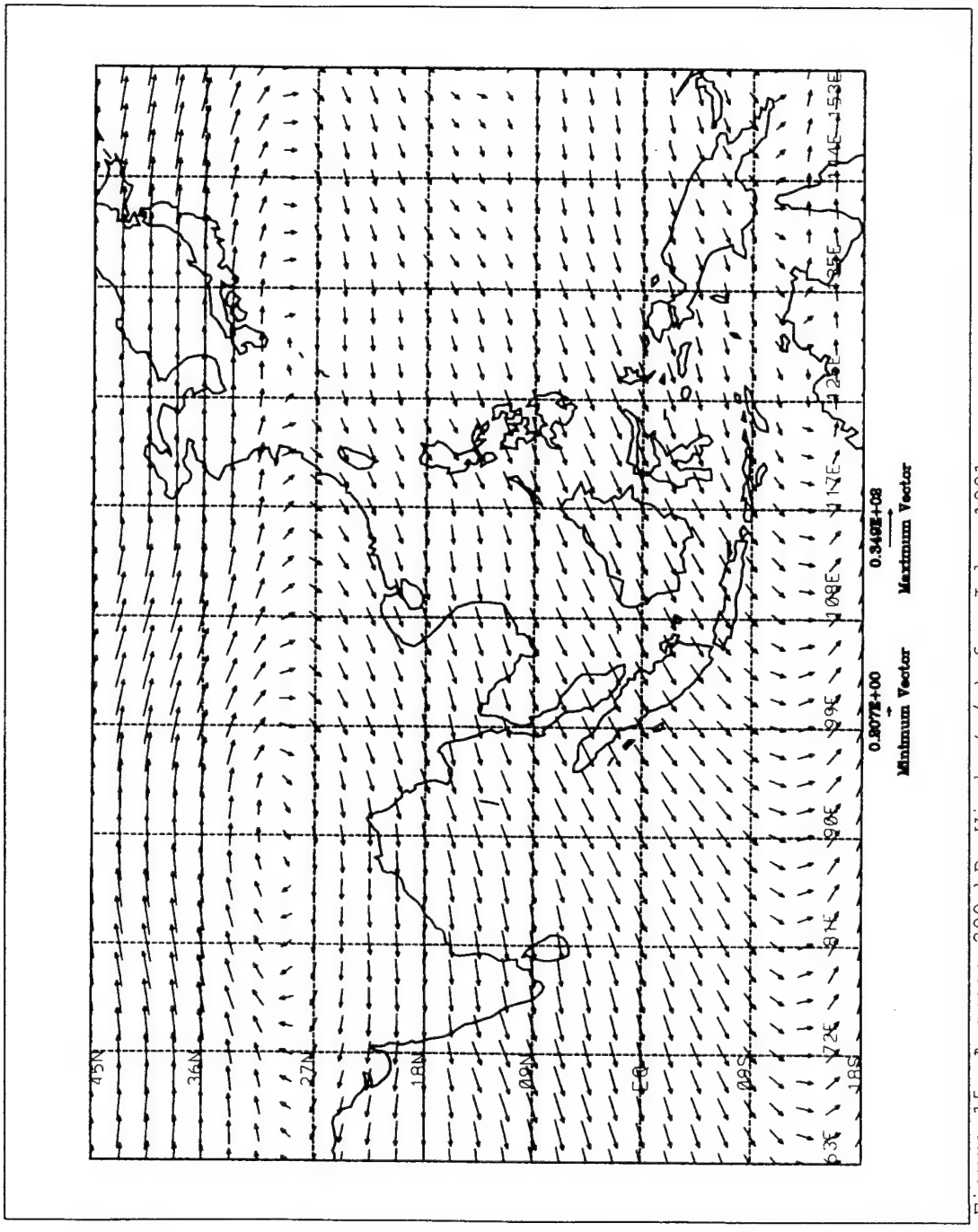

Figure 15. Average 200 hPa Winds (m/s) for July, 1991.

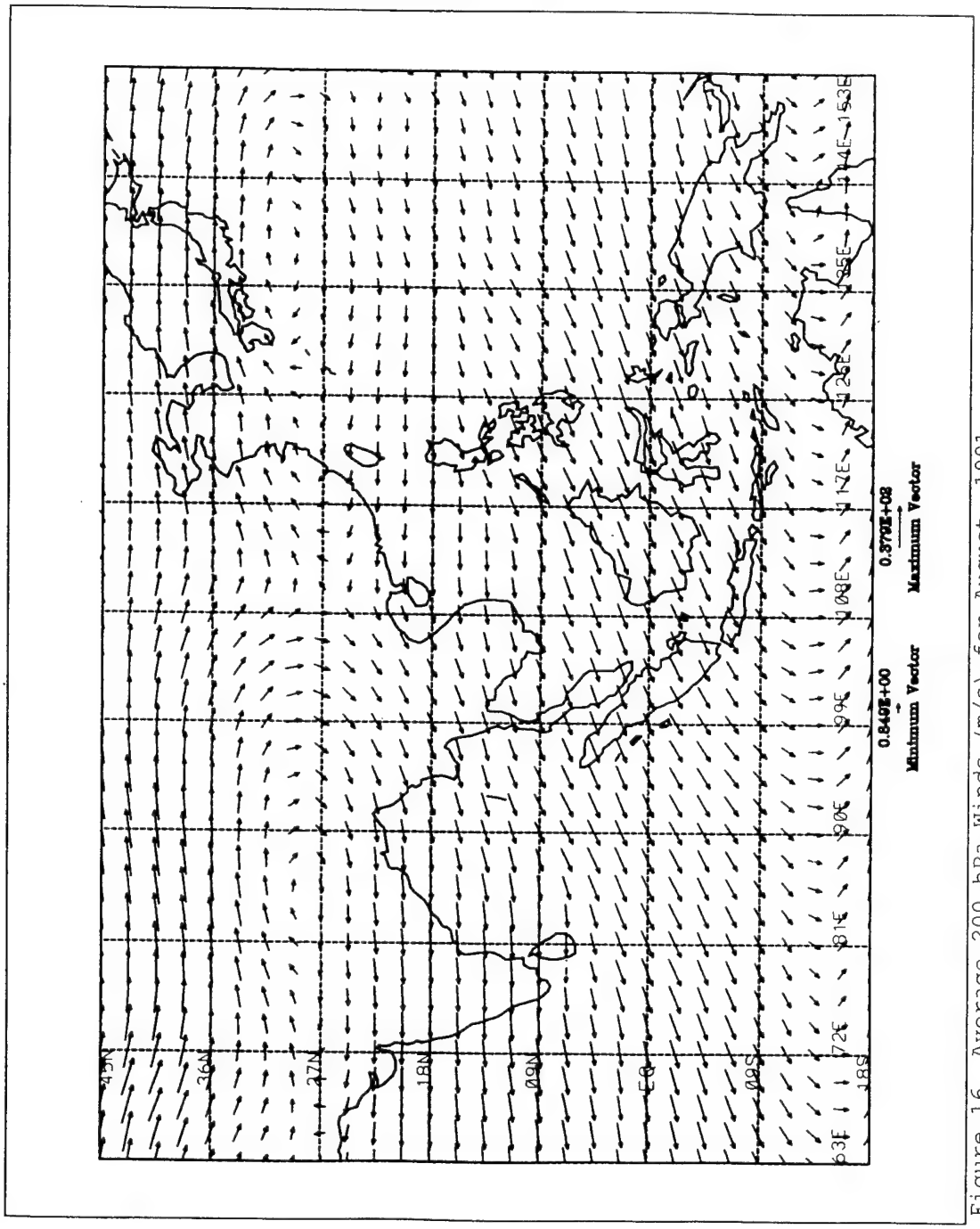

Figure 16. Average 200 hPa Winds (m/s) for August, 1991.

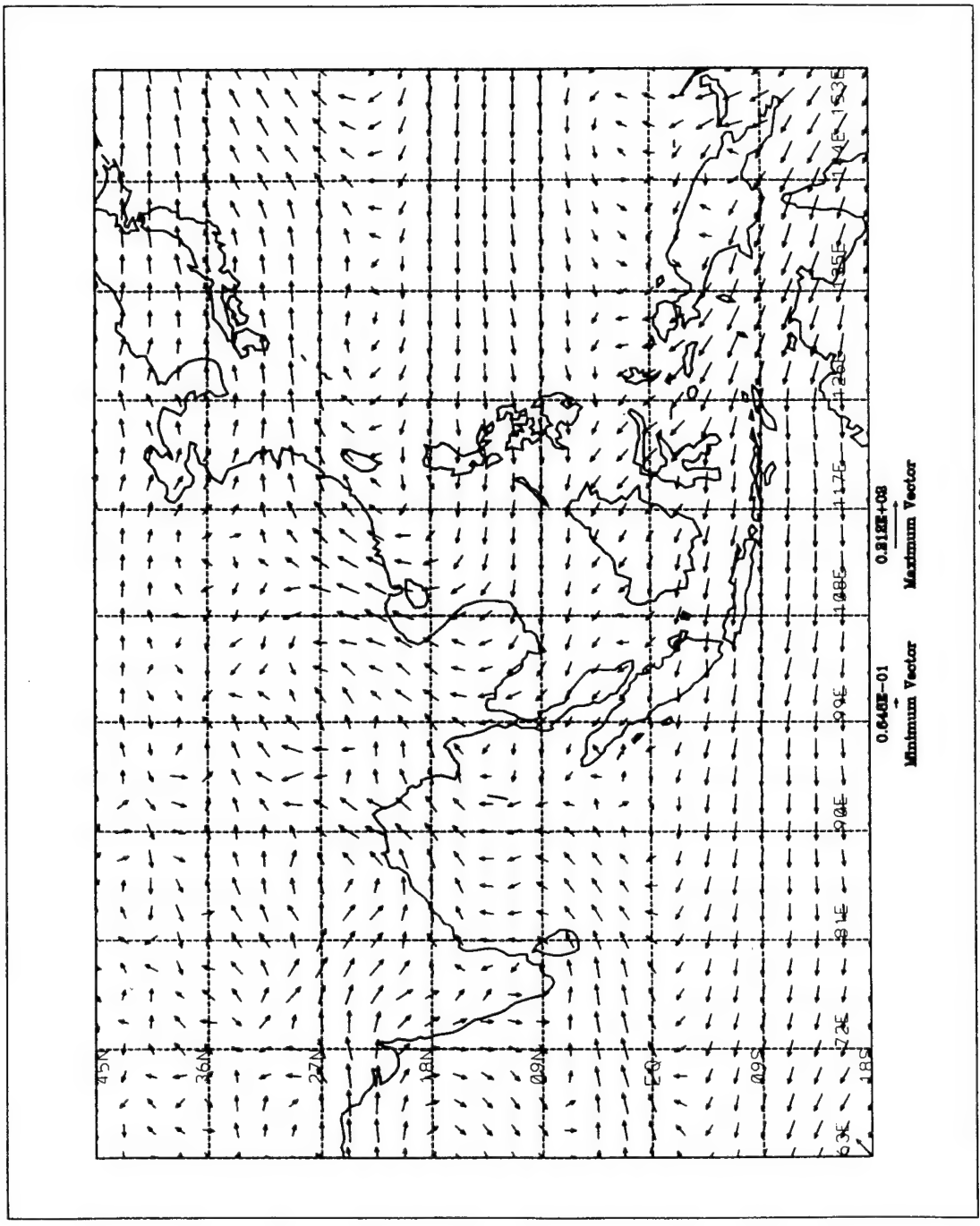

Figure 17. Average 850 hPa Winds (m/s) for May, 1991.

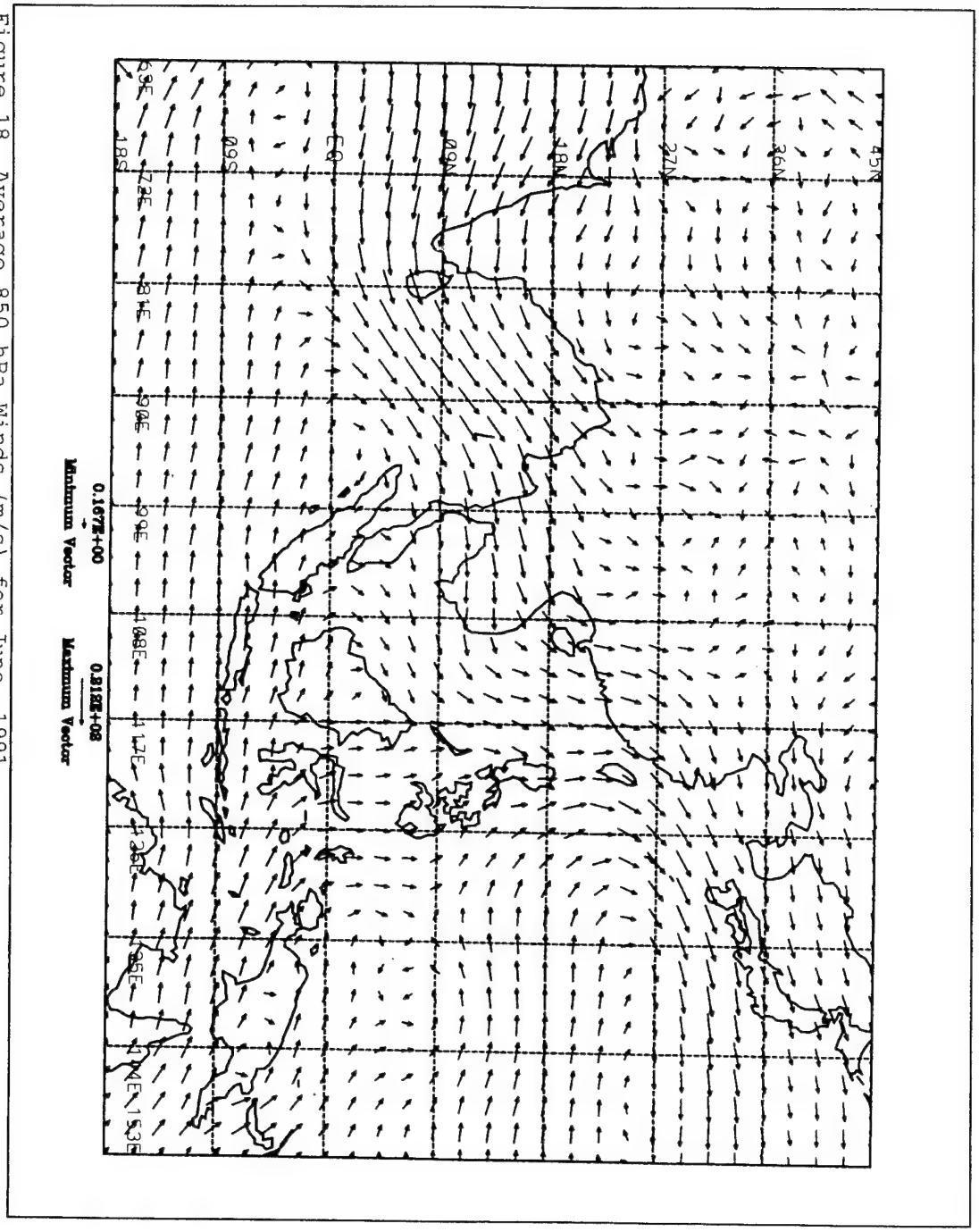

Figure 18. Average 850 hPa Winds (m/s) for June, 1991.

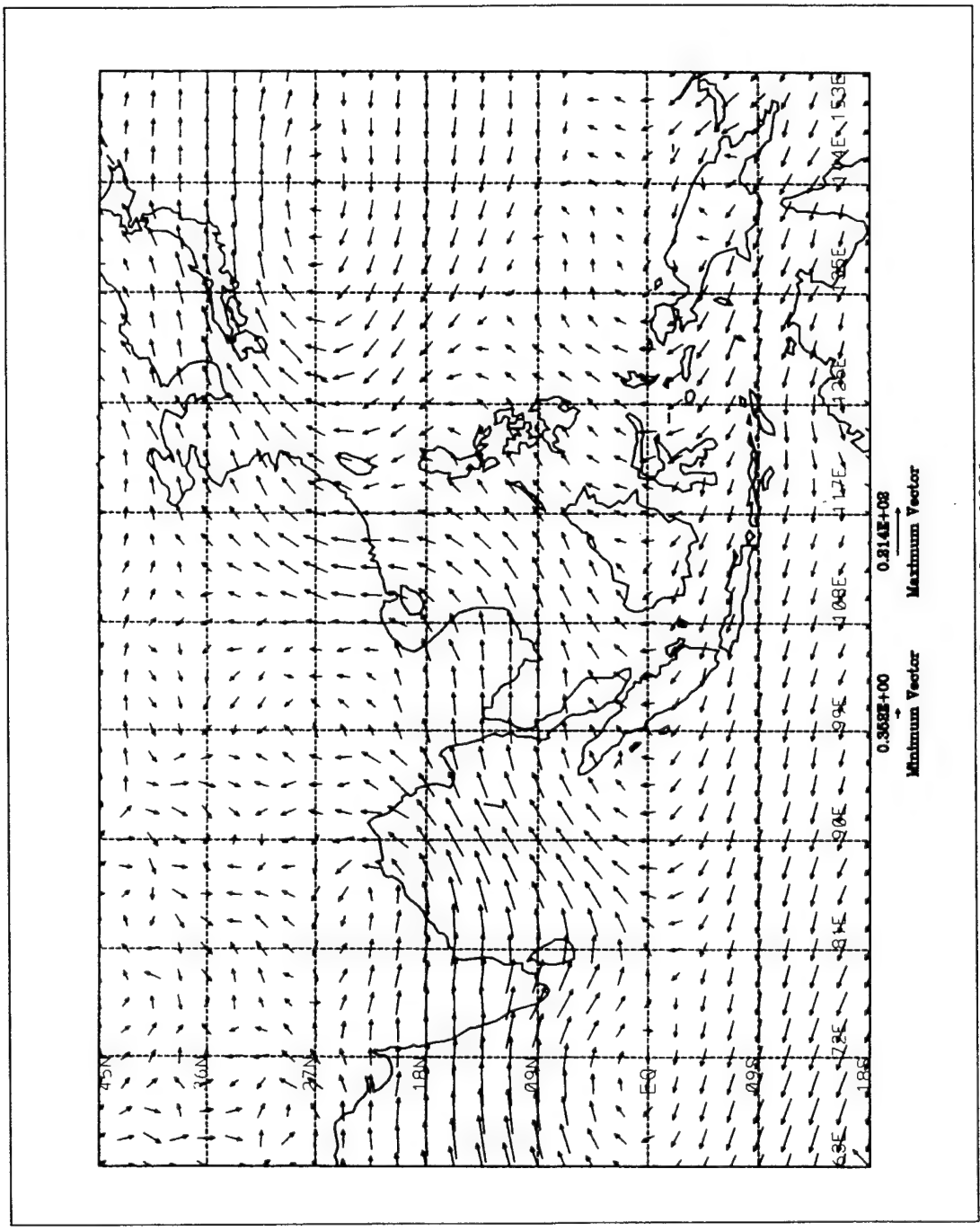

Figure 19. Average 850 hPa Winds (m/s) for July, 1991.

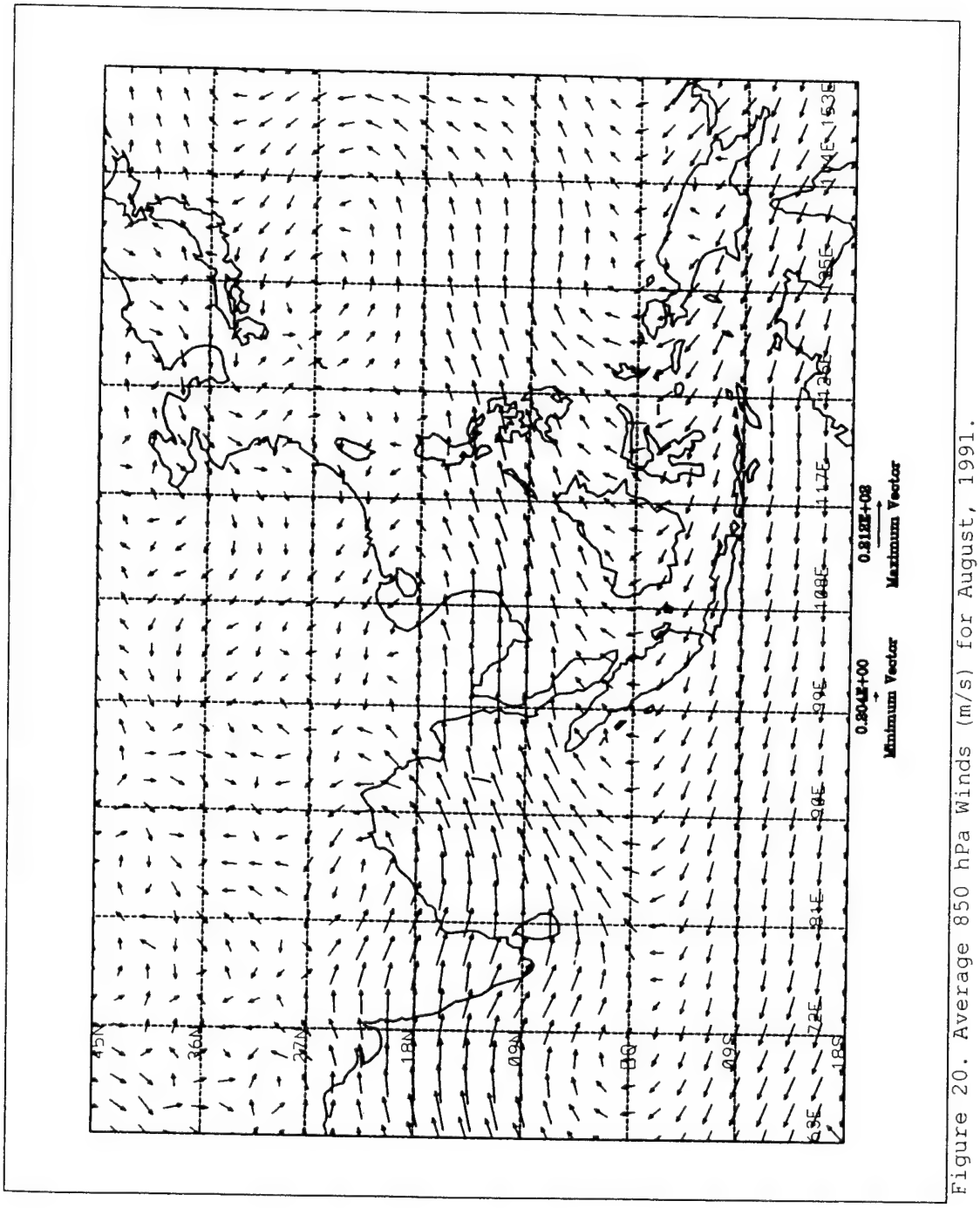

Figure 20. Average 850 hPa Winds (m/s) for August, 1991.

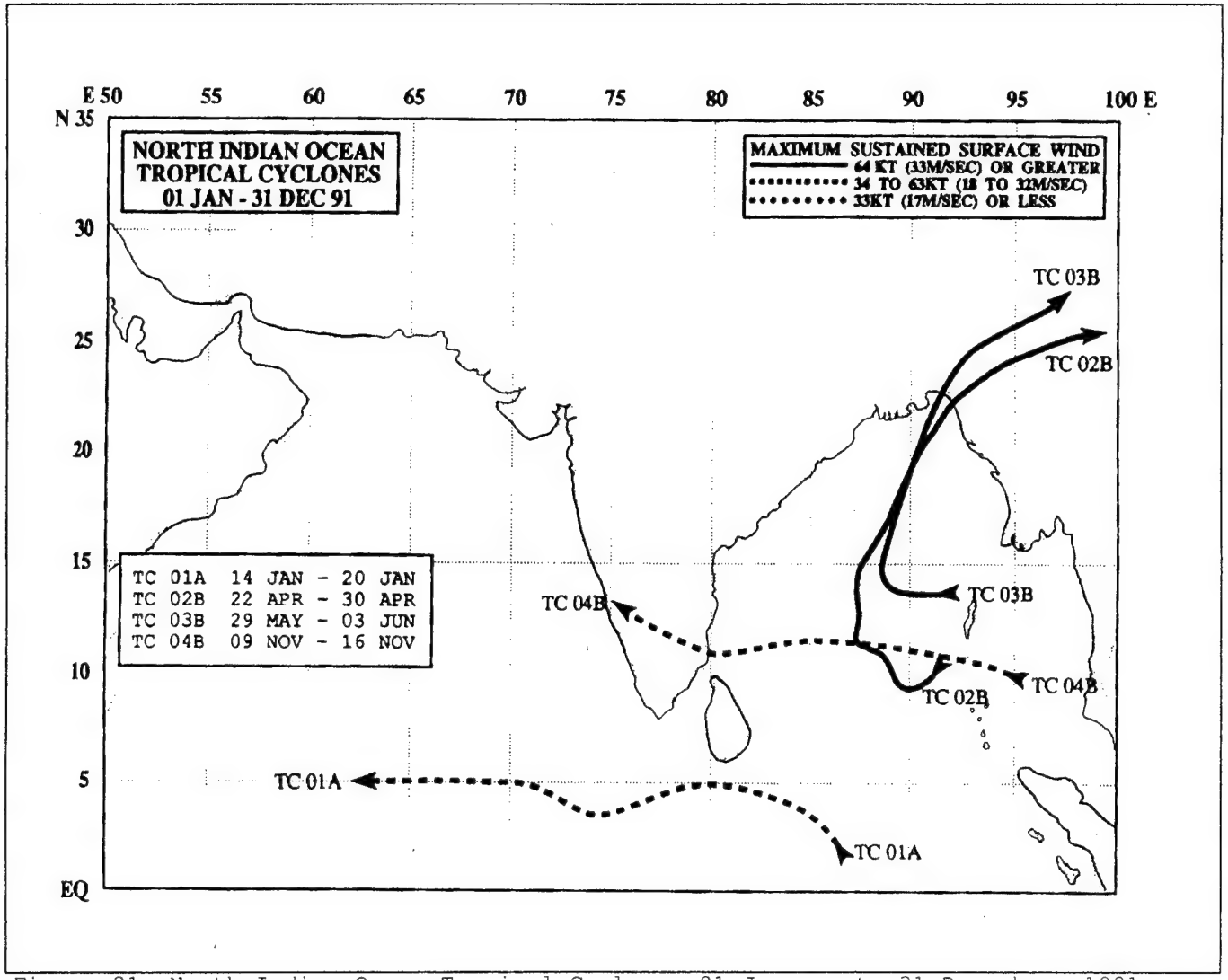

Figure 21. North Indian Ocean Tropical Cyclones 01 January to 31 December, 1991 (From Rudolph and Guard, 1991).

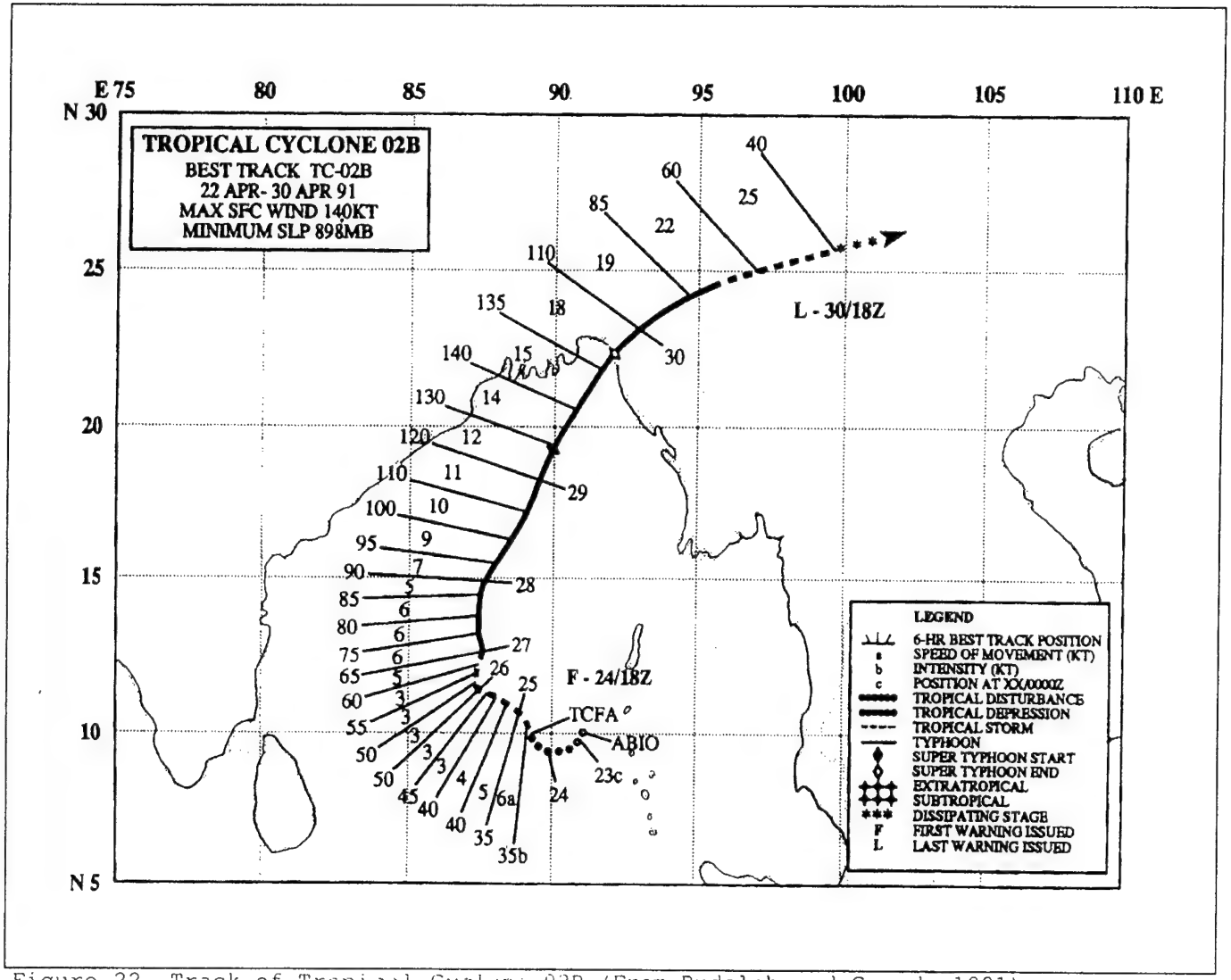

Figure 22. Track of Tropical Cyclone 02B (From Rudolph and Guard, 1991).

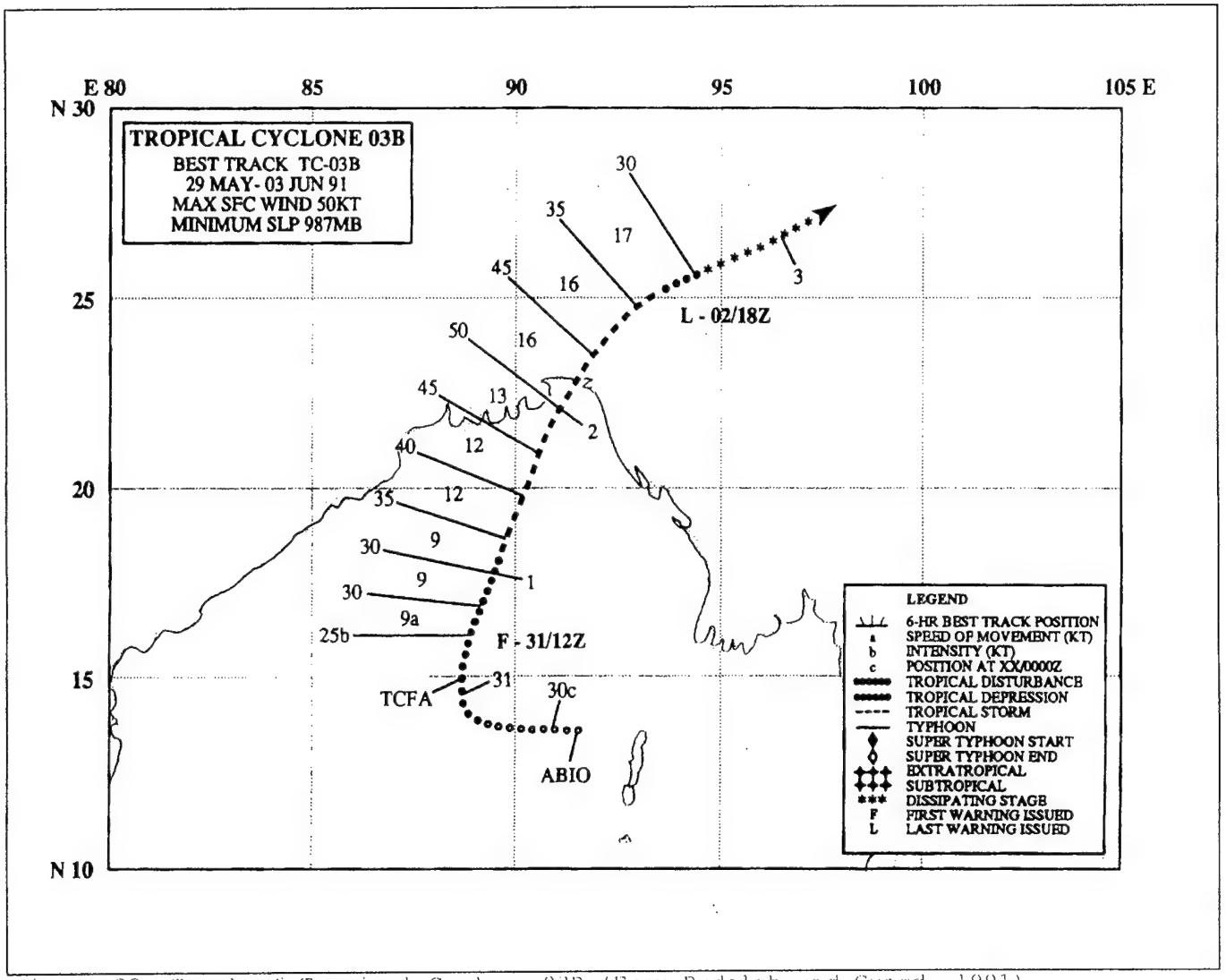

Figure 23. Track of Tropical Cyclone 03B (From Rudolph and Guard, 1991).

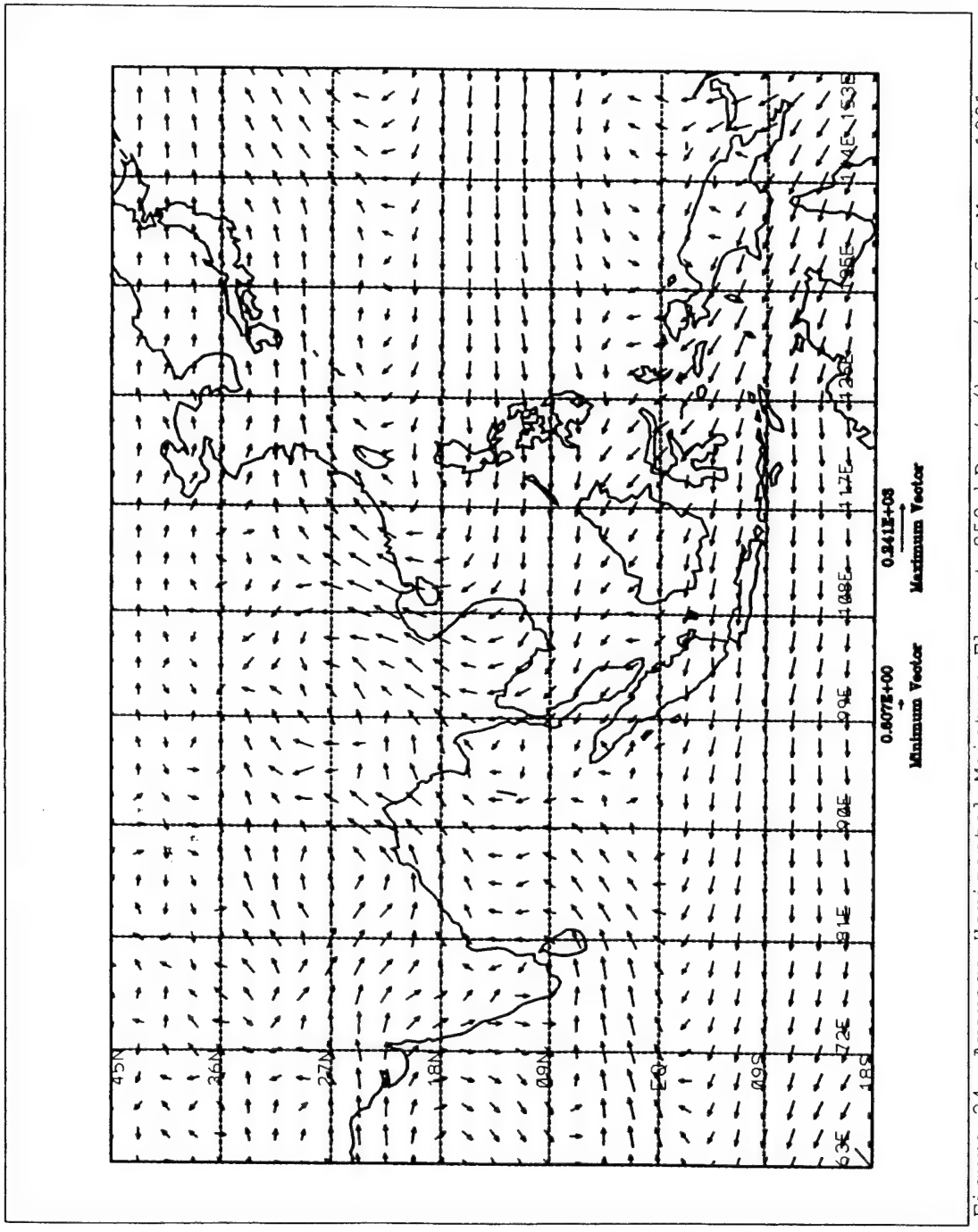

Figure 24. Average Horizontal Moisture Flux at 850 hPa (g/kg m/s) for May, 1991.

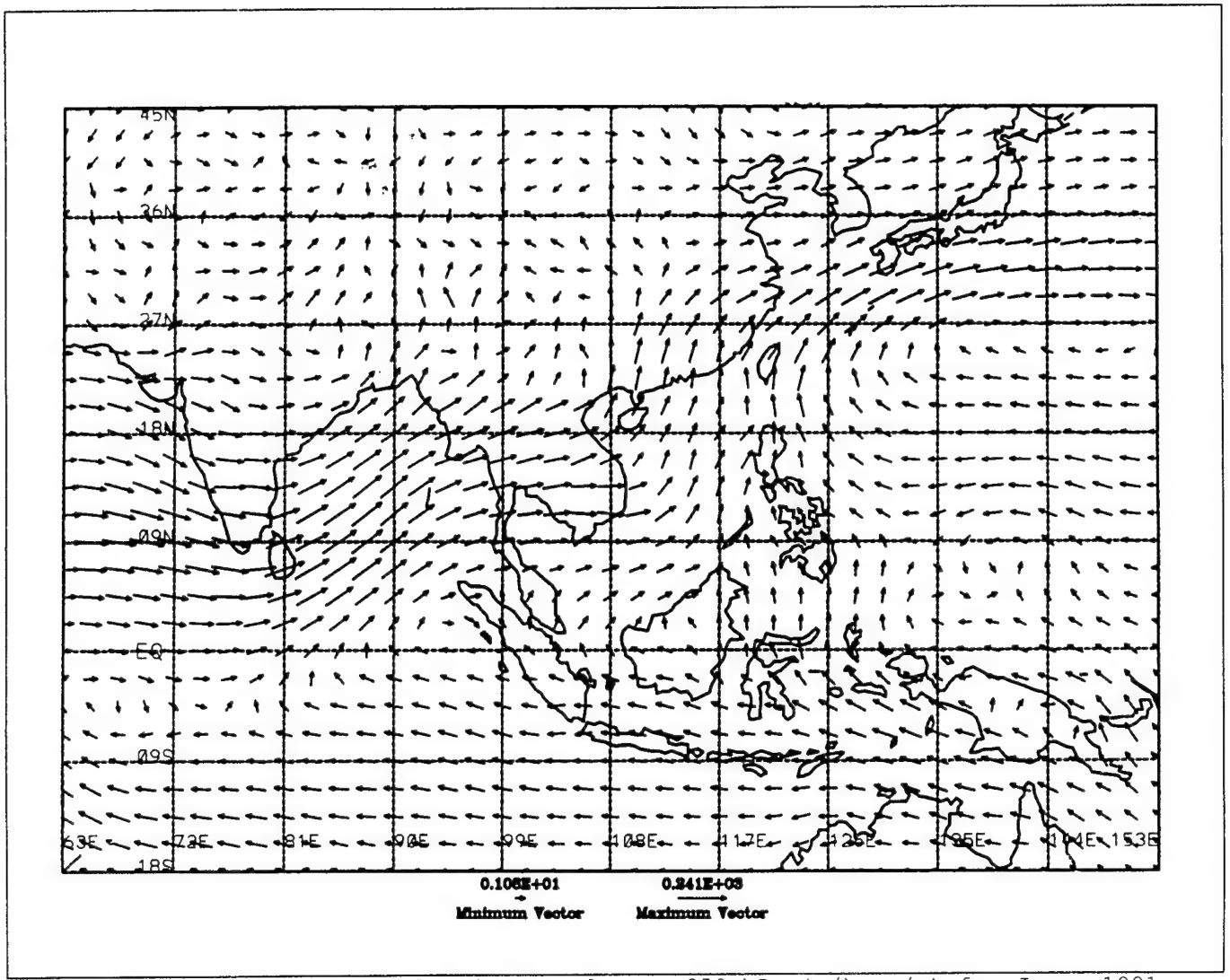

Figure 25. Average Horizontal Moisture Flux at 850 hPa (g/kg m/s) for June, 1991.

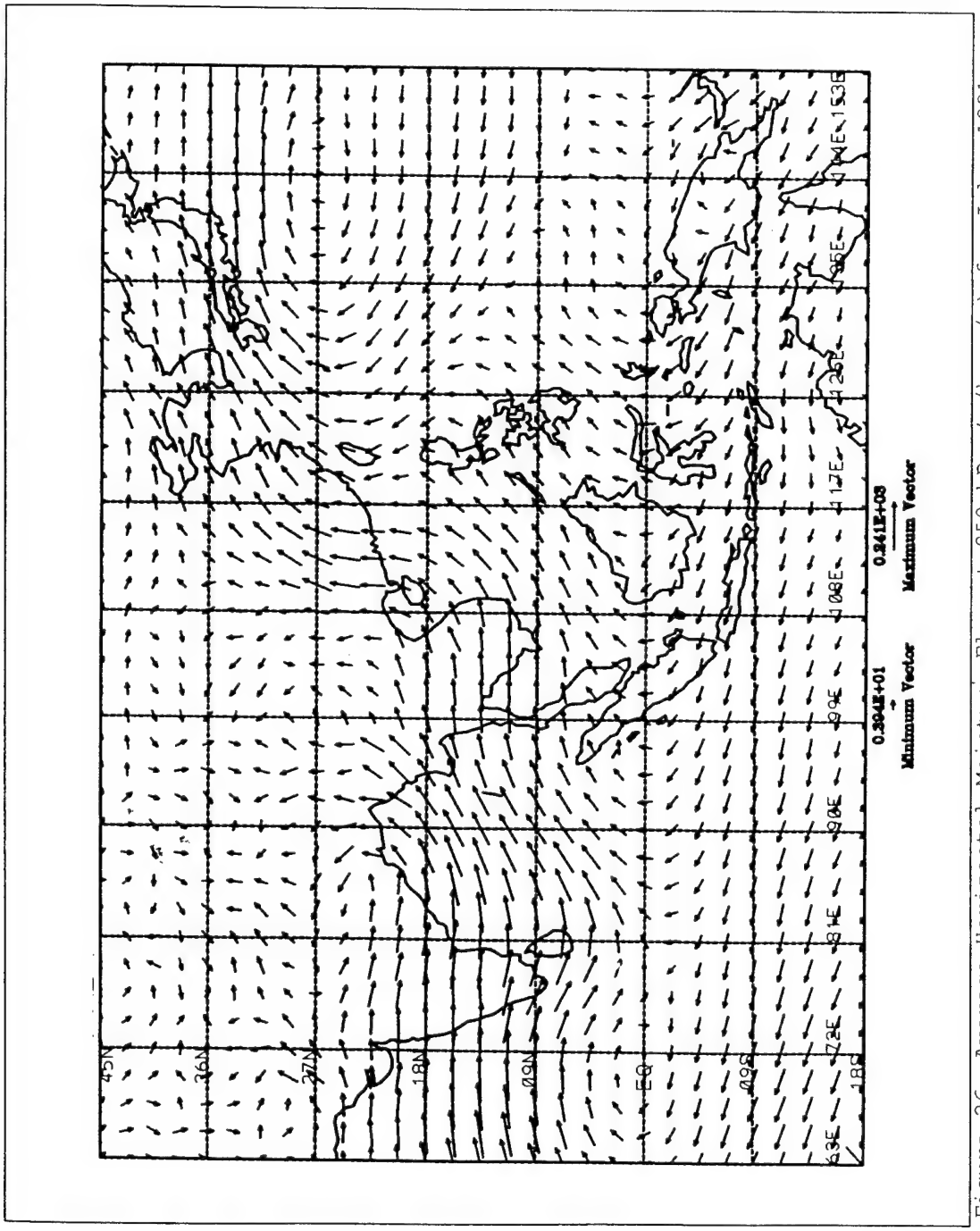

Figure 26. Average Horizontal Moisture Flux at 850 hPa (g/kg m/s) for July, 1991.

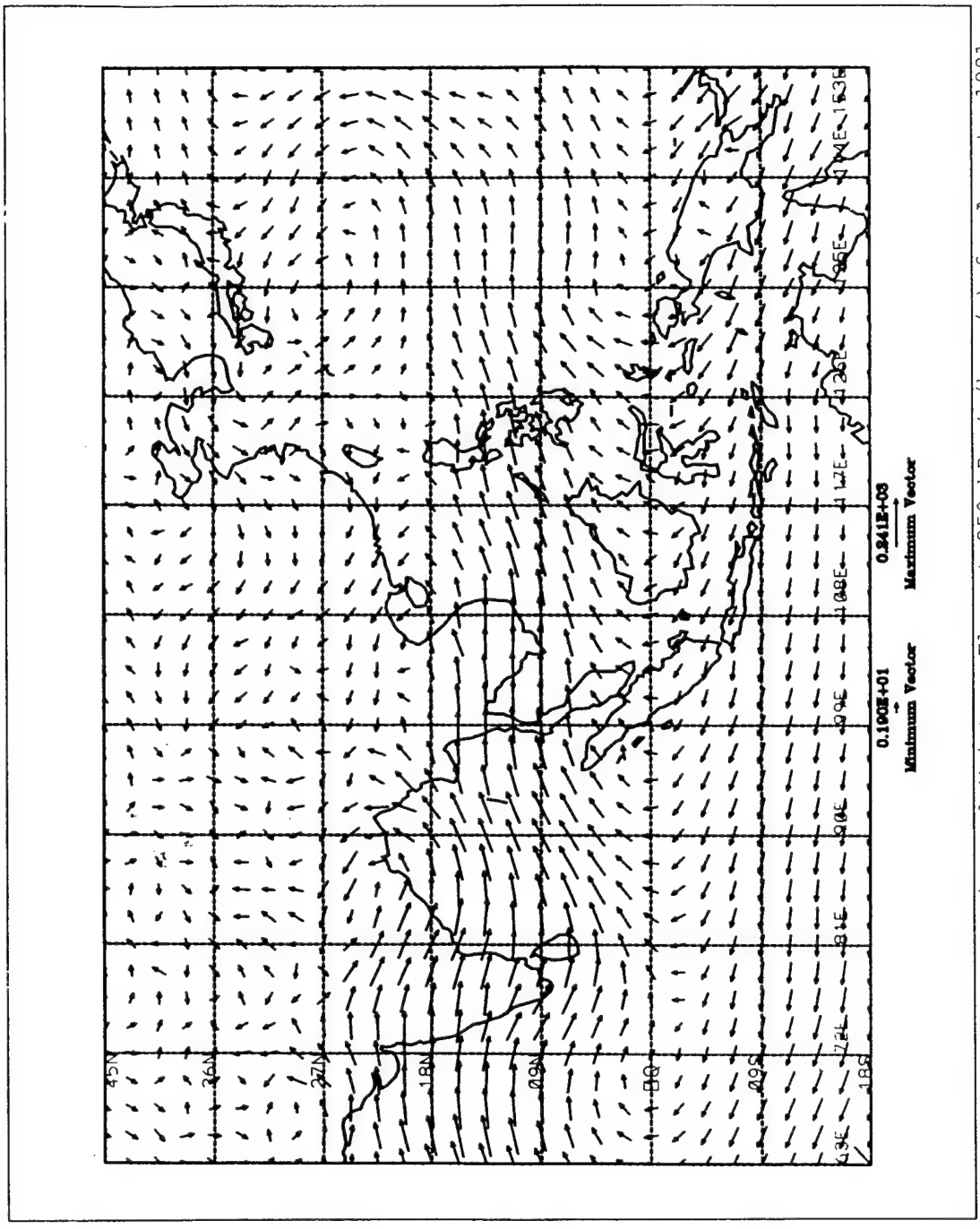

Figure 27. Average Horizontal Moisture Flux at 850 hPa (g/kg m/s) for August, 1991.

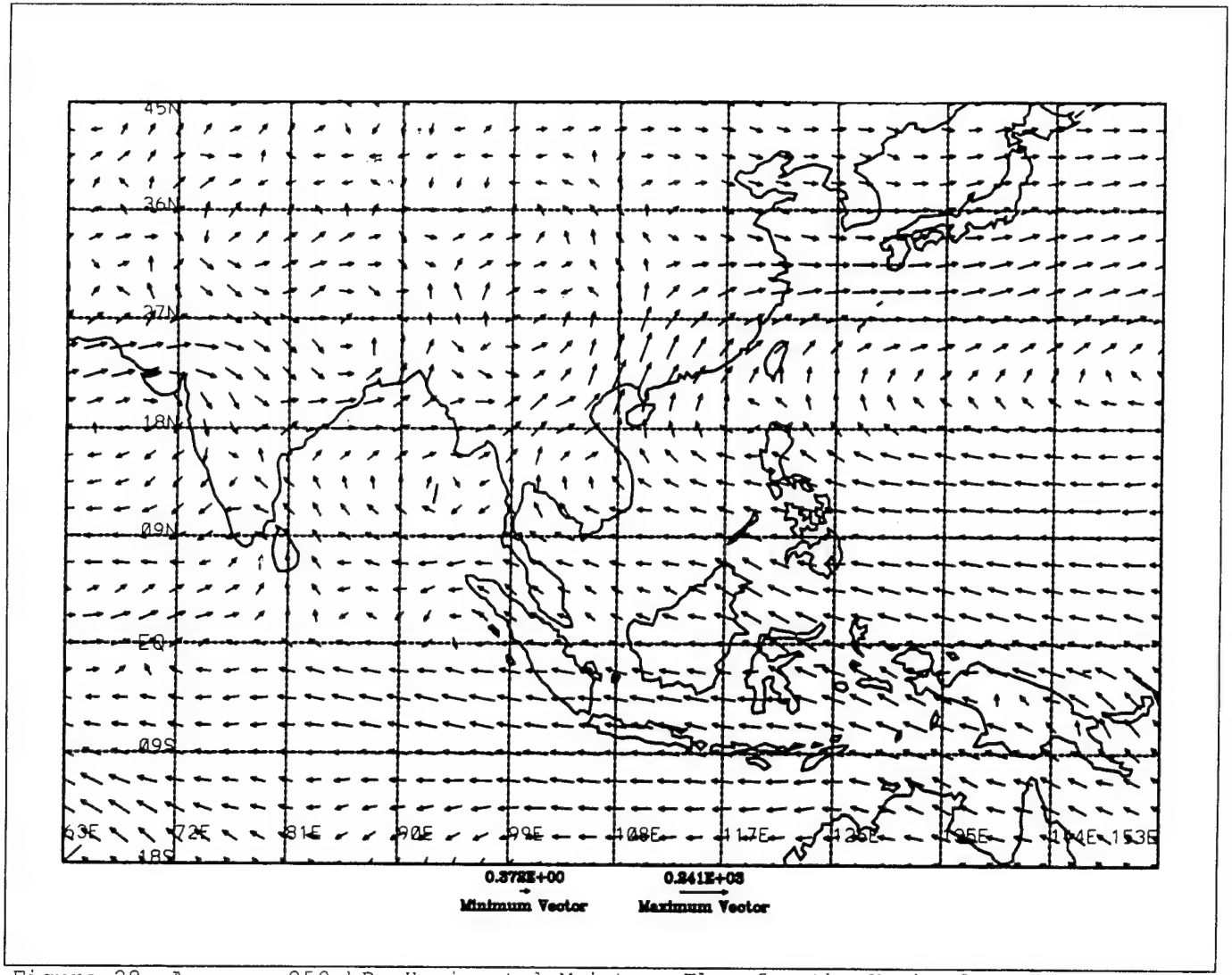

Figure 28. Average 850 hPa Horizontal Moisture Flux for the Week of May 15-22, 1991. Vector quantities in units of g/kg m/s.

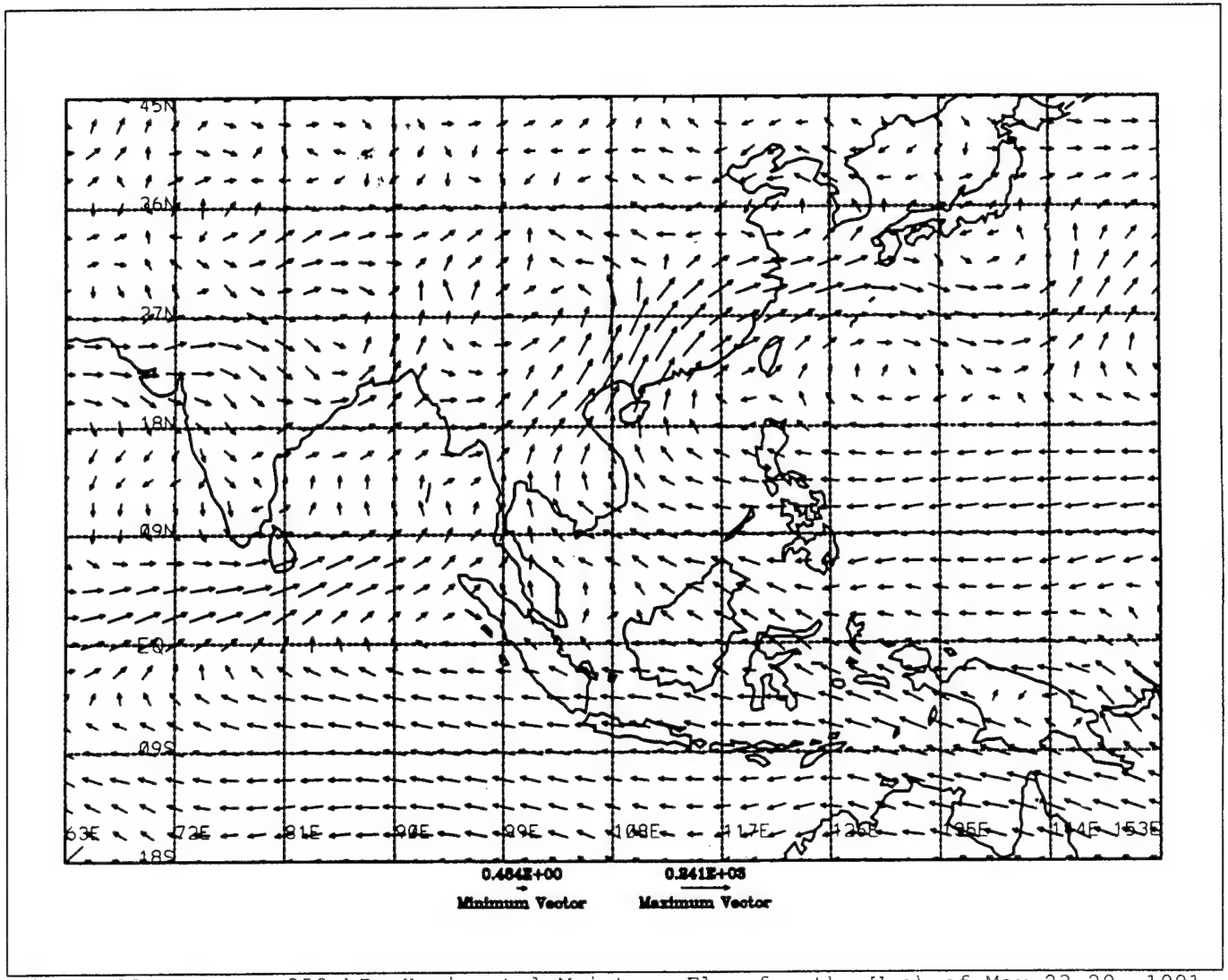

Figure 29. Average 850 hPa Horizontal Moisture Flux for the Week of May 23-29, 1991. Vector quantities in units of g/kg m/s.

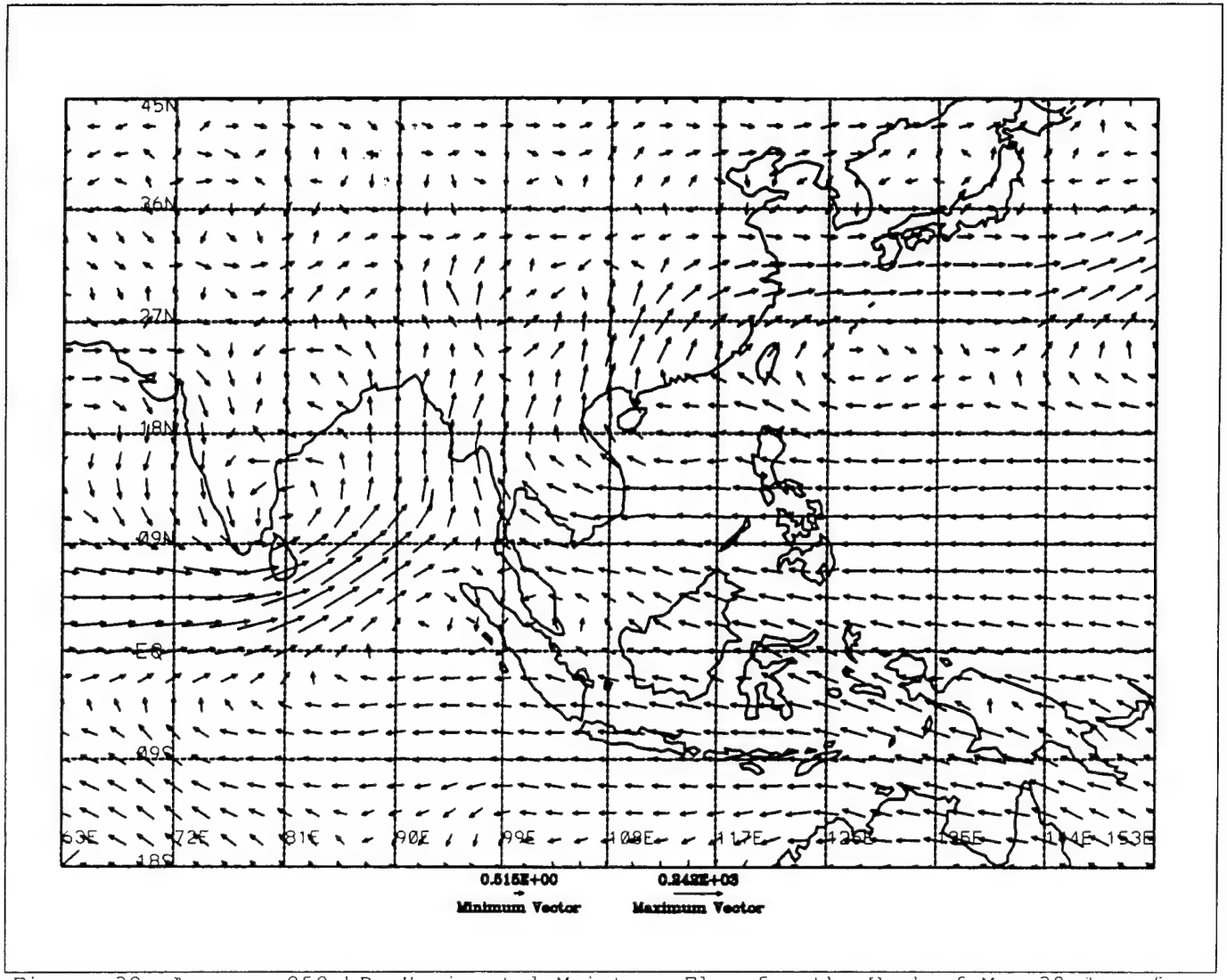

Figure 30. Average 850 hPa Horizontal Moisture Flux for the Week of May 30-June 5, 1991. Vector quantities in units of g/kg m/s.

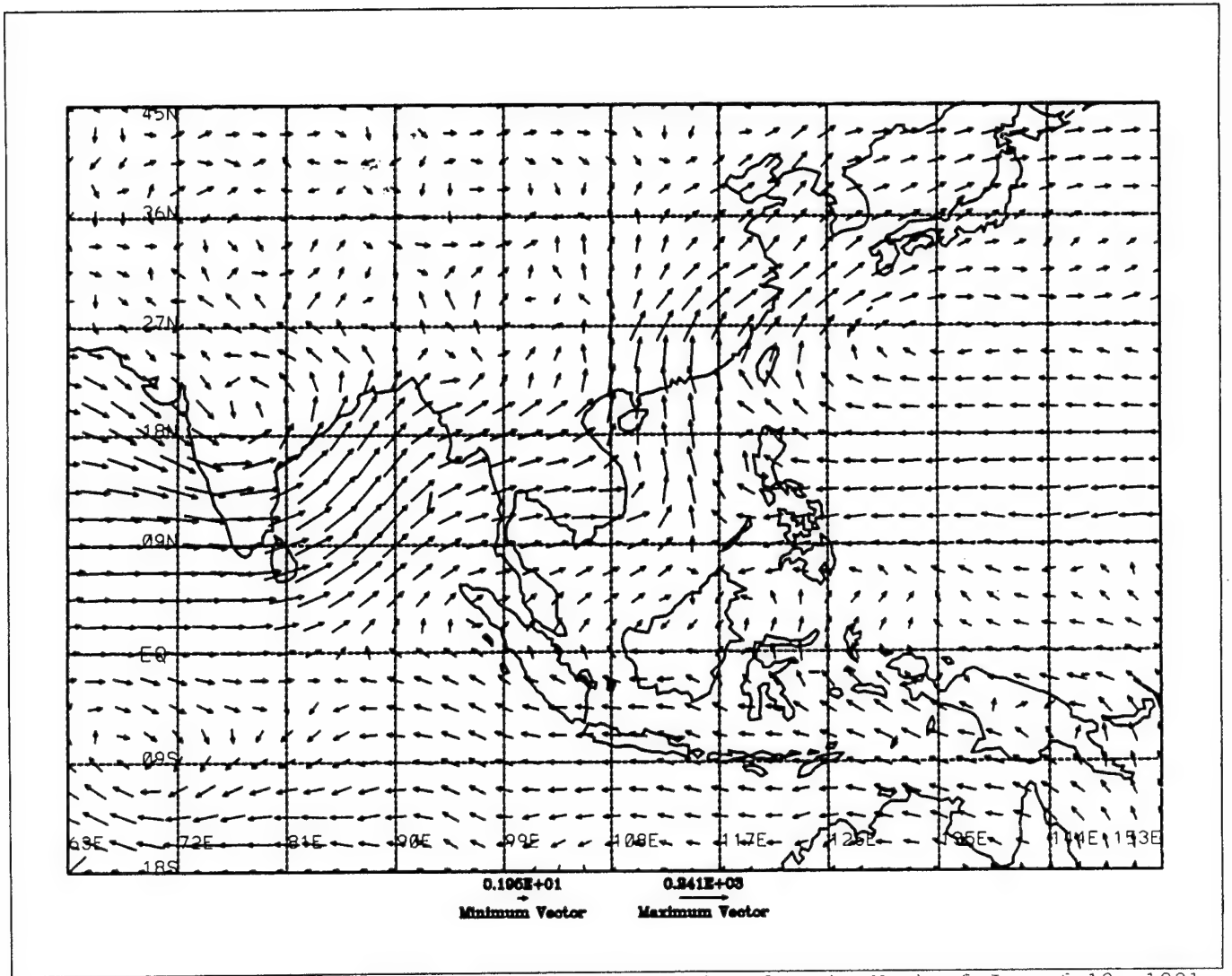

Figure 31. Average 850 hPa Horizontal Moisture Flux for the Week of June 6-12, 1991. Vector quantities in units of g/kg m/s.

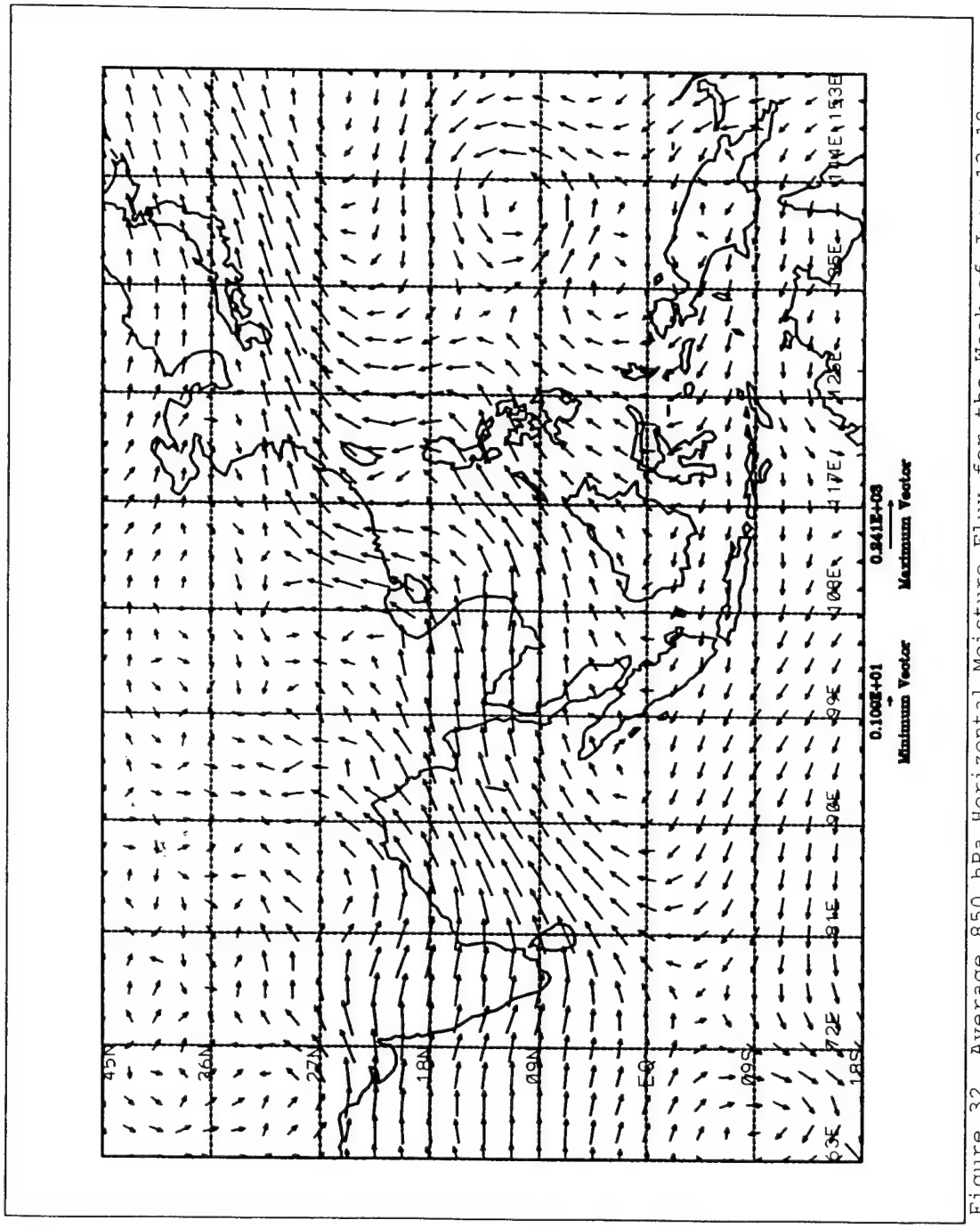

Figure 32. Average 850 hPa Horizontal Moisture Flux for the Week of June 13-18, 1991. Vector quantities in units of g/kg m/s.

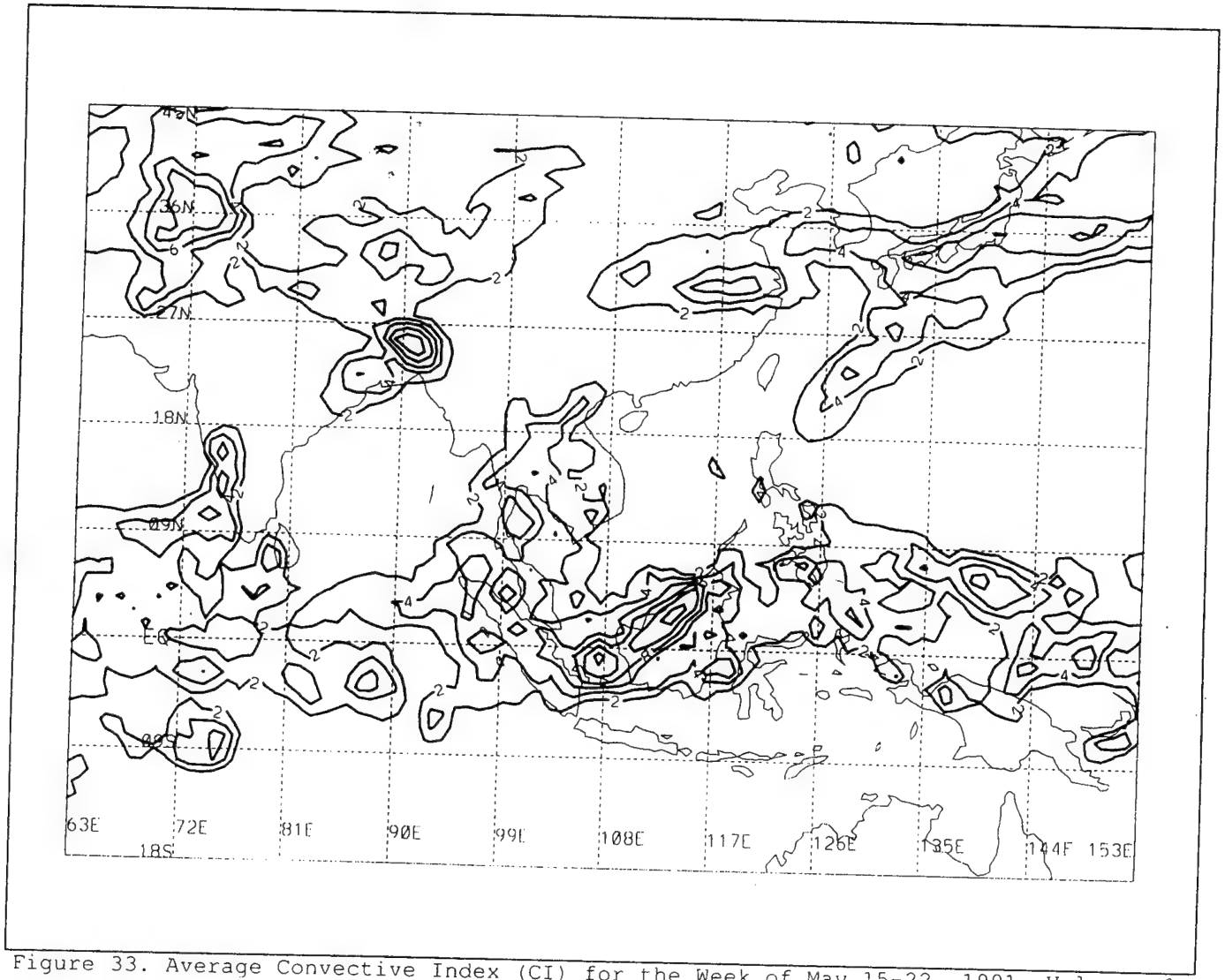

Figure 33. Average Convective Index (CI) for the Week of May 15-22, 1991. Values of CI are in °K.

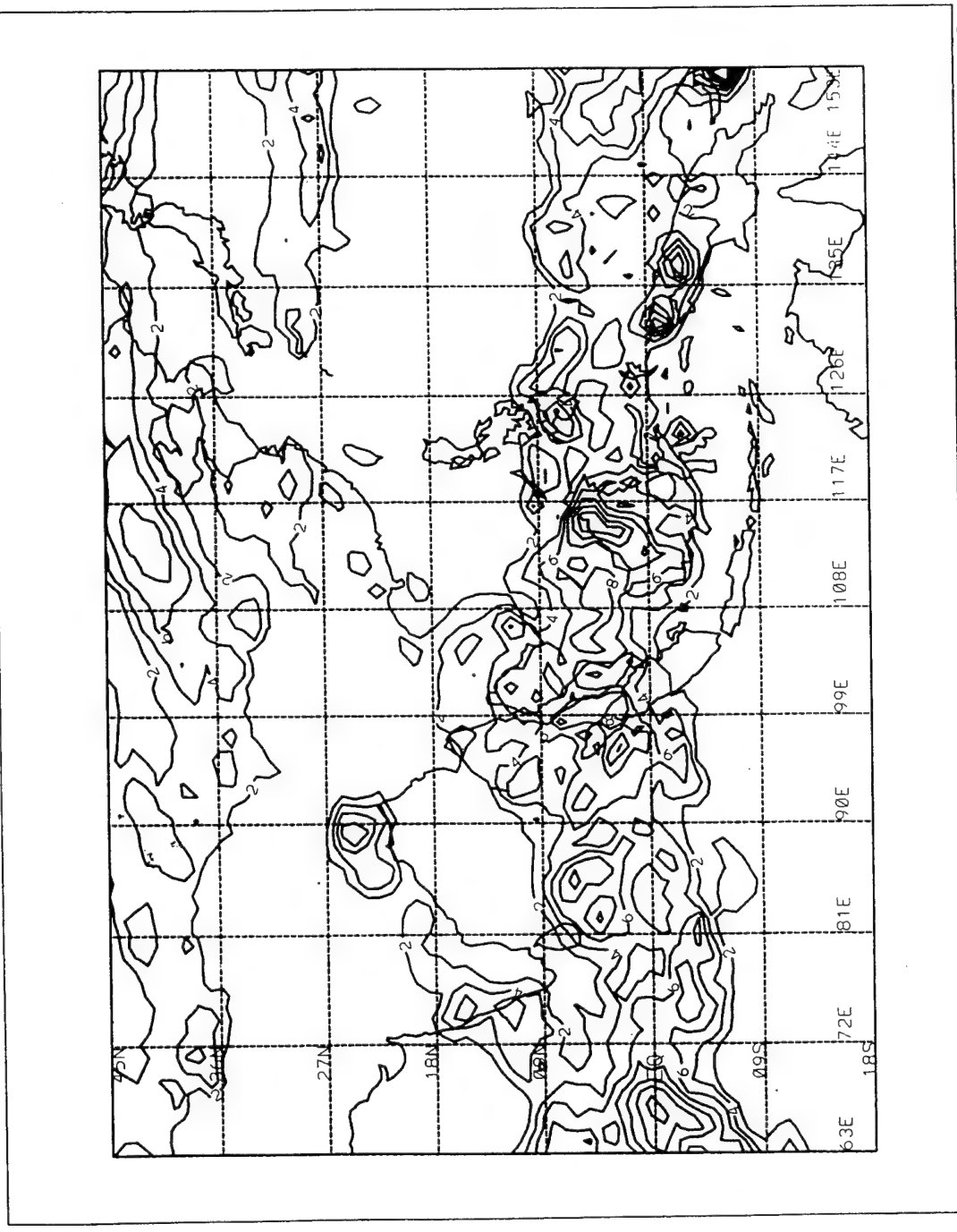

Figure 34. Average Convective Index (CI) for the Week of May 23-29, 1991. Values of CI are in °K.

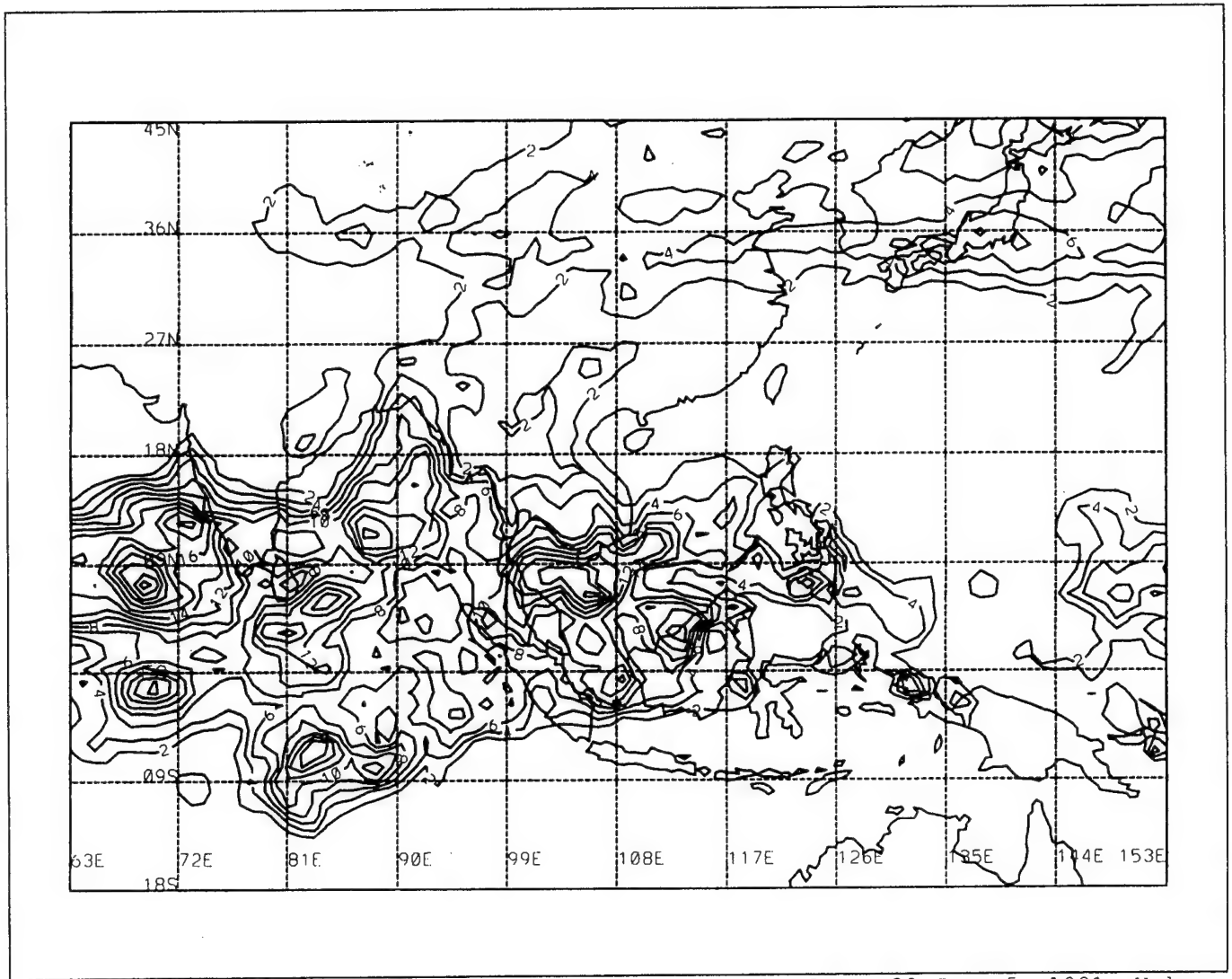

Figure 35. Average Convective Index (CI) for the Week of May 30-June 5, 1991. Values of CI are in °K.

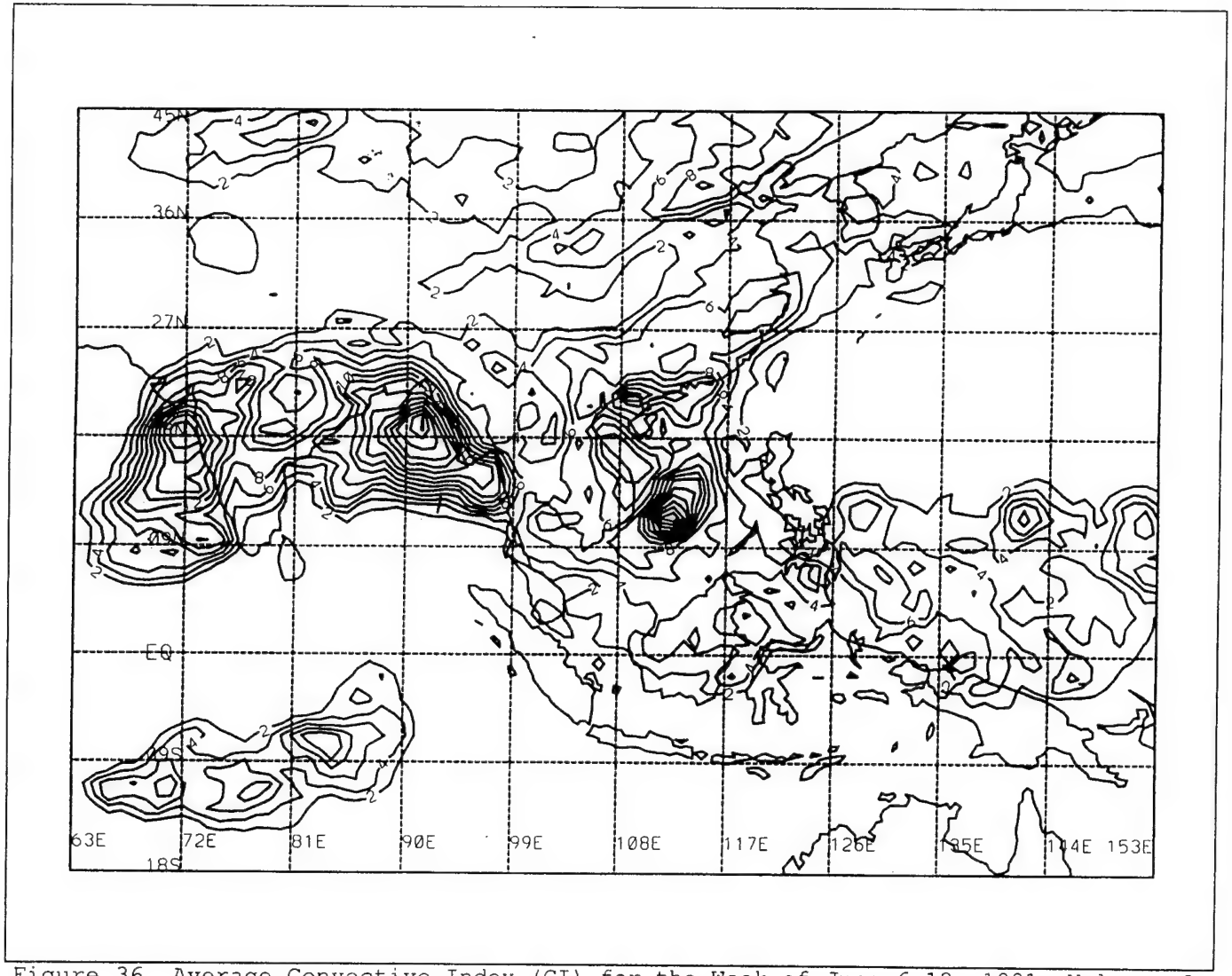

Figure 36. Average Convective Index (CI) for the Week of June 6-12, 1991. Values of CI are in °K.

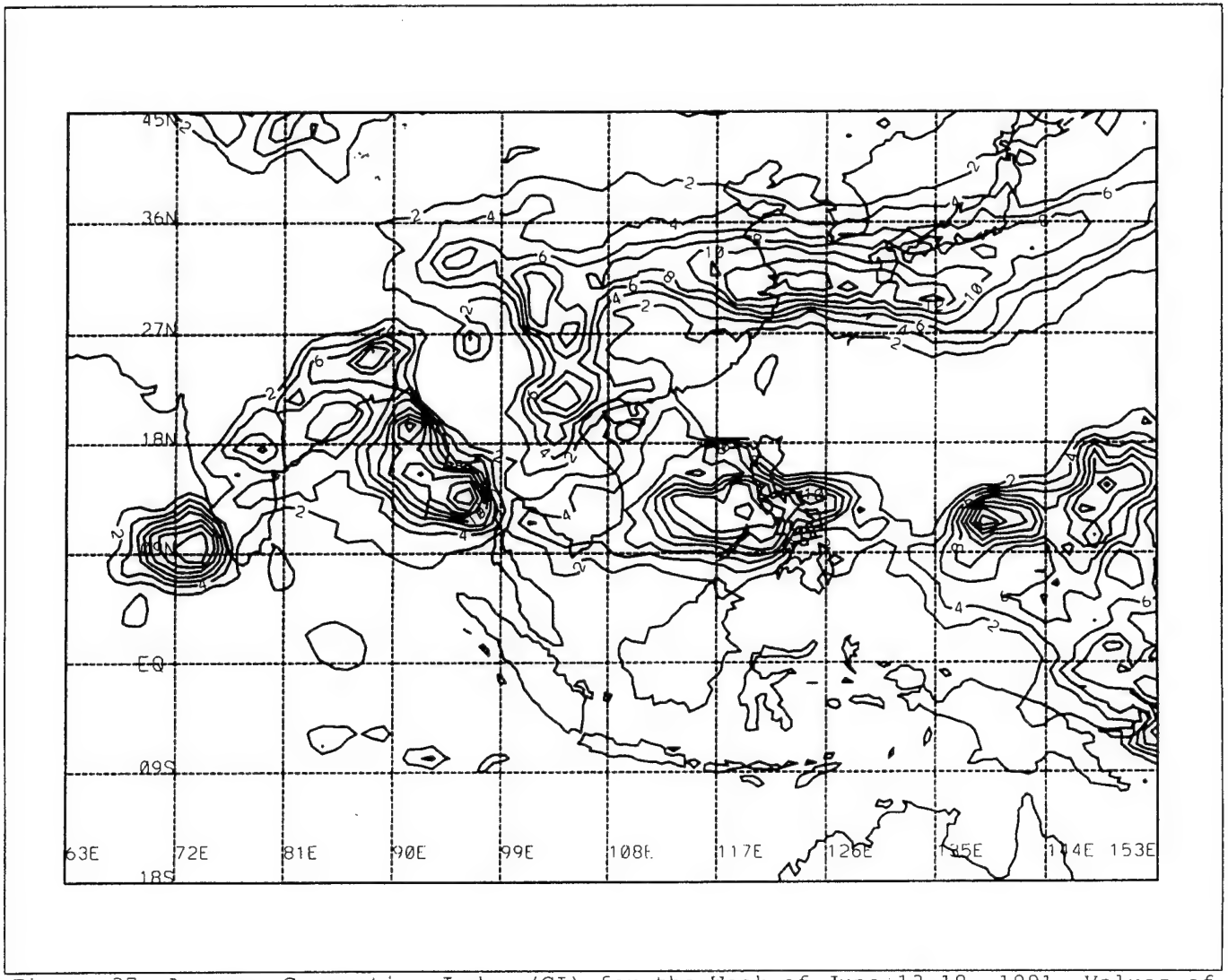

Figure 37. Average Convective Index (CI) for the Week of June 13-18, 1991. Values of CI are in °K.

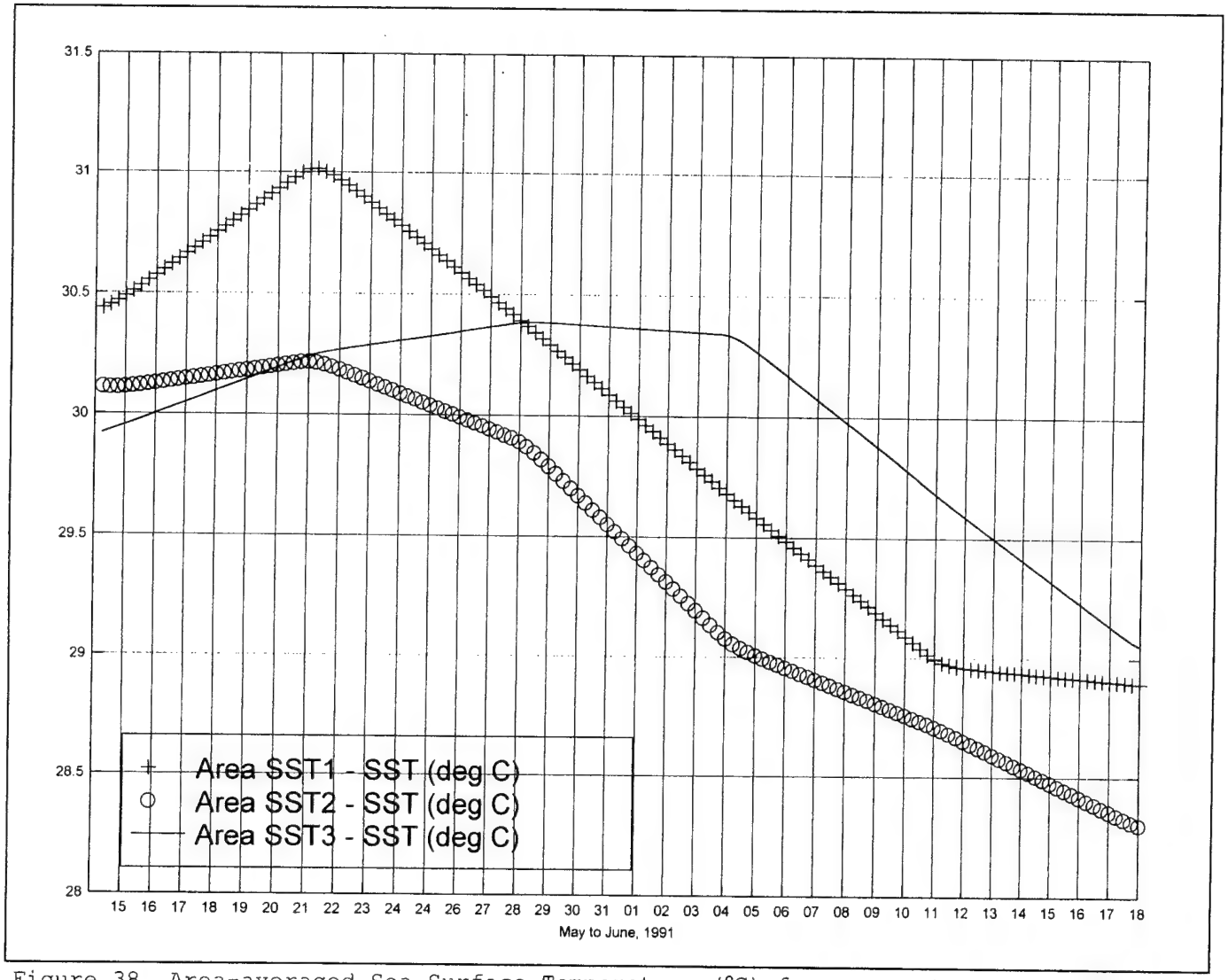

Figure 38. Area-averaged Sea Surface Temperature (°C) for over water areas SST1, SST2, and SST3 during the period May 15-June 18, 1991.

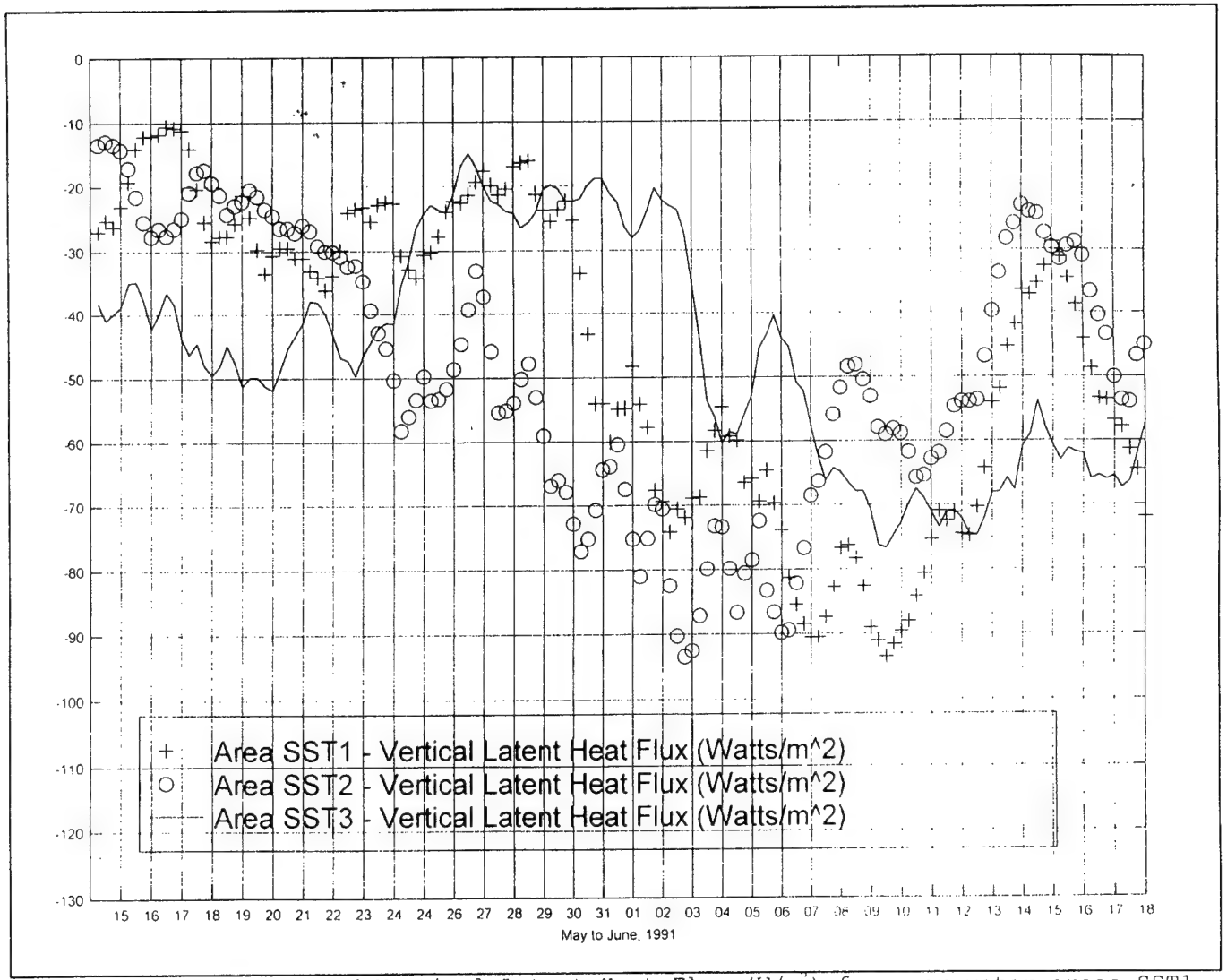

Figure 39. Area-averaged Vertical Latent Heat Flux (W/m^2) for over water areas SST1, SST2, and SST3 during the period May 15-June 18, 1991.

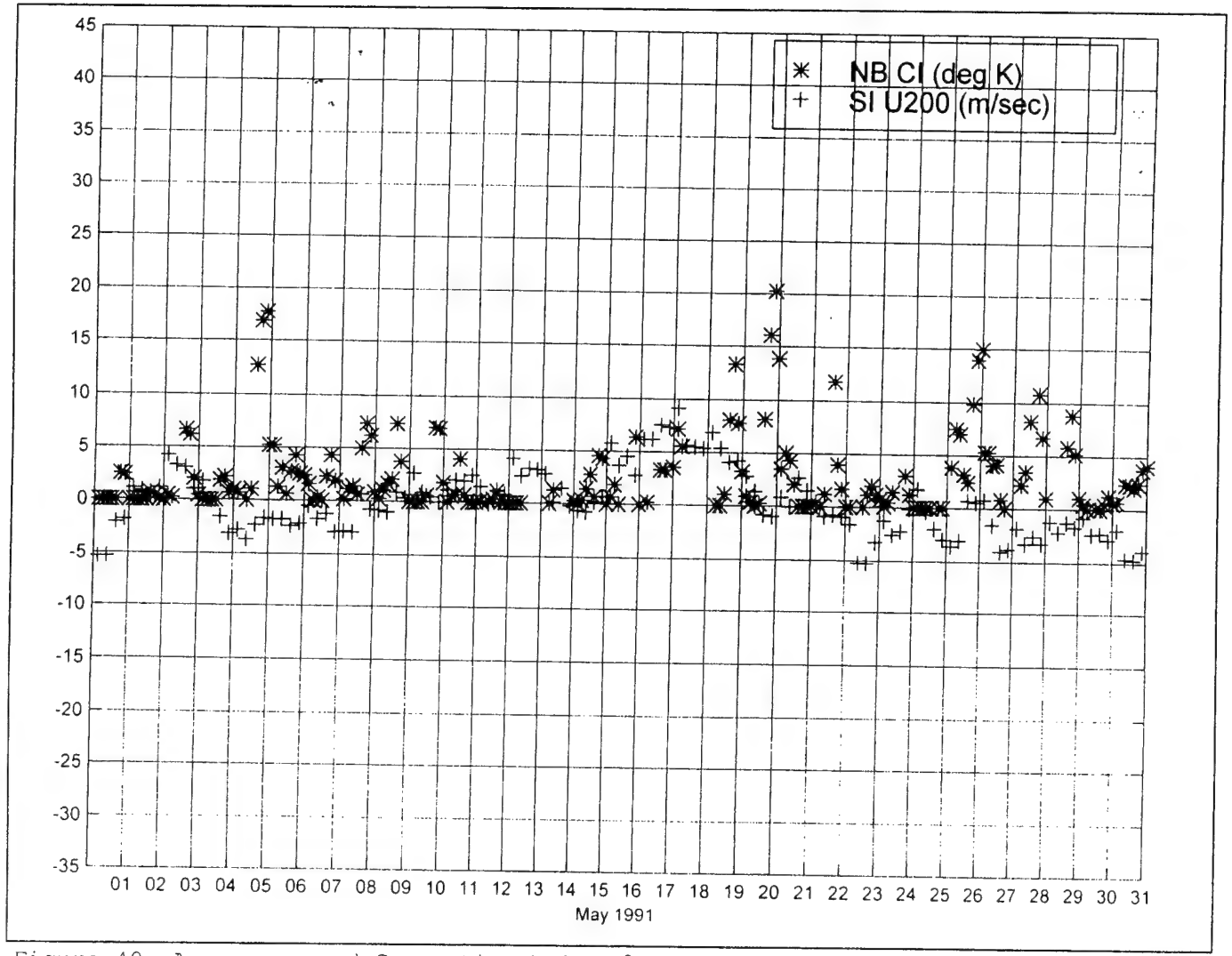

Figure 40. Area-averaged Convective Index (°K) for the northern Bay of Bengal (area NB) versus area-averaged 200 hPa wind (m/s) for southern India (area SI) during May, 1991.

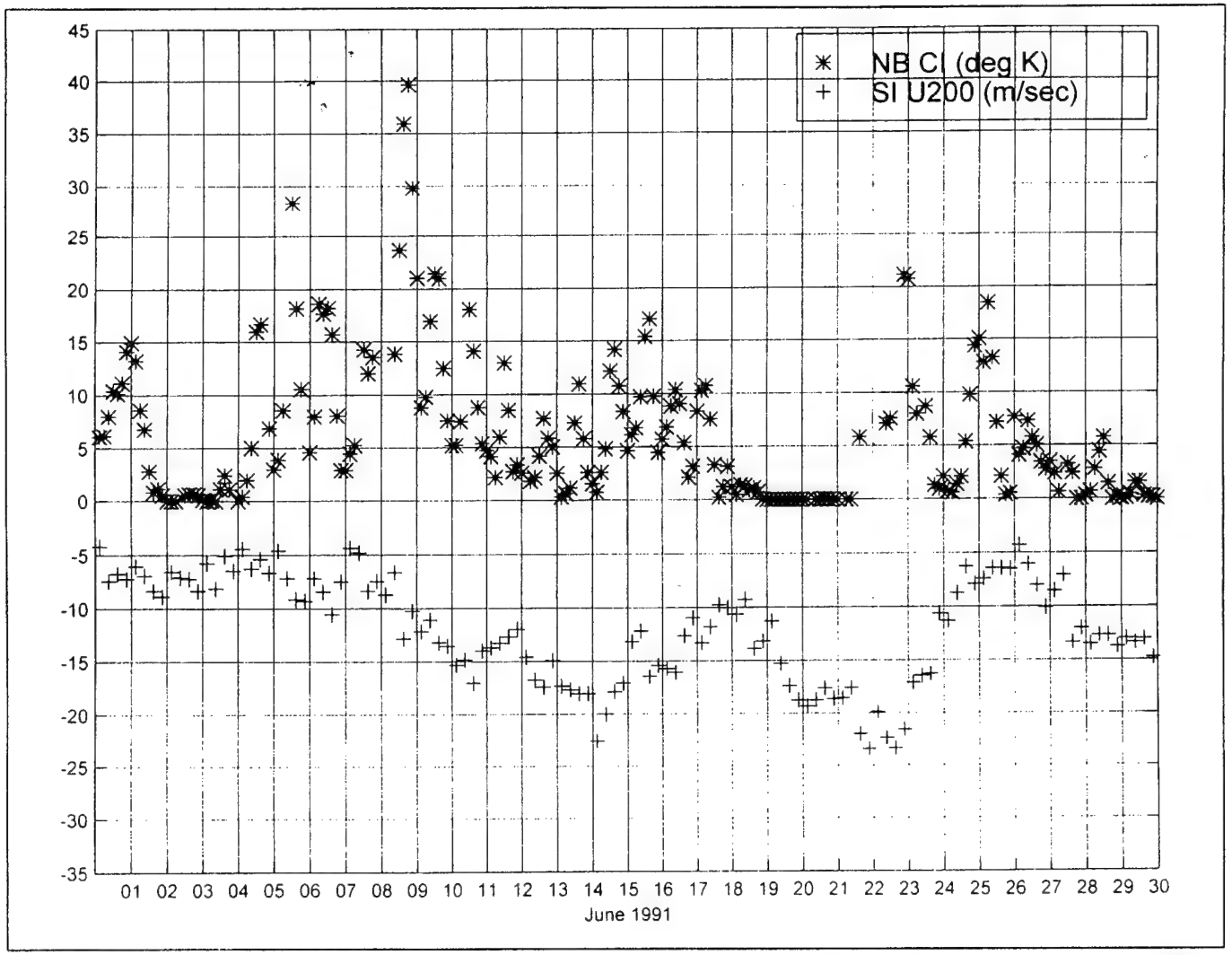

Figure 41. Area-averaged Convective Index (°K) for the northern Bay of Bengal (area NB) versus area-averaged 200 hPa wind (m/s) for southern India (area SI) during June, 1991.

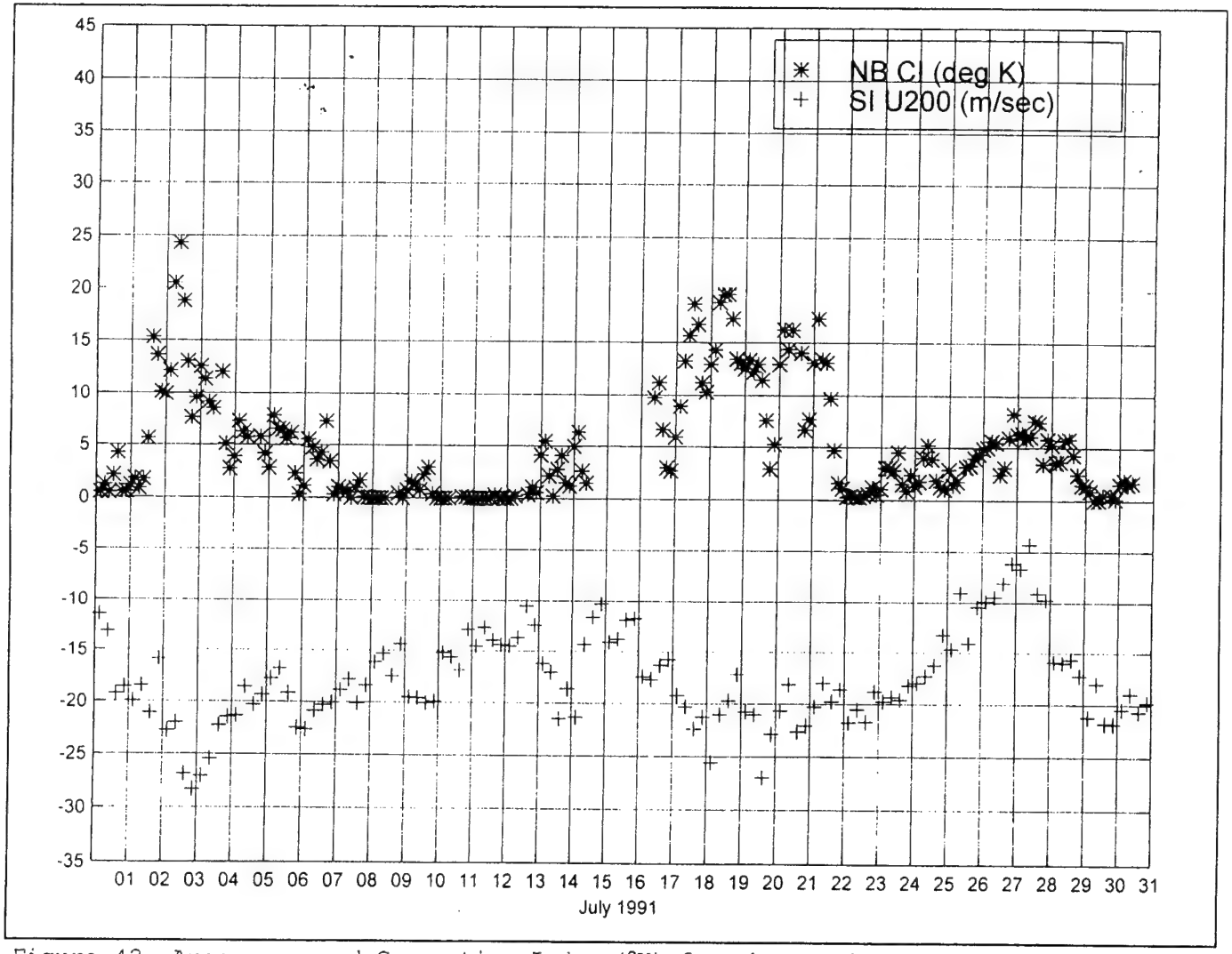

Figure 42. Area-averaged Convective Index (°K) for the northern Bay of Bengal (area NB) versus area-averaged 200 hPa wind (m/s) for southern India (area SI) during July, 1991.

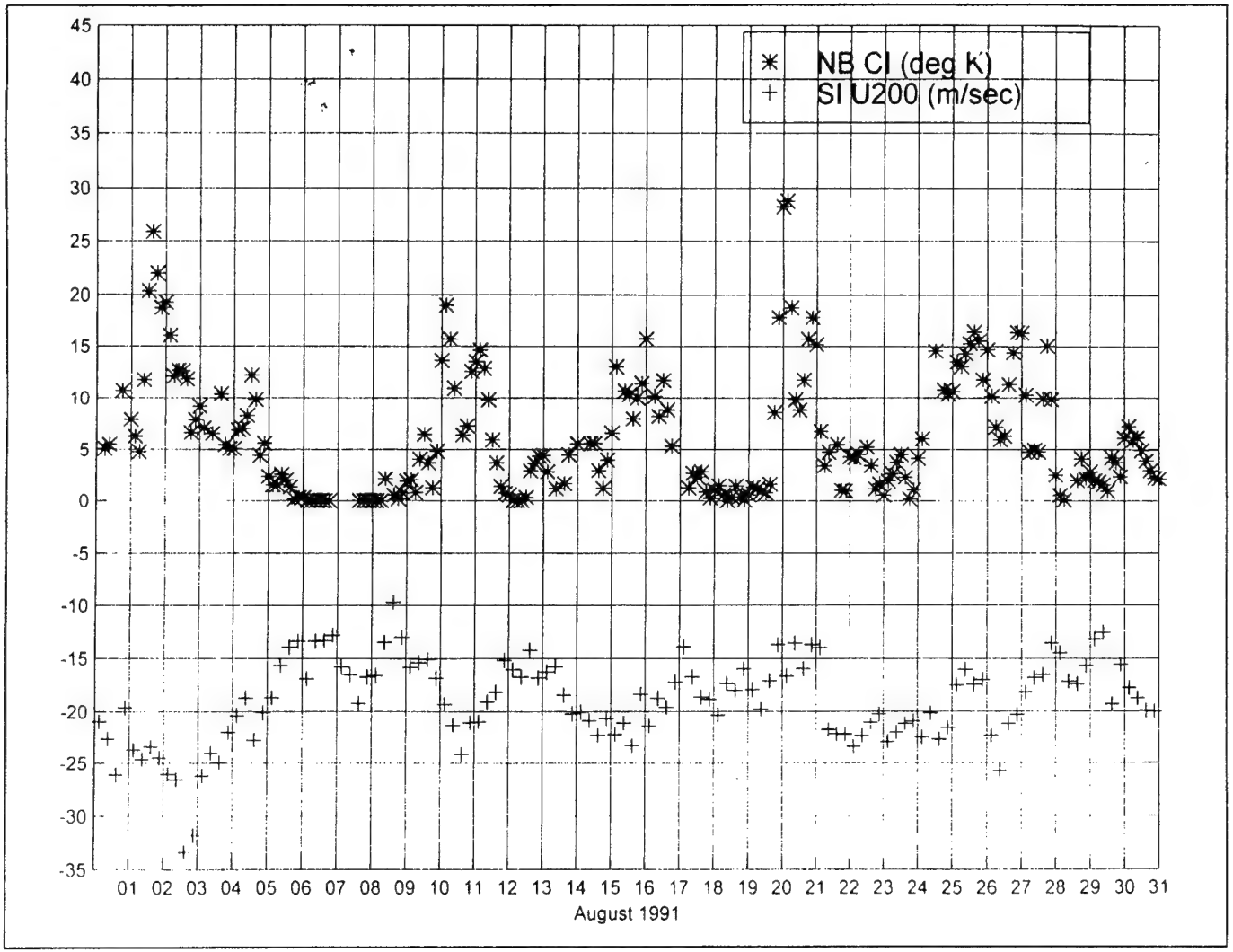

Figure 43. Area-averaged Convective Index (°K) for the northern Bay of Bengal (area NB) versus area-averaged 200 hPa wind (m/s) for southern India (area SI) during August, 1991.

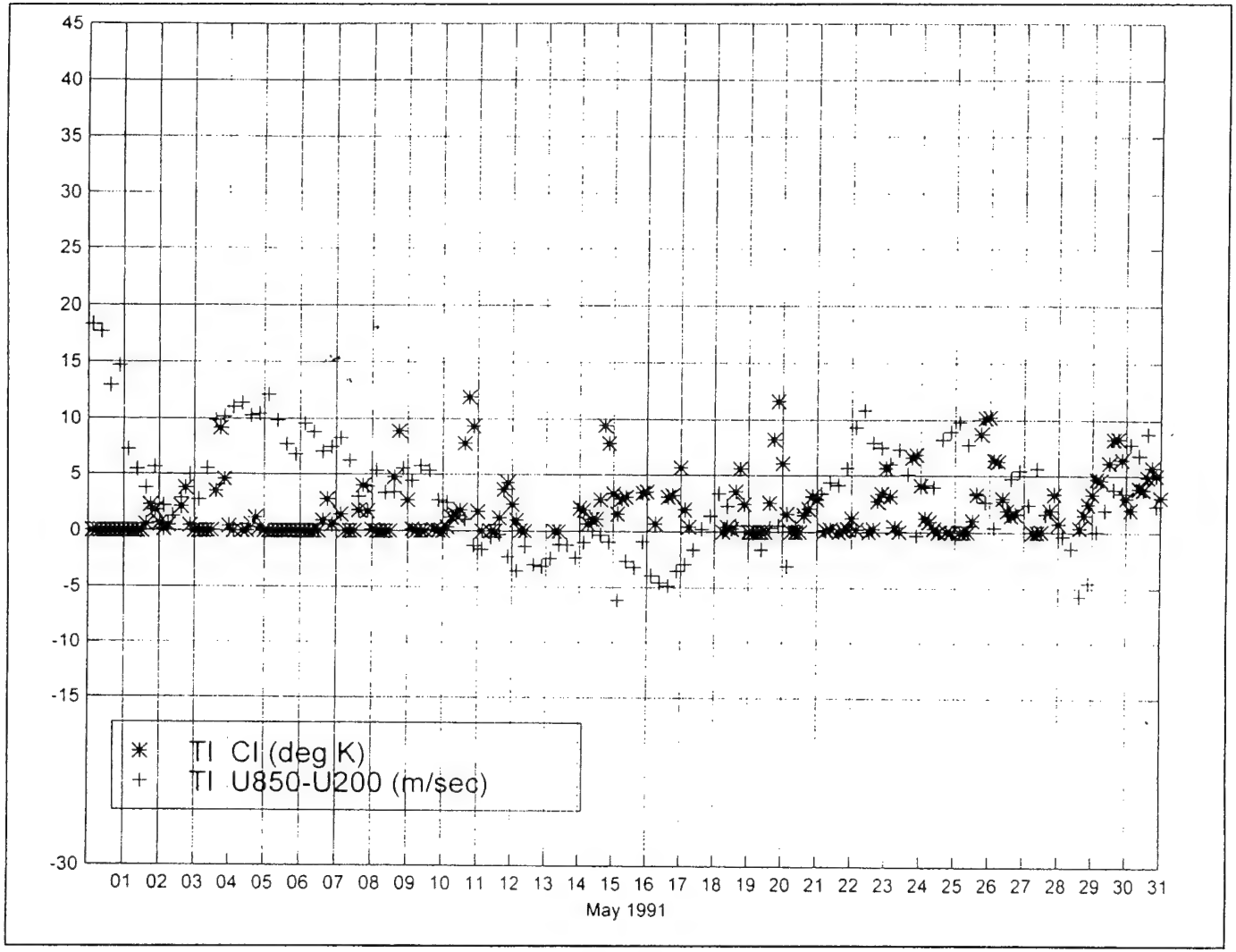

Figure 44. Area-averaged Convective Index (°K) versus area-averaged Vertical Wind Shear (U_{850}-U_{200} in m/s) for the southern tip of India (area TI) during May, 1991.

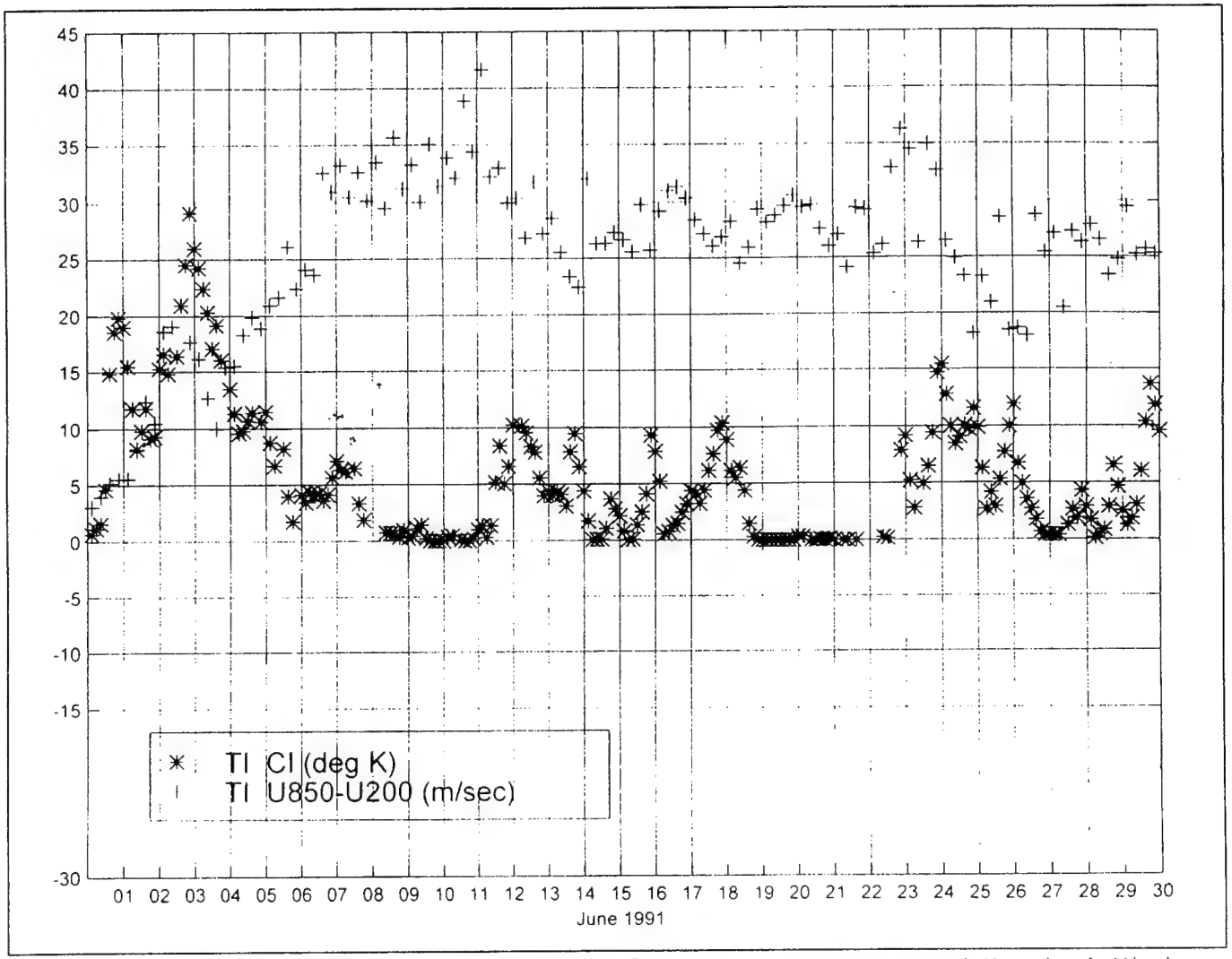

Figure 45. Area-averaged Convective Index (°K) versus area-averaged Vertical Wind Shear (U_{850}-U_{200} in m/s) for the southern tip of India (area TI) during June, 1991.

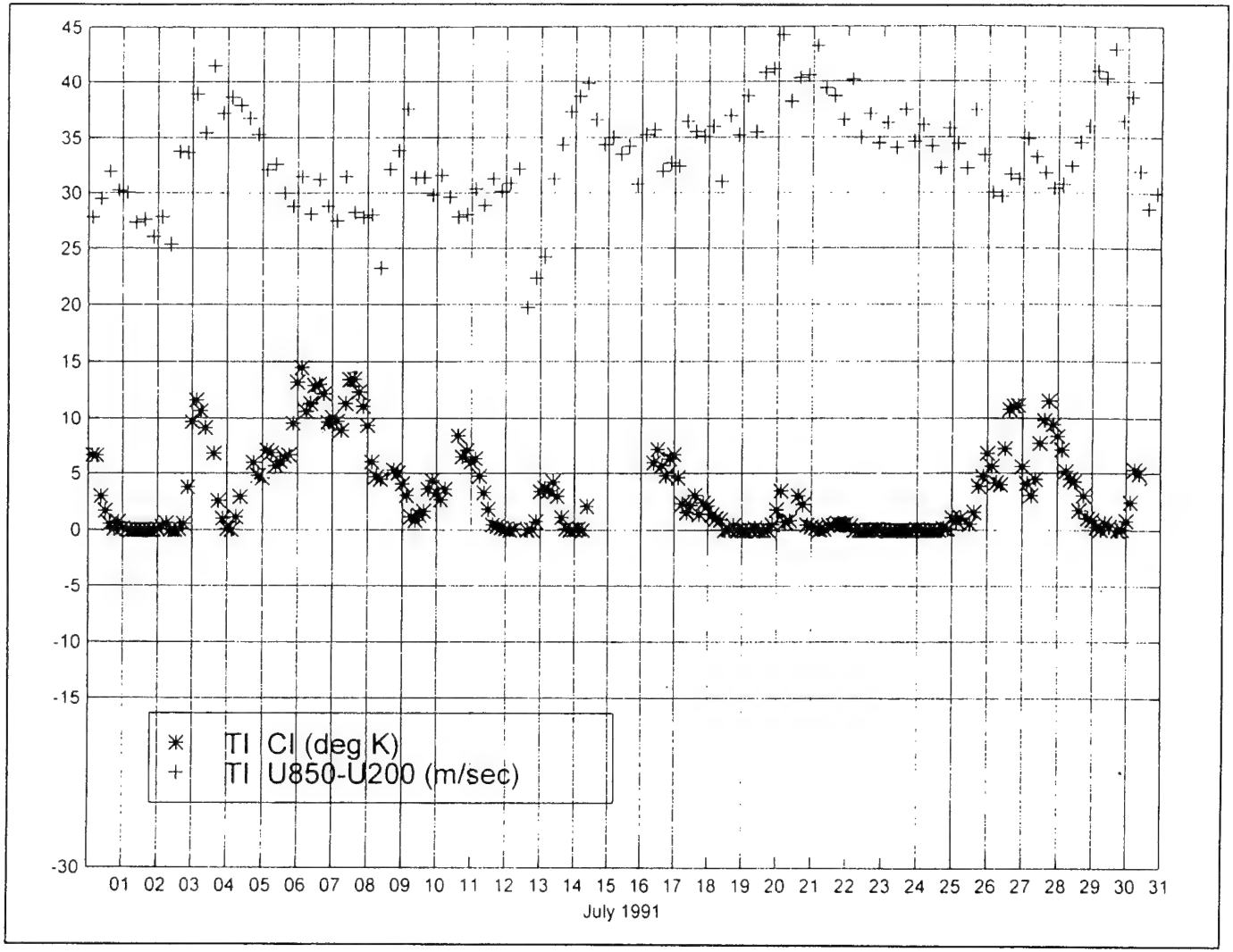

Figure 46. Area-averaged Convective Index (°K) versus area-averaged Vertical Wind Shear (U_{850}-U_{200} in m/s) for the southern tip of India (area TI) during July, 1991.

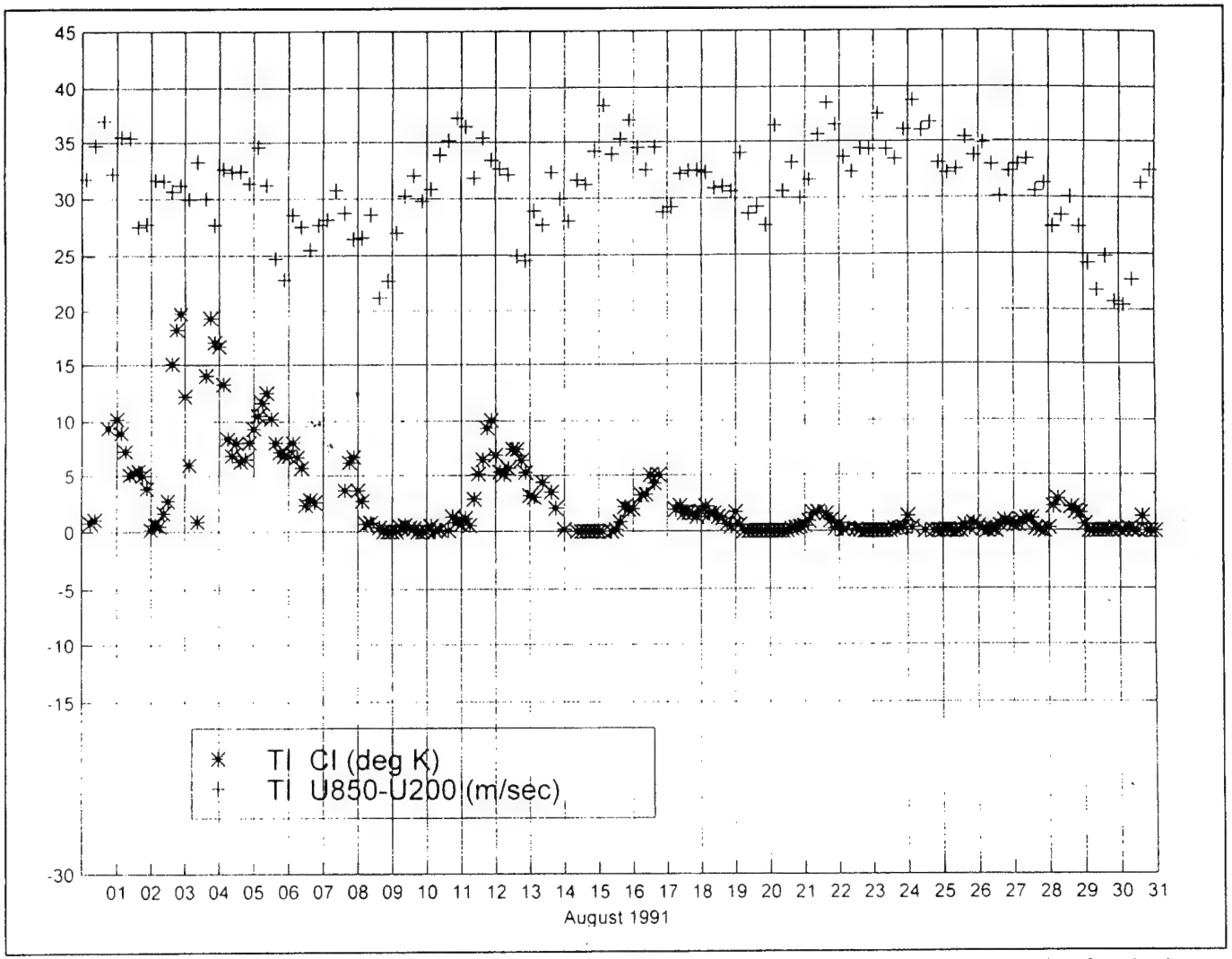

Figure 47. Area-averaged Convective Index (°K) versus area-averaged Vertical Wind Shear (U_{850} -U_{200} in m/s) for the southern tip of India (area TI) during August, 1991.

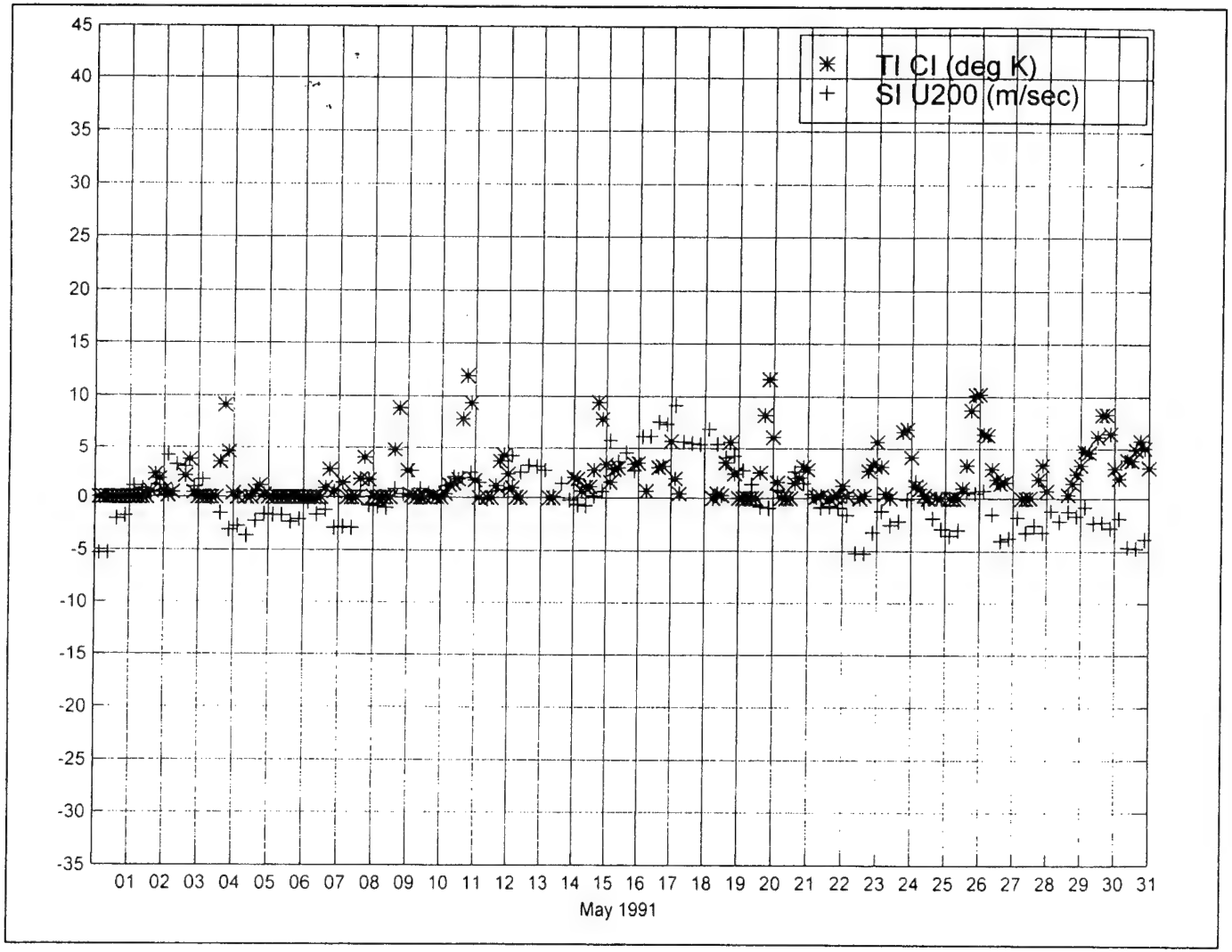

Figure 48. Area-averaged Convective Index (°K) for the southern tip of India (area TI) versus area-averaged 200 hPa wind (m/s) for southern India (area SI) during May, 1991.

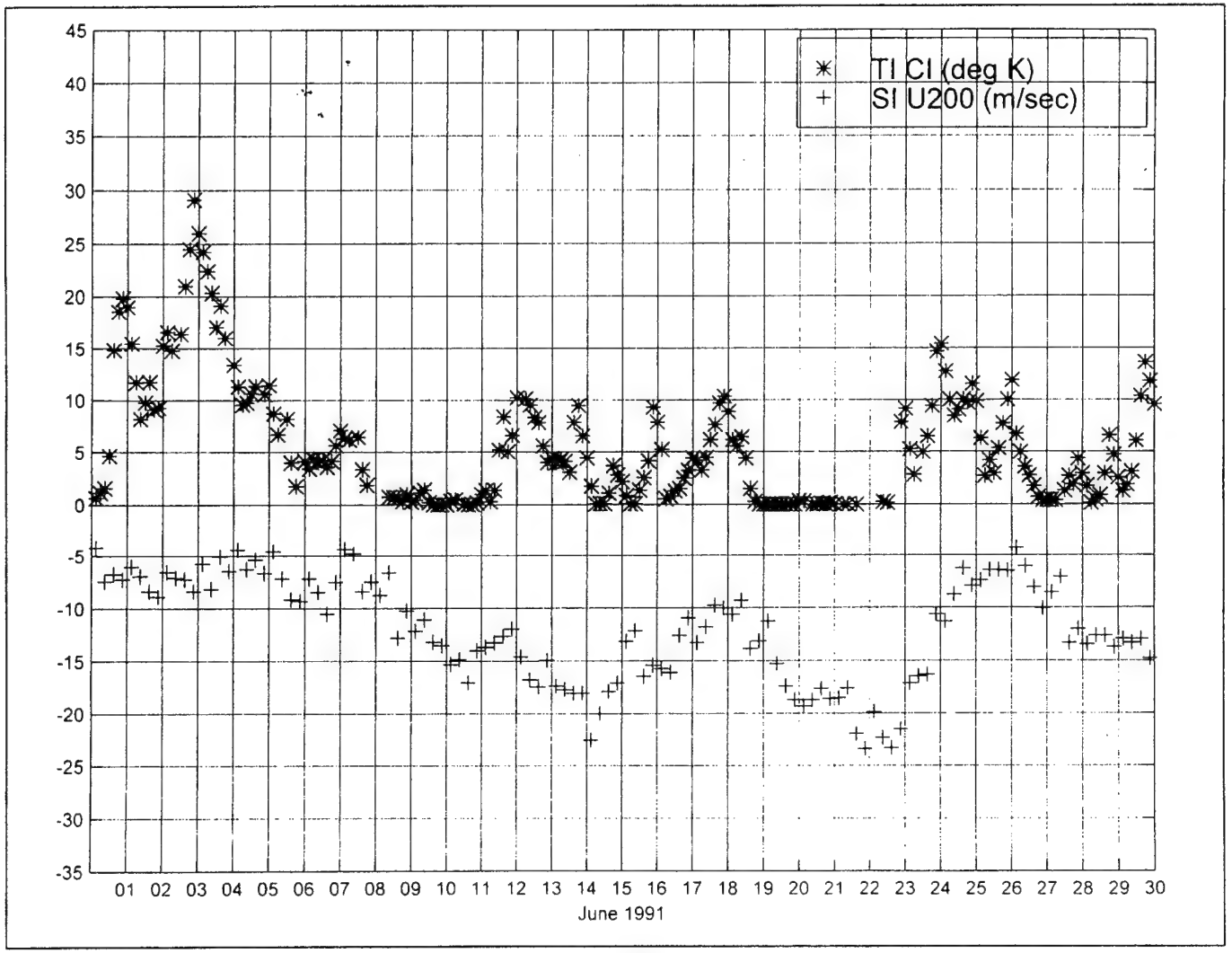

Figure 49. Area-averaged Convective Index (°K) for the southern tip of India (area TI) versus area-averaged 200 hPa wind (m/s) for southern India (area SI) during June, 1991.

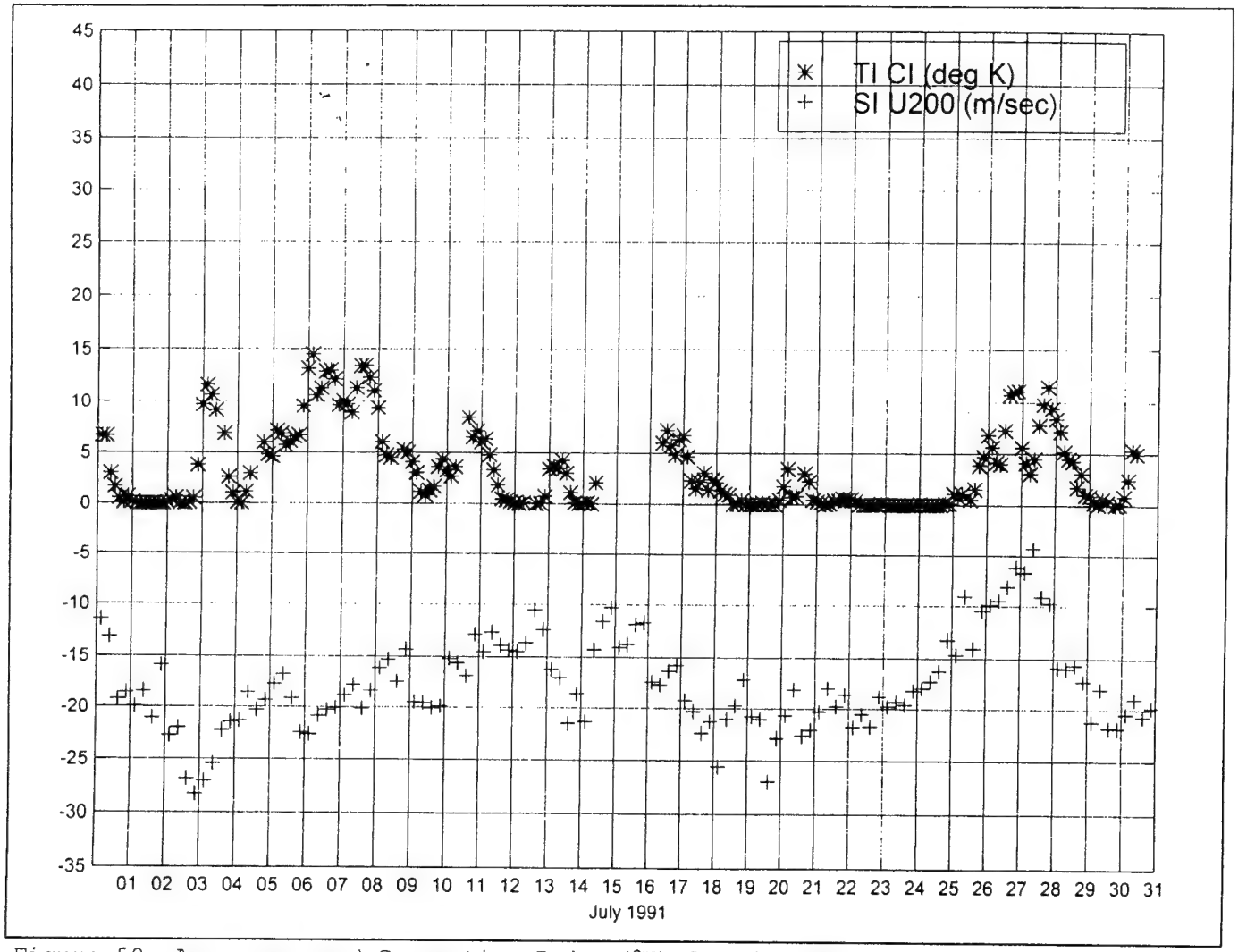

Figure 50. Area-averaged Convective Index (°K) for the southern tip of India (area TI) versus area-averaged 200 hPa wind (m/s) for southern India (area SI) during July, 1991.

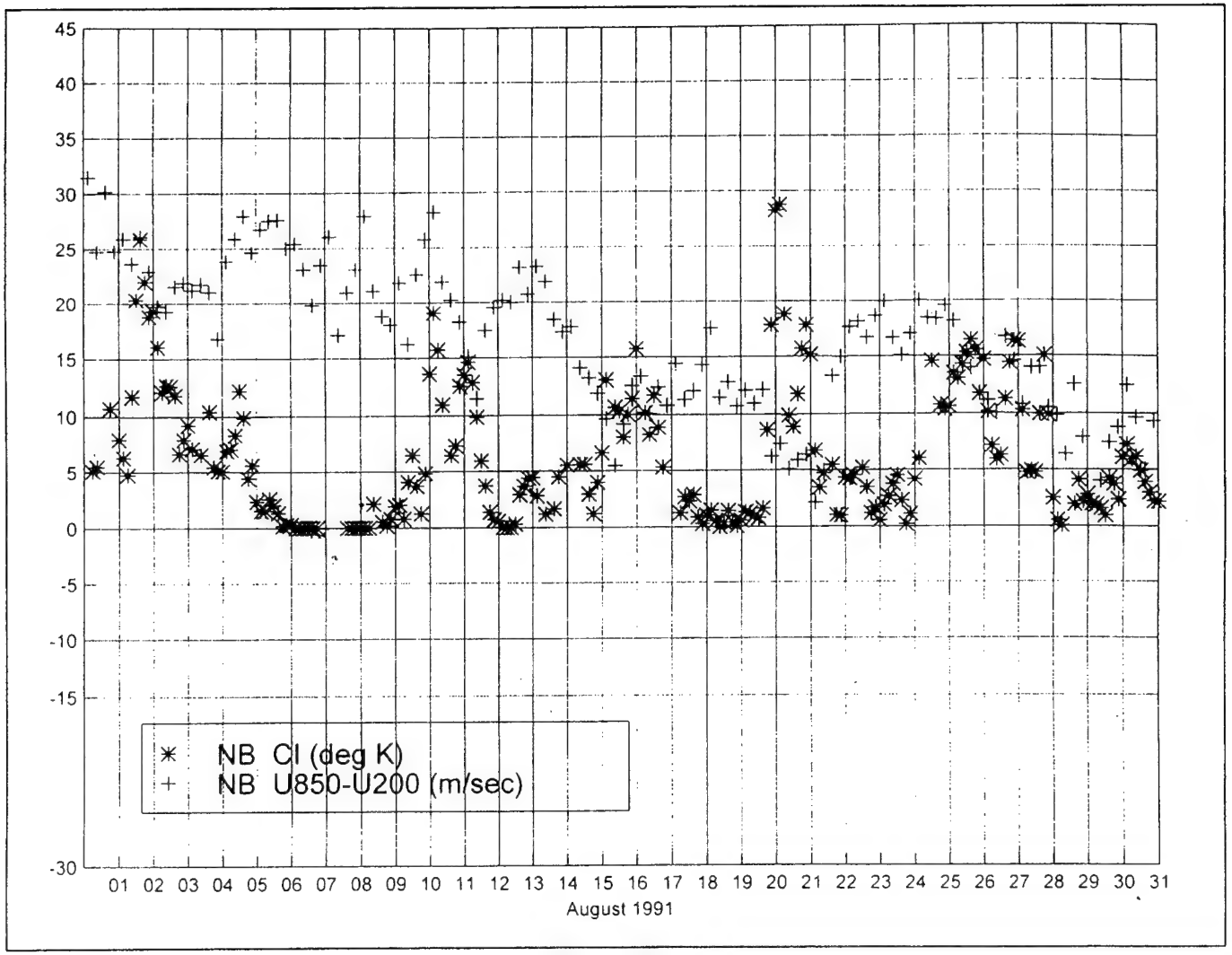

Figure 55. Area-averaged Convective Index (°K) versus area-averaged Vertical Wind Shear (U_{850}-U_{200} in m/s) for the northern Bay of Bengal (area NB) during August, 1991.

IV. SUMMARY

Variations of summer monsoon convection and the tropical upper tropospheric jet over the northern Indian Ocean, India, and south Asia during 1991 are the foci of this study. Using high resolution (1° x 1°, eight times daily) infrared data from both the GMS and INSAT satellites, a convective index (CI) is derived from the black body temperature to analyze the monthly mean and synoptic time scale variations of convective activity over the region. The satellite data is used with 200 and 850 hPa wind and moisture data from ECMWF global re-analyses available four times daily on a 1.125° x 1.125° Gaussian grid. Sea surface temperature data available from NMC, produced weekly on a 1° x 1° grid, is used in conjunction with temperature, relative humidity, and surface wind fields from the ECMWF data set to derive vertical latent heat fluxes. All data and derived fields are optimally interpolated in space to match the grid points of the ECMWF data set.

Average winds at 200 hPa for the months of May-August, 1991, show the presence of an anticyclone aloft over the Indochina Peninsula during May that strengthens and moves towards the northwest. By early July, this anticyclone is situated over the Tibetan Plateau (near 27°N), where it remains through the end of August. An upper level

tropospheric jet maximum forms over northern India (in June) and moves to a position over southern India by early July, where it remains through August. A secondary local jet maximum forms over northern India during late July also remaining through the end of August.

Associated low level winds and at 850 hPa show weak cyclonic turning in May near the tip of India, becoming much stronger in June (after the onset of the northern summer monsoon). Winds align to the west and southwest throughout the Arabian Sea and bay of Bengal, progressively strengthening from July through August.

Significant convection is confined to the near-equatorial region of the Indian Ocean during May, moving northward beginning in June, as the monsoon trough (ITCZ) moves away from the equator to a south of the Tibetan Plateau (becoming roughly aligned vertically with the 200 hPa anticyclone near 27°N through July and August).

The complete development of the northern summer monsoon over the Indian Ocean region during 1991 takes place from approximately May 15 through June 18. This seasonal transition is marked by the development of a low level cyclone over southern India (during May 15-29) that moves northward over the Indian sub-continent from approximately May 30-June 18, eventually merging with the monsoon trough near the

Tibetan Plateau by the end of the transition. As the low level cyclone moves northward, the low level moisture flux to the south increases dramatically and aligns with the wind field to the southwest. Significant convective activity during the transition event corresponds to those areas where low level moisture flux is the highest, beginning near the equator (May 15) and moving north to encompass the entire Indian sub-continent and most of the Bay of Bengal by early June. During July and August, a partial redistribution of significant convective activity occurs, extending north to the foothills of the Tibetan Plateau. Additional characteristics of the observed onset event include a drop in area-averaged sea surface temperatures of 1.5-2.0°C, an increase in area-averaged vertical latent heat flux from the ocean to the atmosphere of approximately 6-7 $W/m^2/day$, and the establishment of a maximum in vertical wind shear (a result of the increased southwesterlies at low levels and the dominance of the tropical upper tropospheric easterly jet which are manifest during the transition).

The onset of the summer monsoon over India and the Bay of Bengal occurred on June 4-6. After the onset, fluctuations of the tropical upper tropospheric easterly jet (at the synoptic time scale) are mostly in phase with those of intense cumulus convection near the rising branch of the local Hadley

circulation whose upward branch is located near the northern Bay of Bengal. Namely, where convection in the northern Bay of Bengal is strong, a corresponding acceleration of the upper easterly jet is observed. This phenomenon is analogous to the northern winter monsoon situation in which the enhancement of monsoon convection over the maritime continent leads to an acceleration of the subtropical westerly jet in the upper troposphere near Japan. In both cases the monsoon convection exerts an influence to the upper tropospheric jet that is downstream from the meridional outflow of the local Hadley cell. This process is probably through the Coriolis torque of the enhanced outflow when the convection flares up.

Another possible effect of the cumulus convection that shows up in the results is the damping of the upper tropospheric easterly jet due to the transport of momentum by cumulus convection. It is expected that such an effect may show up more clearly over regions of strong vertical shear, or strong upper tropospheric wind, especially in view of the marginal observation base for the ECMWF model analysis in the Indian Ocean region.

After the onset, synoptic time variations in the convection over southern India, where the maximum of the upper easterly jet is situated, corresponds with an inverse variation of the jet strength. This correspondence can be

observed during nearly two thirds of the summer monsoon season. This also means increased convection is associated with a reduction of the vertical shear of the zonal wind, with westerly at 850 hPa and easterly at 200 hPa. In the core region of tropical cyclones such correspondence is normally due to the "shearing off" of the vertical column of accumulated condensation heat release, resulting in weakened circulations or cyclone intensity. In the present study, the convection index is area-averaged over a synoptic domain, and the heating and circulation form only a small section of the entire monsoon system. It is unlikely that the shear-off effect is operating here. Therefore the inverse relationship between vertical shear and convection appear to indicate a damping of the vertical shear (or 200 hPa easterly jet) by the cumulus momentum transport.

Further evidence of the cumulus damping mechanism may be seen from the relationship between convective index and the vertical shear over northern Bay of Bengal. This is an area located to the north of the upper easterly jet axis during June and July 1991, but it is occupied by a secondary jet maximum (or maximum vertical shear) during August. No relationship between the convection index and the vertical shear strength is observed during June and July, but a clearly out of phase relationship exists in August, 1991.

LIST OF REFERENCES

Ananthakrishnan, R., 1970: Reversal of pressure gradients and wind circulation across India and the southwest monsoon. *Quart. J. Roy. Met. Soc.*, **96**, 539-542.

Buck, J.S., 1981: Relationship between saturation vapor pressure to temperature for moist air. *J. Appl. Meteor.*, **20**, 1527-1532.

Chang, C.-P. and K.M. Lau, 1980: Northeasterly cold surges and near-equatorial disturbances over the winter MONEX area during December 1974. Part II: Planetary scale aspects. *Mon. Wea. Rev.* **108**, 298-312.

Chang, C.-P., 1977: Viscous internal gravity waves and low frequency oscillation in the tropics. *J. Atmos. Sci.* **24**, 901-910.

Chang, C.-P. and H. Lum, 1985: Tropical mid-latitude interactions over Asia and the western Pacific Ocean during the 1983-1984 northern winter. *Mon. Wea. Rev.* **113**, 1345-1358.

Cornejo-Garrido, A.G. and P.H. Stone, 1977: On the heat balance of the Walker circulation. *J. Atmos. Sci.* **34**, 1155-1162.

Findlater, J., 1969: A major low level air current near the Indian Ocean during the northern summer. *J. Atmos. Sci.*, **95**, 400-403.

Garratt, J.R., 1977: Review of drag coefficients over oceans and continents. *Mon. Wea. Rev.* **105**, 915-929.

Gray, W.M., 1979: Hurricanes: Their formation, structure, and likely role in the tropical circulation. Meteorology Over the Tropical Oceans. Shaw and Collins,eds., James Glaisher House, 155-218.

Holton, J.R. and D.E. Colton, 1972: A diagnostic study of the vorticity balance at 200 mb in the tropics during the northern summer. *J. Atmos. Sci.* **29**, 1124-1128.

Kondo, J., 1975: Air-sea bulk transfer coefficients in

diabatic conditions. *Bound. Layer Meteor.* **9**, 91-112.

Krishnamurti, T.N., 1971: Tropical east-west circulations during northern summer. *J. Atmos. Sci.* **28**, 1342-1347.

Krishnamurti, T.N. and N. Surgi, 1987: Observational aspects of summer monsoon. In: *Monsoon Meteorology*. Chang and Krishnamurti, eds., Oxford Univ. Press.,3-25.

Lau, K.M. and C.-P. Chang, 1987: Planetary scale aspects of the winter monsoon and atmospheric teleconnections. Monsoon Meteorology. Chang and Krishnamurti, eds., Oxford Univ. Press., 161-202.

Lau, K.M., C.-P. Chang, and P.H. Chan, 1983: Short-term planetary scale interaction over the tropics and mid-latitude. II: Winter-MONEX period. *Mon. Wea. Rev.* **111**, 1372-1388.

Liebmann, B. and D.L. Hartmann, 1982: Interannual variations of outgoing IR associated with tropical circulation changes during 1974-1978. *J. Atmos. Sci.*, **39**, 1153-1162.

Murakami, M., 1984: Analysis of deep convective activity over the western Pacific and Southeast Asia. Part II. *J. Meteor. Soc. Jap.* **62**, 88-108.

Nitta, T., 1983: Observational study of heat sources over the eastern Tibetan Plateau during the summer monsoon. *J. Meteor. Soc. Jap.* **61**, 606-618.

Pisharoty, P.R., 1965: Evaporation from the Arabian Sea and the Indian southwest monsoon. In: *Proceedings of the international symposium on meteorological results of the International Indian Ocean Expedition, Bombay India, 22-26 July 1965*. Kurawamis and Dumas, eds., Bombay Univ. Press. 43-54.

Pisharoty, P.R., 1981: Sea surface temperature and monsoon. In: *Monsoon Dynamics*. Lighthill and Pearce, eds., Cambridge Univ. Press. 238-251.

Ramage, C.S. and A.M. Hori, 1981: Meteorological aspects of the El Nino. *Mon. Wea. Rev.*, **109**, 1827-1835.

Rasmussen, E.M. and T.H. Carpenter, 1982: Variations in tropical sea surface temperature and surface wind fields

associated with the Southern Oscillation/El Nino. *Mon. Wea. Rev.*, **110**, 354-384.

Reynolds, R.W. and D.C. Marsico, 1993: An improved real-time global sea surface temperature analysis. *J. Climate,* **6**, 114-119.

Reynolds, R.W., 1988: A real-time global sea surface temperature analysis. *J. Climate,* **1**, 75-86.

Rudolph, D.K. and C.P. Guard, 1991: Northern Indian Ocean Tropical Cyclones. In: *1991 Annual Tropical Cyclone Report of the Joint Typhoon Warning Center*. Rudolph and Guard, eds., National Technical Information Service Press. 150-158.

Sardeshmukh, P.D. and I.M. Held, 1984: The vorticity balance in the tropical upper troposphere of a general circulation model. *J. Atmos. Sci.*, **41**, 768-778.

Schlatter, T.W., 1975: Some experiments with a multivariate statistical objective analysis scheme. *Mon. Wea. Rev.*, **103**, 246-257.

Webster, P.J. and S. Yang, 1992: Monsoon and ENSO; selective interactive systems. *Quart. J. Roy. Met. Soc.*, **118**, 877-926.

Wyrtki, K., 1975: Average annual heat balance of the north Pacific ocean and its relation to ocean circulation. *J. Geo. Res.*, **70**, 4547-4559.

Yasunari, T., 1979: Cloudiness fluctuations associated with the Northern Hemisphere summer monsoon. *J. Meteor. Soc. Jpn.*, **57**, 227-262.

INITIAL DISTRIBUTION LIST

		No. of copies
1.	Defense Technical Information Center 8725 John J. Kingman Rd.,STE 0944 Ft. Belvoir, Virginia 22304-6145	2
2.	Dudley Knox Library Naval Postgraduate School 411 Dyer Rd. Monterey, California 93943-5101	2
3.	Chairman (Code MR/Wx) Department of Meteorology Naval Postgraduate School Monterey, California 93943-5000	1
4.	Chairman (Code OC/Bk) Department of Oceanography Naval Postgraduate School Monterey, California 93943-5000	1
5.	Prof. Chih-Pei Chang (Code MR/Cp) Department of Meteorology Naval Postgraduate School Monterey, California 93943-5000	1
6.	Prof. Peter Chu (Code OC/Cu) Department of Oceanography Naval Postgraduate School Monterey, California 93943-5000	1
7.	LT Michael S. Nicklin 521 Sunshine Loop Fallon, Nevada 89406	2